

A Two-Point Hologram for Everything

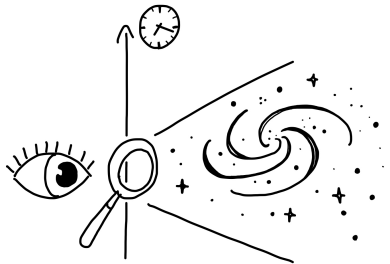
Tamra Nebabu¹, Xiao-Liang Qi², Haifeng Tang^{*2} and Huaijin Wang²

¹ *Department of Physics, Cornell University, Ithaca, New York*

² *Leinweber Institute for Theoretical Physics, Stanford University, Stanford, CA 94305, USA*

Abstract

Known holographic dictionaries, especially AdS/CFT, rely on symmetry matching between the bulk and the boundary. We take a step toward a holographic dictionary with no symmetry requirement and without assuming the geometry being asymptotically AdS. Starting from *any* interacting Majorana generalized free field on a $(0+1)d$ boundary and its two-point function data, we derive a concise analytic formula for the dual $(1+1)d$ bulk geometry, borrowing techniques from unitary matrix integral and inverse scattering. Using this formula, we compute the near-horizon curvature, give conditions for positive versus negative curvature, and identify simple boundary models with de Sitter or anti-de Sitter near-horizon duals. We also study the large- q SYK model, finding an unusual temperature dependence of the near-horizon curvature, related to the discrepancy between physical temperature and the “fake disk” temperature. We also construct, directly from boundary operators, approximate algebras generated by null translations and boost that become exact at the bifurcate horizon.



*hftang@stanford.edu

Contents

1	Introduction	3
2	Derive bulk geometry from boundary correlator	5
2.1	Review of Nebabu-Qi's discrete circuit construction	5
2.2	Method I: via unitary matrix integral	7
2.3	Method II: via inverse scattering	12
3	Curvature near horizon and AdS universality	17
4	Examples: finite QNMs	19
4.1	Two QNMs	19
4.2	Three QNMs and a concrete de Sitter model	21
4.3	A Gaussian Lindbladian boundary model	22
5	Examples: large-q SYK	24
5.1	General setup	24
5.2	Zero temperature limit	28
5.3	Finite temperature geometry	28
6	Algebra near the horizon	29
7	Discussion	31
A	Convention for the Fourier transformation	34
B	Determinant formula for multi-flavor fermions	35
C	Technical details of applying BOGC formula	38
D	An elementary calculation of determinants in one and two QNM models	41
D.1	BOGC evaluation of determinant	41
D.2	Elementary evaluation of determinant	43
E	An alternative inverse formula via contour integral of S-matrix	47
F	Match with bulk QFT	49
F.1	Boundary condition	49
F.2	Causal kernel decomposition from bulk QFT	50
F.3	Analytic property of Jöst function	52
F.4	One QNMs model from bulk QFT	56
F.5	Two QNMs model from bulk QFT	56
G	Technical detail of deriving inverse scattering formula	60
H	Technical details of near horizon algebra	64
H.1	$\mathfrak{sl}(2, \mathbb{R})$ algebra in AdS ₂ -Rindler	64
H.2	Curvature from algebra at bifurcate horizon	65
I	Examples of two-point function that doesn't have a continuous limit	71

1 Introduction

Is there a gravitational dual for a *generic* quantum many-body system? This question is motivated by the success of holographic principle [1], which relates a bulk quantum gravity theory to a non-gravitational boundary theory in one lower dimension, applied to the *special* setting of AdS (Anti-de Sitter)/CFT (conformal field theory) duality [2, 3, 4, 5]. A canonical example is the duality between supergravity on AdS_D and $\mathcal{N} = 4$ super Yang-Mills theory on Mink_{D-1} [2].

In AdS/CFT, the dictionary is tightly constrained by symmetry matching: the isometry group of AdS_D equals the conformal group of Mink_{D-1} . It is therefore natural to ask whether a more general holographic principle [1] exists— one with weaker, or even no, reliance on symmetry— particularly given the renewed interest in quantum gravity in de Sitter spacetime [6, 7, 8, 9, 10, 11, 12, 13, 14, 15].

Constructing such a dictionary at the fully *non-perturbative* level is difficult: microscopic boundary models with quantum gravity bulk duals typically require large numbers of degrees of freedom and strong coupling [16]. Here we instead pursue a *phenomenological* dictionary: given only two-point correlation data on the boundary, what can be inferred about the semiclassical bulk geometry and about bulk operators expressed in terms of boundary ones?

A concrete step in this direction was taken in [17]. Building on the Hamilton–Kabat–Lifschytz–Lowe (HKLL) construction [18, 19, 20], they proposed a reconstruction scheme that uses only boundary data and assumes neither prior knowledge of the bulk geometry nor (approximate) conformal symmetry.

One limitation of [17] is that the construction is numerical, relying on two-point functions on some discrete time points; the reconstructed bulk theory is specified as a circuit. In this work, we take the continuum limit and obtain analytic results. A main outcome is an explicit formula for the semiclassical bulk geometry reconstructed from the spectral function of a boundary generalized free field (GFF). Concretely, consider a time-translation-invariant Majorana GFF $\chi(t)$ in $(0+1)\text{d}$, and suppose we are given its anti-commutator two-point function $A(t, t') := \langle \{\chi(t), \chi(t')\} \rangle$. We show that the dual $(1+1)\text{d}$ bulk theory is a minimally coupled Majorana field of mass m on a geometry with metric

$$ds^2 = \Omega(z)^2(-dt^2 + dz^2) \tag{1.1}$$

where the conformal factor $\Omega(z)$ is determined as follows. Denote the Fourier transformation of $A(t, t')$ as $\mathcal{A}(\omega)$. Assume¹ that $\mathcal{A}(\omega)$ has simple poles $\{iJ_n\}$ and zeros $\{i\lambda_i\}$ in the upper half-plane, and associate to each λ_i the coefficient

$$\beta_i := 2\lambda_i \times \prod_{k \neq i} \frac{\lambda_k + \lambda_i}{\lambda_k - \lambda_i} \times \prod_n \frac{J_n - \lambda_i}{J_n + \lambda_i} \tag{1.2}$$

Physically, $-i\beta_i$ is the residue of the S-matrix $\mathcal{S}(\omega)$ at the pole $i\lambda_i$. Then

$$m^2 \Omega(z)^2 = -\partial_z^2 \log \det[\mathbf{1} - B(z)^2], \quad \text{with } B(z)_{ij} := \frac{\beta_j e^{-\lambda_j 2z}}{\lambda_i + \lambda_j} \tag{1.3}$$

Equation (1.3) is the main result of this work. Based on this result, we investigate several examples of two-point functions and various aspects of the bulk geometry. In particular, we

¹A more general formula without this assumption appears in (2.57),(2.58).

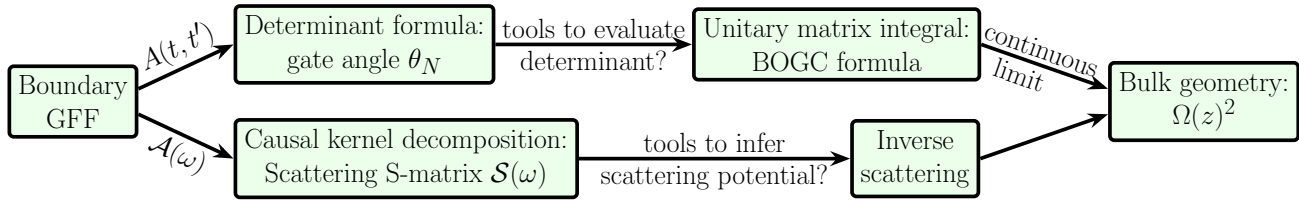


Figure 1: Roadmap from the boundary GFF two-point function to the dual bulk geometry, via two complementary approaches.

derive a concise formula for the scalar curvature near the black hole horizon.

The remainder of the paper is organized as follows. In [section 2](#) we first overview the key results in Ref. [17], and then provide derivations of the main results (1.2) and (1.3) using the following two methods.

- Method I (unitary matrix integral): We start from the discrete Gaussian-circuit construction of [17] (reviewed in [section 2.1](#)), and in [section 2.2](#) derive a determinant formula expressing the gate angles in terms of determinants of sub-matrices of $A(t, t')$, and evaluate the resulting Toeplitz determinants using the Borodin–Okounkov–Geronimo–Case (BOGC) formula [21, 22], familiar from giant graviton expansion in the context of unitary matrix integral [23, 24, 25, 26, 27, 28, 29, 30, 31, 32].
- Method II (inverse scattering): In [section 2.3](#), we work directly in the continuum, interpret $\Omega(z)$ as the scattering potential, extract the scattering amplitude $\mathcal{S}(\omega)$ from $\mathcal{A}(\omega)$ via causal kernel decomposition, and reconstruct $\Omega(z)$ using inverse scattering [33].

These methods are sketched in [fig. 1](#). We then study how the horizon curvature R_h depends on the boundary correlator.

In [section 3](#), we obtain the generic asymptotic behavior of metric and curvature near the horizon. We show that for generic $A(t, t')$ the near-horizon region is universally AdS, with $R_h/m^2 = -2$, independent of microscopic details. Only if the first and second zero of $\mathcal{A}(\omega)$ has exactly ratio 3, the curvature can take other values including dS, flat space or AdS with different value of R_h/m^2 .

In [section 4](#), we analyze correlators with finitely many quasi-normal modes (QNMs) [34, 35]. For $N_{\text{qnm}} = 2$ the geometry is always constant-curvature AdS₂. For $N_{\text{qnm}} = 3$ we exhibit a family with $R_h/m^2 > 0$, realizing de Sitter near horizon. A generic feature of finite-QNM examples is that $\Omega(z)$ remains finite at the boundary (i.e. the boundary is not at the asymptotic AdS boundary), naturally realizing finite-cutoff holography [36, 10, 37]. We also show how such spectra with finitely QNMs arise from Gaussian Lindbladian dynamics as a boundary model, and in particular we record an explicit realization of such $N_{\text{qnm}} = 3$ model with de Sitter near horizon.

In [section 5](#), we turn to the large- q SYK model [38, 39, 40, 41], which has infinitely many QNMs. In [section 5.1](#) we obtain the general formula for SYK model two-point function and curvature. In [section 5.2](#), we study the zero-temperature limit and recover constant-curvature AdS₂ with the correct R_h/m^2 . In [section 5.3](#), we study finite temperature and find that R_h/m^2 has an unusual dependence on T_{syk} , changing sign and diverging in an almost periodic fashion, due to collisions between poles and zeros of $\mathcal{S}(\omega)$ induced by the mismatch between T_{syk} and the “fake disk” temperature T_{fake} [40, 42].

In [section 6](#), we discuss the operator algebra in the near horizon region. For AdS₂ or dS₂ geometry there is an $\mathfrak{sl}(2, \mathbb{R})$ algebra generated by the null translations P^\pm and boost B , while for flat space we expect to find a Poincaré algebra. We show that for a generic boundary theory whose dual bulk geometry doesn't exhibit maximal symmetry, these three operators can also be defined, which form an approximate algebra; when acting on fermion modes at the bifurcate horizon, the algebra becomes exact.

Finally, in [section 7](#) we present the conclusion and discuss potential future directions.

2 Derive bulk geometry from boundary correlator

2.1 Review of Nebabu-Qi's discrete circuit construction

In this section we briefly review the aspects of the discrete-circuit reconstruction of Nebabu-Qi [\[17\]](#) needed for our continuum analysis.

We start from a $(0+1)$ d boundary theory containing an interacting Majorana GFF χ , with anti-commutator two-point function $A(t, t') := \langle \{\chi(t), \chi(t')\} \rangle$. The goal is to map this data to a $(1+1)$ d free massive Majorana field Ψ_L, Ψ_R living on the geometry [\(1.1\)](#), with the boundary at $z = 0$.

Ref. [\[17\]](#) focused on the two-point function at discretized time points $t := \mathbf{t}\Delta t$ with $\mathbf{t} \in \mathbb{Z}$. The corresponding bulk coordinate is given by

$$\begin{aligned} u &= \mathbf{u}\Delta t, v = \mathbf{v}\Delta t \\ z &= \frac{v - u}{2}, t = \frac{v + u}{2} \end{aligned} \tag{2.1}$$

with $\mathbf{u}, \mathbf{v} \in \mathbb{Z}$, $\mathbf{v} - \mathbf{u} \geq 0$. Each value of (\mathbf{u}, \mathbf{v}) labels a gate in a semi-infinite “brickwall” circuit, as is illustrated in [fig. 2\(a\)](#). The circuit fermions satisfy the canonical anti-commutation relations

$$\{\psi_a(\mathbf{z}, \mathbf{t}), \psi_b(\mathbf{z}', \mathbf{t}')\} = \delta_{ab}\delta_{\mathbf{z}\mathbf{z}'}, \quad a, b \in \{L, R\} \tag{2.2}$$

where we distinguish $\psi_a(\mathbf{z}, \mathbf{t})$ (circuit fermions) from $\Psi_a(z, t)$ (continuum QFT fields).

Since the bulk evolution is unitary, each gate in [fig. 2\(a\)](#) is an $SO(2)$ rotation U parametrized by an angle $\theta(\mathbf{z}, \mathbf{t})$. For example, the gate in [fig. 2\(c\)](#) acts as

$$\begin{bmatrix} \psi_c \\ \psi_d \end{bmatrix} = U \begin{bmatrix} \psi_a \\ \psi_b \end{bmatrix} = \begin{bmatrix} \cos \theta & -\sin \theta \\ \sin \theta & \cos \theta \end{bmatrix} \begin{bmatrix} \psi_a \\ \psi_b \end{bmatrix} \tag{2.3}$$

More generally, there could be multiple flavors at each location. When there are n fermions at each time labeled by $\chi_a(t)$, $a = 1, 2, \dots, n$, there is the same number of fermions at each link of the bulk circuit, and the gate is an $SO(2n)$ matrix.

The bulk fermions are linear combinations of boundary fermions via future/past kernels,

$$\psi_L(\mathbf{z}, \mathbf{t}) = \sum_{\mathbf{t}'} K^P(\mathbf{z}, \mathbf{t}|\mathbf{t}')\chi(\mathbf{t}'), \quad \psi_R(\mathbf{z}, \mathbf{t}) = \sum_{\mathbf{t}'} K^F(\mathbf{z}, \mathbf{t}|\mathbf{t}')\chi(\mathbf{t}') \tag{2.4}$$

Following the HKLL construction, $K^{p,f}: K^{p,f}(\mathbf{z}, \mathbf{t}|\mathbf{t}')$ are required to be nonzero only when the bulk point (\mathbf{z}, \mathbf{t}) is spacelike separated from the boundary point $(0, \mathbf{t}')$, as is shown in [Fig. 2 \(b\)](#).

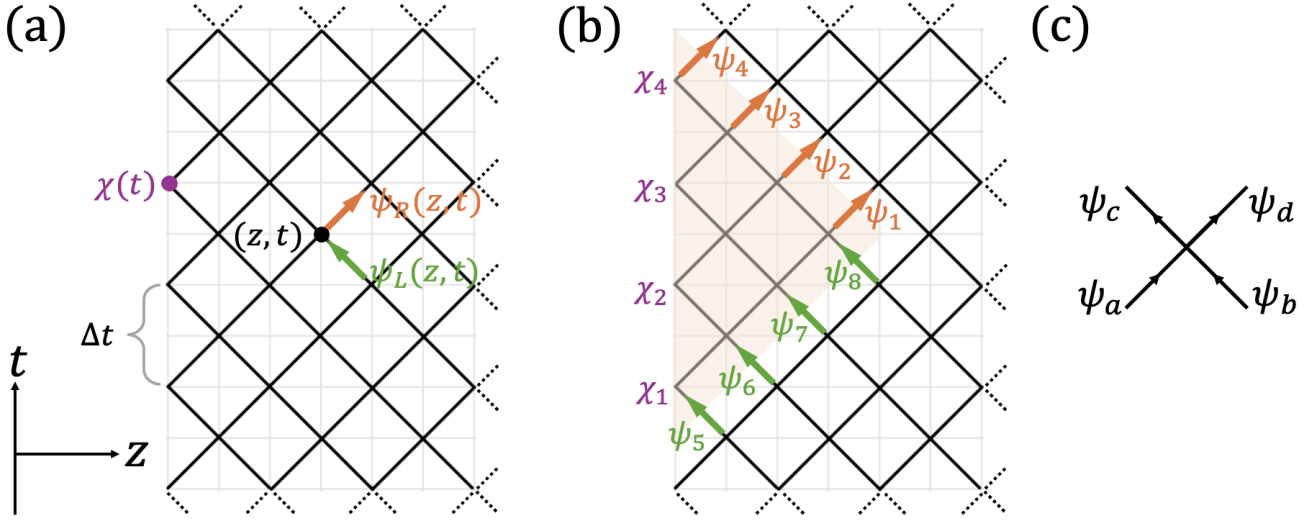


Figure 2: **(a)** The Nebabu–Qi circuit [17]. **(b)** Causal-wedge reconstruction (cf. (2.5)). **(c)** Each “cross” is an SO(2) gate, with the convention in (2.3).

As shown in [17], the kernels can be constructed wedge-by-wedge. For the illustrative wedge in fig. 2(b), one reconstructs $\psi_{1\sim 4}, \psi_{5\sim 8}$ from $\chi_{1\sim 4}$, where $\psi_{1\sim 4}$ and $\psi_{5\sim 8}$ form two mutually orthonormal sets. The causal wedge condition enforces triangularity of $K^{p,f}$:

$$\begin{bmatrix} \psi_5 \\ \psi_6 \\ \psi_7 \\ \psi_8 \end{bmatrix} = \begin{bmatrix} 1 & 0 & 0 & 0 \\ K_{61}^p & K_{62}^p & 0 & 0 \\ K_{71}^p & K_{72}^p & K_{73}^p & 0 \\ K_{81}^p & K_{82}^p & K_{83}^p & K_{84}^p \end{bmatrix} \begin{bmatrix} \chi_1 \\ \chi_2 \\ \chi_3 \\ \chi_4 \end{bmatrix}, \quad \begin{bmatrix} \psi_1 \\ \psi_2 \\ \psi_3 \\ \psi_4 \end{bmatrix} = \begin{bmatrix} K_{11}^f & K_{12}^f & K_{13}^f & K_{14}^f \\ 0 & K_{22}^f & K_{23}^f & K_{24}^f \\ 0 & 0 & K_{33}^f & K_{34}^f \\ 0 & 0 & 0 & K_{44}^f \end{bmatrix} \begin{bmatrix} \chi_1 \\ \chi_2 \\ \chi_3 \\ \chi_4 \end{bmatrix} \quad (2.5)$$

The canonical anti-commutation relations (2.2) then require

$$K^f A (K^f)^\top = \mathbf{1}, \quad K^p A (K^p)^\top = \mathbf{1} \quad (2.6)$$

Here $A_{ij} := \langle \{\chi_i, \chi_j\} \rangle$ is the 4×4 submatrix of the boundary anti-commutator matrix $A(t, t')$.

Equations (2.5) and (2.6) implement a step-by-step orthonormalization procedure. For example, $\psi_4 = \chi_4$; ψ_3 is the component of χ_3 orthogonal to χ_4 ; ψ_2 is the component of χ_2 orthogonal to both χ_3 and χ_4 ; and so on. In linear algebra this is related to the Cholesky decomposition² [43], which determines $K^{p,f}$: writing $A = R^f (R^f)^\top = R^p (R^p)^\top$ with R^p lower triangular and R^f upper triangular, one has³ $K^p = (R^p)^{-1}$ and $K^f = (R^f)^{-1}$.

Once the kernels are fixed, the gate angles are fixed as well. For the gate in fig. 2(c), from (2.3) the orthogonal matrix U (and hence θ) is determined by

$$\begin{bmatrix} \text{---} K_c \text{---} \\ \text{---} K_d \text{---} \end{bmatrix} \begin{bmatrix} | \\ | \\ \chi \\ | \\ | \end{bmatrix} = U \begin{bmatrix} \text{---} K_a \text{---} \\ \text{---} K_b \text{---} \end{bmatrix} \begin{bmatrix} | \\ | \\ \chi \\ | \\ | \end{bmatrix} \longrightarrow U = \begin{bmatrix} K_c^\top A K_a & K_c^\top A K_b \\ K_d^\top A K_a & K_d^\top A K_b \end{bmatrix} \quad (2.7)$$

²For any positive semidefinite matrix, a Cholesky decomposition exists. The matrix $A(t, t')$ is positive semidefinite since $\sum_{t, t'} f(t) f(t')^* A(t, t') \geq 0$ for any test function $f(t)$, and any submatrix inherits this property.

³The inverse (when it exists) of an upper/lower triangular matrix is upper/lower triangular.

The main goal of the current paper is to obtain more analytic results about the continuum limit of the circuit construction above. We would like to consider the following limit:

$$\Delta t \rightarrow 0 \text{ and } \mathbf{z}, \mathbf{t} \rightarrow \infty, \text{ while } (\mathbf{z}\Delta t), (\mathbf{t}\Delta t) \rightarrow \text{const.} \quad (2.8)$$

Since the bulk quantum circuit is Gaussian, and it has a sharp light cone, in the continuum limit we expect it to describe a free Majorana fermion in (1+1)d which is relativistic. To determine the continuum limit theory, we can compare the quantum circuit with a massive (1+1)d Majorana QFT minimally coupled to the metric (1.1), which has the action

$$S = \frac{1}{4\pi} \int dt dz \cdot i\Psi_L \partial_t \Psi_L + i\Psi_R \partial_t \Psi_R - i\Psi_L \partial_z \Psi_L + i\Psi_R \partial_z \Psi_R + 2im\Omega(z)\Psi_L \Psi_R \quad (2.9)$$

The circuit and continuum fields are related by

$$\Psi_a(z, t) = \frac{1}{\sqrt{\Delta t}} \psi_a(\mathbf{z}, \mathbf{t}) \quad (2.10)$$

such that $\Psi_a(z, t)$ satisfies the Dirac δ -function canonical anti-commutation relation

$$\{\Psi_a(z, t), \Psi_b(z', t)\} = \delta_{ab}(2\pi)\delta(z - z') \quad (2.11)$$

Matching equations of motion in $\Delta t \rightarrow 0$ limit [17] relates the geometry to the gate angle:

$$m\Omega(z, t) = \lim_{\Delta t \rightarrow 0} \frac{\pi - 2\theta(\mathbf{z}, \mathbf{t})}{\Delta t} \quad (2.12)$$

Physically, $m\Omega(z, t)\Delta t$ determines the small probability that a right-moving fermion becomes a left-moving fermion in Δt time, which depends on the scale factor $\Omega(z, t)$ in the geometry. In the circuit language, this probability is given by the deviation of gate angle θ from $\pi/2$. $\theta = \pi/2$ corresponds to SWAP gate, which means the left-mover and right-mover completely decouple. The reflection probability amplitude is determined by $\cos \theta \simeq \frac{\pi}{2} - \theta$, and there is a factor of 2 because in $\Delta t \times \Delta t$ area in the bulk there are two gates. Eq. (2.12) is the key relation that allows us to determine the curved geometry (up to a length unit m) from the bulk fermion dynamics.

However, we would like to note that $\pi - 2\theta(\mathbf{z}, \mathbf{t})$ is not always guaranteed to be order $O(\Delta t)$ in continuous limit. We are going to discuss different examples later in the draft. For the examples in section 4 and section 5, this scaling holds strictly, ensuring $m\Omega(z, t)$ is well-defined. In section I we give explicit correlators for which θ does *not* scale as $\pi/2 - O(\Delta t)$ and hence admit no such continuum QFT limit.

While the reconstruction algorithm does not require time translation invariance, the remainder of this work focuses on the time translation invariant case, when $\theta(\mathbf{z}, \mathbf{t}) \equiv \theta(\mathbf{z}), \Omega(z, t) \equiv \Omega(z)$ only depends on z or \mathbf{z} .

2.2 Method I: via unitary matrix integral

In this section we derive (1.2) and (1.3) by taking the continuum limit of the discrete circuit. In section 2.2.1, we first obtain a determinant formula expressing the gate angle θ directly in terms of determinants of submatrices of the boundary correlator $A(\mathbf{t}, \mathbf{t}')$ (viewing \mathbf{t}, \mathbf{t}' as matrix indices), bypassing the intermediate construction of $K^{p,f}$ in (2.7). For a time-translation-

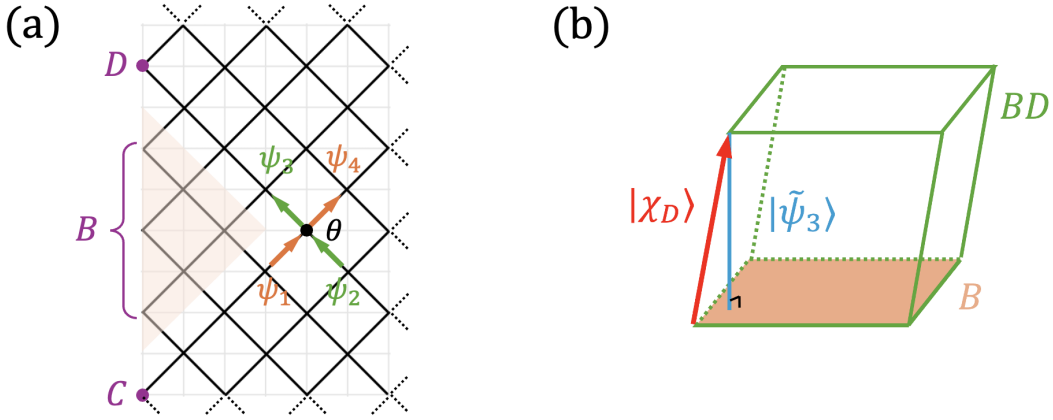


Figure 3: (a) An illustration of the determinant formula (2.18). (b) The parallelepiped used in its derivation.

invariant boundary theory, $A(\mathbf{t}, \mathbf{t}')$ and its submatrices are Toeplitz⁴. In section 2.2.2, we evaluate these determinants using tools from unitary matrix integral [23, 30, 31], in particular the Borodin–Okounkov–Geronimo–Case (BOGC) formula [21, 22].

2.2.1 A determinant formula for gate angle

It is convenient to view the collection of boundary operators at different time points $\{\chi(\mathbf{t}), \mathbf{t} \in \mathbb{Z}\}$ as spanning an infinite dimensional linear space. We will sometimes use vector notation $|\chi\rangle$. This space carries the natural inner product $\langle \chi(\mathbf{t}_1) | \chi(\mathbf{t}_2) \rangle := A(\mathbf{t}_1, \mathbf{t}_2)$ (see footnote 2). The bulk circuit fermions ψ provide another basis, chosen so that spacelike separated ψ 's are orthonormal.

For the gate angle θ in fig. 3(a), causal wedge reconstruction implies that it depends only on data in the region CBD : D and C each contain a single time point, while B contains the intervening time points. As in fig. 3(a), we denote the input fermions of the gate as $\psi_{1,2}$ and the output fermions as $\psi_{3,4}$. By definition of gate angle (2.3),

$$\sin^2 \theta = \langle \psi_3 | \psi_2 \rangle^2. \quad (2.13)$$

As explained in section 2.1, the circuit implements step-by-step orthonormalization. Let $\tilde{\psi}_{2,3}$ denote the unnormalized vectors

$$|\tilde{\psi}_2\rangle = (1 - P_{CB})|\chi_D\rangle, \quad |\tilde{\psi}_3\rangle = (1 - P_B)|\chi_D\rangle, \quad (2.14)$$

where P_{CB} projects $|\chi_D\rangle$ onto the span of $|\chi\rangle$ in region CB , and similarly for P_B . Using $(1 - P_{CB})(1 - P_B) = (1 - P_{CB})^2$, one finds $\langle \tilde{\psi}_3 | \tilde{\psi}_2 \rangle = \langle \tilde{\psi}_2 | \tilde{\psi}_2 \rangle$, and hence

$$\sin^2 \theta = \frac{\langle \tilde{\psi}_3 | \tilde{\psi}_2 \rangle^2}{\langle \tilde{\psi}_3 | \tilde{\psi}_3 \rangle \langle \tilde{\psi}_2 | \tilde{\psi}_2 \rangle} = \frac{\langle \tilde{\psi}_2 | \tilde{\psi}_2 \rangle}{\langle \tilde{\psi}_3 | \tilde{\psi}_3 \rangle}. \quad (2.15)$$

Now consider the submatrix A_{BD} of $A(\mathbf{t}, \mathbf{t}')$ with indices restricted to region BD . Then $\det(A_{BD})$ equals the squared volume of the parallelepiped spanned by the vectors $\{|\chi\rangle\}$ in BD ⁵.

⁴A Toeplitz matrix M_{ij} depends only on $i - j$.

⁵Recall the volume element in general relativity $dV = \sqrt{\det g} d^n x$, where $g_{\mu\nu}$ is the inner-product matrix of

In [fig. 3\(b\)](#), we schematically draw this parallelepiped in green. The orange shaded parallelepiped is spanned by $|\chi\rangle$ in region B and has squared volume $\det(A_B)$. Since $\langle\tilde{\psi}_3|\tilde{\psi}_3\rangle$ is the squared height of the BD -parallelepiped with respect to B -parallelepiped, it is given by the ratio of squared volumes:

$$\langle\tilde{\psi}_3|\tilde{\psi}_3\rangle = \det(A_{BD})/\det(A_B). \quad (2.16)$$

The same reasoning applies to $\langle\tilde{\psi}_2|\tilde{\psi}_2\rangle$:

$$\langle\tilde{\psi}_2|\tilde{\psi}_2\rangle = \det(A_{CBD})/\det(A_{CB}). \quad (2.17)$$

Together with [\(2.15\)](#), this yields

$$\sin^2 \theta = \frac{\det(A_{CBD}) \det(A_B)}{\det(A_{BD}) \det(A_{CB})}. \quad (2.18)$$

In [section B](#), we provide an alternative way of deriving the above determinant formula without using parallelepiped, instead using elementary properties of block matrix determinant. The benefit of the alternative method is that it directly generalizes to the case where fermions have multi-flavor, see [\(B.18\)](#).

Let $A_{[\mathbf{t}_1, \mathbf{t}_2]}$ denote the submatrix of $A(\mathbf{t}, \mathbf{t}')$ with indices $\mathbf{t}, \mathbf{t}' \in [\mathbf{t}_1, \mathbf{t}_2]$, within a time band. Then $A_{[\mathbf{t}, \mathbf{t}+(N-1)\Delta t]}$ is an $N \times N$ Toeplitz matrix independent of \mathbf{t} by time-translation invariance; we denote it by A_N and define

$$\tilde{F}_N := \log \det A_N, \quad N \geq 1. \quad (2.19)$$

The determinant formula for the N^{th} -layer gate angle θ_N becomes

$$\sin^2 \theta_N = \exp [\tilde{F}_{N+1} + \tilde{F}_{N-1} - 2\tilde{F}_N], \quad N \geq 2. \quad (2.20)$$

The first-layer angle θ_1 is special and is not captured by [\(2.20\)](#); it determines the boundary condition for the continuum fields $\Psi_{L,R}(z, t)$:

$$(\partial_t - \mu)\Psi_L = (\partial_t + \mu)\Psi_R, \quad z = 0, \quad \text{with } \mu := -\left. \frac{\partial_t A(0, t)}{A(0, 0)} \right|_{t \rightarrow 0^+} \geq 0. \quad (2.21)$$

For more detailed derivation of this boundary condition, see [section F.1](#).

In the next subsection we take the continuum limit of [\(2.20\)](#) with

$$N \rightarrow \infty, \Delta t \rightarrow 0, \quad (N\Delta t) \rightarrow T = 2z = \text{const}. \quad (2.22)$$

Here T is the width of the time band and z is the depth of the causal wedge. In this limit, the second difference in [\(2.20\)](#) becomes the second derivative appearing in [\(1.3\)](#).

2.2.2 Evaluate Toeplitz matrix determinant

In this section we evaluate \tilde{F}_N using the systematic large- N expansion of Toeplitz determinants. These techniques are standard in unitary matrix integral, since the partition function of a single

line element dx^μ .

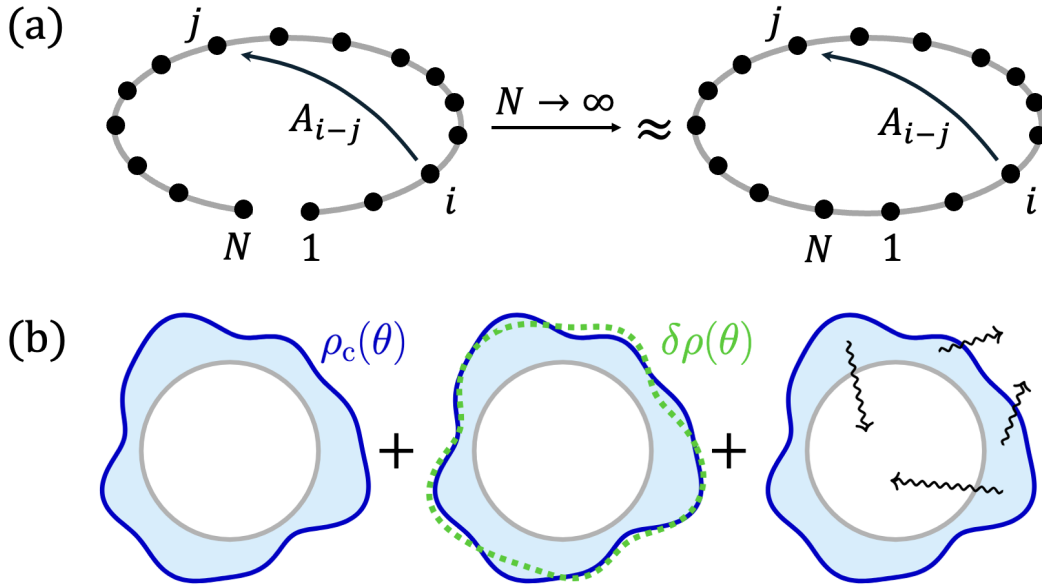


Figure 4: **(a)** Illustration of Szegő's limit theorem: a Toeplitz matrix may be viewed as a single particle hopping on a one-dimensional lattice with OBC. In the large- N limit, the leading spectrum is well approximated by the corresponding PBC lattice. **(b)** Illustration of the physical meaning of the three terms in (2.23) for the unitary matrix integral. The gray line is the unit circle on complex plane. The blue line and the shaded region represent the classical eigenvalue density $\rho_c(\theta)$. The wavy lines represent eigenvalue tunneling.

unitary matrix can be written as a Toeplitz determinant [30, 31].

To take the limit (2.22), we first consider $N \rightarrow \infty$ at fixed Δt . In this standard limit, the log determinant admits an expansion

$$\tilde{F}_N = O(N) + O(1) + O(e^{-\#N}). \quad (2.23)$$

The $O(N)$ and $O(1)$ terms are governed by Szegő's limit theorem [44]. A useful intuition is to view the Toeplitz matrix as a translation-invariant hopping Hamiltonian on a 1D chain with open boundary conditions (OBC). At large N , most of the spectrum is insensitive to boundary effects, so one may replace open by periodic boundary conditions (PBC) and diagonalize in Fourier space, with order one eigenvalue $\eta^{\text{pbc}}(k)$, where lattice momentum $k \in [-\pi, \pi]$ are within first the Brillouin zone. This gives rise to the $O(N)$ term in (2.23): $O(N) = N \int_{-\pi}^{\pi} dk \log \eta^{\text{pbc}}(k)$. See fig. 4(a) for illustration.

In our application of evaluating the gate angle, the $O(N)$ and $O(1)$ pieces don't contribute because (2.20) involves a second difference. We therefore focus on the exponentially small corrections $O(e^{-\#N})$, which encode the geometric data in the continuum limit.

A systematic description of these exponentially small subleading terms is available from the theory of unitary matrix integral:

$$\mathcal{Z}_N = \int_{U(N)} dU \exp \left[\sum_{k=1}^{+\infty} \frac{t_k^+}{k} \text{Tr}(U^k) + \frac{t_k^-}{k} \text{Tr}(U^{-k}) \right] \quad (2.24)$$

where $\{t_k^\pm\}$ are parameters. Physically, such an integral arises, for example, from the thermal

partition function of $\mathcal{N} = 4$ super Yang–Mills theory on $S^1 \times S^{D-1}$ [23]: integrating out Kaluza–Klein modes of matter fields and gauge fields leaves an effective partition function⁶ for the holonomy matrix U of gauge field around the thermal circle S^1 .

The partition function \mathcal{Z}_N can be written as a Toeplitz determinant (see appendix A of [45] for a review). Define $\varphi(\theta) := \exp[V(\theta)]$ with external potential $V(\theta) := \sum_{k=1}^{\infty} (\frac{t_k^+}{k} e^{ik\theta} + \frac{t_k^-}{k} e^{-ik\theta})$, and Fourier coefficients $\varphi(\theta) = \sum_{n \in \mathbb{Z}} \varphi_n e^{in\theta}$. The associated $N \times N$ Toeplitz matrix is $(A_N)_{ij} := \varphi_{i-j}$, and one has:

$$\mathcal{Z}_N = \det(A_N) \quad (2.25)$$

In this language, the free energy $\tilde{F}_N = \log \mathcal{Z}_N$ in (2.23) admits a standard physical interpretation term-by-term (see fig. 4(b) for illustration):

- The $O(N)$ term is the action⁷ of the saddle-point eigenvalue density $\rho_c(\theta)$ on the unit circle, determined by the competition between the external potential $V(\theta)$ and Coulomb repulsion from the Vandermonde determinant.
- The $O(1)$ term captures one-loop fluctuations $\delta\rho(\theta)$ around $\rho_c(\theta)$.
- The exponentially small corrections $O(e^{-\#N})$ (with associated asymptotic series in N^{-1}) describe eigenvalue instantons [46, 32], in which finitely many eigenvalues tunnel off the unit circle to locations on the complex planes, inside or outside the unit circle. These contributions are equivalent to the giant-graviton expansion [32].

We now recall a theorem, applied to unitary matrix integral first by Murthy [30], that resums the full set of exponentially small corrections. This is the Borodin–Okounkov–Geronimo–Case (BOGC) formula, which we will use for bulk reconstruction later:

Theorem. (Borodin–Okounkov–Geronimo–Case) [21, 22]. *Given a $N \times N$ real symmetric Toeplitz matrix A_N , with matrix element $(A_N)_{ij} := f_{|i-j|}$, $i, j = 1, \dots, N$. View $\{f_n\}$ as Fourier coefficient of $f(\theta) := \sum_{n \in \mathbb{Z}} f_n e^{in\theta}$. Assume⁸ $g(\theta) := \log f(\theta)$ exist everywhere on $\theta \in (0, 2\pi]$, with $\{g_n\}$ its Fourier coefficient given by $g(\theta) = \sum_{n \in \mathbb{Z}} g_n e^{in\theta}$. Further define $g_+(\theta) := \sum_{n=1}^{+\infty} g_n e^{in\theta}$, $g_-(\theta) := \sum_{n=-\infty}^{-1} g_n e^{in\theta}$, and $b^-(\theta) := e^{g_-(\theta) - g_+(\theta)}$, with Fourier coefficient $\{b_n^-\}$ given by $b^-(\theta) = \sum_{n \in \mathbb{Z}} b_n^- e^{in\theta}$. Now, define a Hankel matrix B_N on half infinite lattice $L^2(\mathbb{Z}_{\geq 0})$ via $(B_N)_{ij} := b_{i+j+N+1}^-$, $i, j \geq 0$. We then have:*

$$\log \det A_N = N g_0 + \left(\sum_{k=1}^{\infty} k g_k g_{-k} \right) + \log \det [\mathbf{1} - (B_N)^2] \quad (2.26)$$

In section D.2, we benchmark the BOGC formula in simple cases where $A(t, t')$ admits a finite (N_{qnm}) quasi-normal-mode expansion, see (4.1). For $N_{\text{qnm}} = 1, 2, 3$, we verify that the deter-

⁶Following such procedure [23], one would actually end up with a matrix integral with a double trace potential $\tilde{\mathcal{Z}}_N = \int_{U(N)} dU \exp \left[\sum_{k=1}^{+\infty} \frac{g_k}{k} \text{Tr}(U^k) \text{Tr}(U^{-k}) \right]$. Then, one perform a Hubbard-Stratonovich transformation [30] going from $\tilde{\mathcal{Z}}_N$ to \mathcal{Z}_N in (2.24).

⁷In most matrix models the leading free energy scales as $O(N^2)$, which corresponds to inserting an additional factor of N in the exponent of (2.24). We will not need this distinction.

⁸The assumption that $f(\theta) > 0, \forall \theta \in (0, 2\pi]$ is equivalent to condition that A_N is positive definite: $x^\top A_N x = \sum_{i,j=1}^N \int \frac{d\theta}{2\pi} e^{-i(i-j)\theta} f(\theta) x_i x_j = \int \frac{d\theta}{2\pi} f(\theta) |x(\theta)|^2 > 0$. For our purpose of bulk reconstruction, A_N is always positive definite, as discussed in footnote 2.

minant computed from the BOGC formula agrees with an elementary evaluation (via Gauss elimination), which is technically feasible in these three cases.

We now apply the BOGC formula and show that, under the scaling limit (2.22), all exponentially small terms contribute at the same order:

$$\lim_{(2.22)} \log \det[\mathbf{1} - (B_N)^2] = \log \det[\mathbf{1} - B(z)^2], \quad (2.27)$$

with $B(z)$ as in (1.2),(1.3), which we repeat it here for completeness:

$$B(z)_{ij} := \frac{\beta_j e^{-\lambda_j 2z}}{\lambda_i + \lambda_j}, \quad \text{with: } \beta_i := 2\lambda_i \times \prod_{k \neq i} \frac{\lambda_k + \lambda_i}{\lambda_k - \lambda_i} \times \prod_n \frac{J_n - \lambda_i}{J_n + \lambda_i} \quad (2.28)$$

where $\{iJ_n\}$ and $\{i\lambda_i\}$ are simple zeros and poles of $\mathcal{A}(\omega)$ in the upper half-plane.

We relegate the uninteresting technical derivation to section C. To extract the conformal factor $\Omega(z)$, note that the continuum limit of (2.20) is

$$\lim_{(2.22)} \frac{1 - \sin^2 \theta_N}{(\Delta t)^2} = -\frac{1}{4} \partial_z^2 \log \det[\mathbf{1} - B(z)^2]. \quad (2.29)$$

Combining this with (2.12) yields (1.3):

$$m^2 \Omega(z)^2 = -\partial_z^2 \log \det[\mathbf{1} - B(z)^2] \quad (2.30)$$

2.3 Method II: via inverse scattering

In this section we provide an alternative derivation of the key result (1.2) and (1.3). Instead of starting from the discrete circuit, we directly work in the continuum and derive (1.2) and (1.3) using inverse scattering. In section 2.3.1, starting from the boundary spectral function $\mathcal{A}(\omega)$, we first extract the S-matrix $\mathcal{S}(\omega)$ via causal kernel decomposition, which captures the scattering phase between modes leaving the static patch through the future horizon and modes entering the static patch from the past horizon. Given $\mathcal{S}(\omega)$, reconstructing $m\Omega(z)$ becomes a classic inverse scattering problem [33]: determine the scattering potential from its scattering amplitude. In section 2.3.2, we generalize the standard scalar field construction in [33] to the Majorana system and re-derive (1.2),(1.3).

2.3.1 Causal kernel decomposition and horizon modes

It is convenient to work in lightcone coordinates

$$u := t - z, \quad v = t + z. \quad (2.31)$$

As in the discrete setting (2.4), in the continuum a bulk fermion can be reconstructed from boundary fermions via causal kernels:

$$\Psi_R(u, v) = \int_u^v dt' K^f(z, t') \chi(t'), \quad \Psi_L(u, v) = \int_u^v dt' K^p(z, t') \chi(t') \quad (2.32)$$

As shown in [fig. 5](#), we can further define horizon ‘future’ and ‘past’ modes, which can be reconstructed directly in terms of boundary operators:

$$\begin{aligned}\Psi^f(u) &:= \lim_{v \rightarrow +\infty} \Psi_R(u, v) := \int_u^{+\infty} dt' K^f(t' - u) \chi(t') \\ \Psi^p(v) &:= \lim_{u \rightarrow -\infty} \Psi_L(u, v) := \int_{-\infty}^v dt' K^p(t' - v) \chi(t')\end{aligned}\tag{2.33}$$

The kernels $K^{p,f}$ are causal:

$$K^f(t) \equiv K^f(t)\Theta(t), \quad K^p(t) \equiv K^p(t)\Theta(-t)\tag{2.34}$$

In Fourier space⁹, this implies:

$$\mathcal{K}^f(\omega) \text{ is analytic in upper half plane.} \quad \mathcal{K}^p(\omega) \text{ is analytic in lower half plane.}\tag{2.35}$$

The horizon modes satisfy the standard anti-commutation relations of chiral fermions:

$$\{\Psi^f(u), \Psi^f(u')\} = (2\pi)\delta(u - u'), \quad \{\Psi^p(v), \Psi^p(v')\} = (2\pi)\delta(v - v')\tag{2.36}$$

In Fourier space, this requires the continuum analogue of [\(2.6\)](#):

$$\mathcal{K}^f(\omega)\mathcal{A}(\omega)\mathcal{K}^f(-\omega) = 1, \quad \mathcal{K}^p(\omega)\mathcal{A}(\omega)\mathcal{K}^p(-\omega) = 1\tag{2.37}$$

Due to reality condition, for real ω we have $\mathcal{A}(\omega) \geq 0$ and $\mathcal{K}^{p,f}(-\omega) = \mathcal{K}^{p,f}(\omega)^*$. Thus [\(2.37\)](#) fixes only the modulus of $\mathcal{K}^{p,f}(\omega)$ on the real axis. To determine the phase (and hence the analytic continuation to the complex plane), one imposes [\(2.35\)](#) and applies a Kramers–Kronig relation [\[47\]](#) to $\log \mathcal{K}^f(\omega)$ ¹⁰. Once \mathcal{K}^f is fixed, defining

$$\mathcal{K}^p(\omega) := \mathcal{K}^f(-\omega)\tag{2.38}$$

automatically satisfies the lower-half-plane analyticity of \mathcal{K}^p .

One may also ask about the analyticity of the inverse kernels $\mathcal{R}^{f,p}(\omega) := [\mathcal{K}^{f,p}(\omega)]^{-1}$. In the discrete setting, the inverses automatically inherit triangularity from finite-dimensional linear algebra. In the continuum, however, analyticity of $\mathcal{R}^{f,p}$ does not follow from [\(2.35\)](#); in particular, \mathcal{K}^f analytic in the upper half-plane does not by itself imply that \mathcal{R}^f is analytic there. \mathcal{K}^f and \mathcal{R}^f are both analytic only if \mathcal{K}^f has no zero or pole on the upper half-plane.

Given the causal kernels, one can compute the S-matrix:

$$\{\Psi^f(\omega'), \Psi^p(\omega)\} := \mathcal{S}(\omega)\delta(\omega + \omega'), \quad \mathcal{S}(\omega) = \frac{\mathcal{K}^f(-\omega)}{\mathcal{K}^f(\omega)}\tag{2.39}$$

For real ω , $\mathcal{S}(\omega)$ is a pure phase.

In [section F](#), we re-derive this causal kernel decomposition directly in the bulk QFT. We show

⁹In [section A](#), we collect our Fourier transform conventions.

¹⁰If $g(\omega)$ is analytic in the upper half-plane and $\text{Re } g(\omega)$ is known on the real axis, then $\text{Im } g(\omega)$ is fixed by the Hilbert transform $\text{Im } g(\omega) = -\frac{1}{\pi} \mathcal{P} \int_{\mathbb{R}} d\omega' \frac{\text{Re } g(\omega')}{\omega' - \omega}$, and $g(\omega)$ in the upper half-plane follows from Cauchy’s theorem. Here one takes $g(\omega) = \log \mathcal{K}^f(\omega)$.

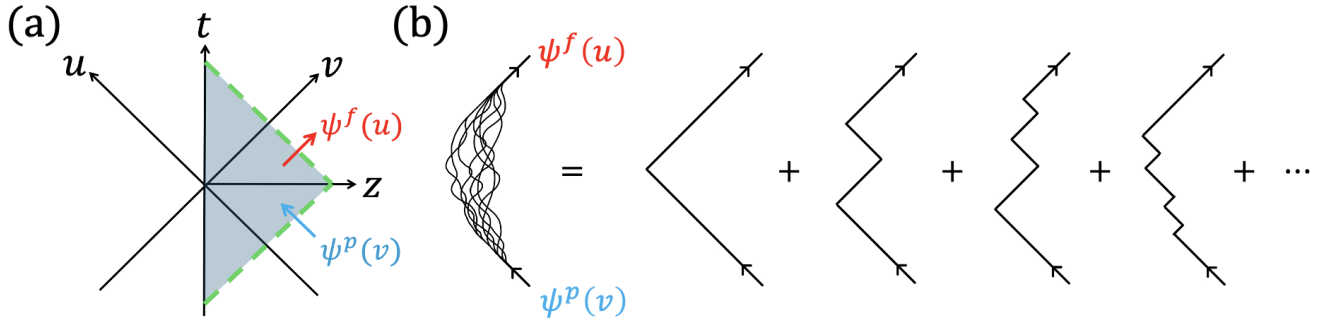


Figure 5: **(a)** Past/future horizon modes defined in (2.33). The horizon is indicated by the green dashed line. **(b)** The “forward scattering” expansion (2.48).

that if

$$\int_0^{+\infty} dz \cdot \Omega(z) < \infty \quad (2.40)$$

then, comparing with (F.22), the causal kernel $\mathcal{K}^f(\omega)$ exists and is given by the Jöst function $\mathcal{J}(\omega)$ [48, 49, 50]. In section F.3, we further show that zeros of $\mathcal{J}(\omega)$ in the upper half plane correspond to bound states. Assuming there are no such bound states for the Majorana equation (F.7), the inverse kernel $\mathcal{R}^f(\omega) := \frac{1}{\mathcal{J}(\omega)}$ is also analytic in the upper half plane.

2.3.2 Inverse scattering

From the Majorana equation (F.7), the conformal factor $m\Omega(z)$ plays the role of a scattering potential. Given scattering amplitude $\mathcal{S}(\omega)$, reconstructing $\Omega(z)$ is therefore an inverse scattering problem.

Before addressing the inverse problem, it is useful to recall the corresponding ‘forward scattering’ problem: determine $\mathcal{S}(\omega)$ from a given $\Omega(z)$. A convenient approach is the interaction picture. From the action (2.9) we read off the Hamiltonian H and decompose it into a free part H_0 describing a massless Majorana fermion (with decoupled left/right movers)¹¹ and an interaction V that couples left and right movers. Near the horizon, $\Omega(z) \rightarrow 0$ exponentially as $z \rightarrow +\infty$, so the left/right movers become asymptotically non-interacting; the horizon modes $\Psi^f(u)$ and $\Psi^p(v)$ furnish the out- and in-states of the scattering problem.

We denote by $\Psi^{(0)}(u, v)$ the interaction-picture fields evolved by H_0 . They satisfy the standard chiral fermion anti-commutation relations:

$$\{\Psi_L^{(0)}(u, v), \Psi_L^{(0)}(u', v')\} = (2\pi)\delta(v - v'), \quad \{\Psi_R^{(0)}(u, v), \Psi_R^{(0)}(u', v')\} = (2\pi)\delta(u - u') \quad (2.41)$$

In the interaction picture, the potential is time dependent: $V^{(0)}(t) := e^{iH_0(t-t_0)} V e^{-iH_0(t-t_0)}$, where t_0 is a reference time. We can now compute the scattering matrix at finite location:

$$S(u_f, v_f | u_i, v_i) := \{\Psi_R(u_f, v_f), \Psi_L(u_i, v_i)\} \quad (2.42)$$

We choose the interaction-picture reference time t_0 to coincide with the initial operator $\Psi_L(u_i, v_i)$,

¹¹Left/right scattering arises from both the mass term $m\Omega(z)$ and the boundary at $z = 0$; we include both effects in V . More precisely, H_0 describes a massless Majorana fermion on the full line $z \in (-\infty, +\infty)$.

so that $\Psi_L(u_i, v_i) = \Psi_L^{(0)}(u_i, v_i)$. We therefore only need to expand the final operator $\Psi_R(u_f, v_f)$ in a Dyson series:

$$\Psi_R(u_f, v_f) = \Psi_R^{(0)}(u_f, v_f) + \sum_{n=1}^{+\infty} i^n \int dt_1 \cdots dt_n [V^{(0)}(t_1), \cdots [V^{(0)}(t_n), \Psi_R^{(0)}(u_f, v_f)]], \quad (2.43)$$

with integration region $\frac{v_i+u_i}{2} < t_1 < \cdots < t_n < \frac{v_f+u_f}{2}$. The resulting finite-location S-matrix can be resummed into an integral equation:

$$S(u_f, v_f | u_i, v_i) / (2\pi) = m\Omega\left(\frac{v_i - u_f}{2}\right) - \int_{u_i}^{u_f} du' \int_{v_i}^{v_f} dv' m\Omega\left(\frac{v' - u'}{2}\right) m\Omega\left(\frac{v' - u_f}{2}\right) S(u', v' | u_i, v_i) \quad (2.44)$$

The asymptotic S-matrix

$$S(u, v) := S(u, +\infty | -\infty, v) \quad (2.45)$$

is obtained by taking the horizon limit of the finite-location quantity:

$$S(u, v) := \{\Psi^f(u), \Psi^p(v)\} \quad (2.46)$$

By time-translation invariance, $S(u, v)$ depends only on the radial coordinate $z = \frac{v-u}{2}$. Using (2.39), its Fourier representation is:

$$S(u, v) / (2\pi) = S(2z), \quad S(z) := \int \frac{d\omega}{2\pi} e^{i\omega z} \mathcal{S}(\omega) \quad (2.47)$$

Taking the limit of (2.44), we obtain a formal relation between the S-matrix and the conformal factor¹²:

$$S(u, v) / (2\pi) = m\Omega\left(\frac{v-u}{2}\right) + \sum_{n=1}^{+\infty} (-1)^n m^{2n+1} \int dv_1 \cdots dv_n \int du_1 \cdots du_n \prod_{k=1}^n \left[\Omega\left(\frac{v_k - u_k}{2}\right) \right] \prod_{k=1}^{n+1} \left[\Omega\left(\frac{v_{k-1} - u_k}{2}\right) \right] \quad (2.48)$$

with $v_0 := v$ and $u_{n+1} := u$, and integration region $v < v_1 < \cdots < v_n < +\infty$ and $-\infty < u_1 < \cdots < u_n < u$. Equation (2.48) is a small-mass expansion in which a timelike trajectory is resolved into a sum over zig-zag null trajectories, as in fig. 5(b).

Although (2.48) does not admit a simple recursive form like (2.44), inverse scattering methods still allow one to invert it and reconstruct $m\Omega(z)$ from $S(z)$. We defer the derivation to section G and record the result:

$$m^2 \Omega(z)^2 = -\partial_z^2 \log \det [1 - (P_z h P_z)^2] \quad (2.49)$$

$$\text{with: } h(z_1, z_2) := S(z_1 + z_2), \quad P_z(z_1, z_2) := \delta(z_1 - z_2) \Theta(z_1 - z_2) \quad (2.50)$$

Here h and P_z are operators on $L^2(\mathbb{R})$, with $P_z \equiv \mathbf{1}_{[z, +\infty)}$ the projector onto $L^2(\mathbb{R}_{\geq z})$.

To connect with the explicit expressions (1.2)–(1.3), we specialize to spectral functions ad-

¹²This formula holds for $z = \frac{v-u}{2} > 0$; for $z < 0$ the S-matrix includes the boundary scatterer at $z = 0$.

mitting a quasi-normal-mode expansion, assuming $\mathcal{A}(\omega)$ has no branch cut:

$$A(t, t') = \sum_i c_i e^{-J_i |t-t'|}, \quad \mathcal{A}(\omega) = \sum_i \frac{c_i J_i}{J_i^2 + \omega^2} \quad (2.51)$$

where $\{iJ_i\}$ are poles of $\mathcal{A}(\omega)$ in the upper half plane. If $\mathcal{A}(\omega)$ has zeros at $\{i\lambda_k\}$ on the upper half plane, we can combine these into the rational form

$$\mathcal{A}(\omega) = C \frac{\prod_k (\lambda_k^2 + \omega^2)}{\prod_i (J_i^2 + \omega^2)} \quad (2.52)$$

where C is an irrelevant positive constant.

Assuming there are no bound states in the upper half-plane, both $\mathcal{K}^f(\omega)$ and its inverse $\mathcal{R}^f(\omega)$ are analytic there. This uniquely fixes the causal factorization:

$$\mathcal{K}^f(\omega) = \sqrt{C} \frac{\prod_i (\omega + iJ_i)}{\prod_k (\omega + i\lambda_k)} \quad (2.53)$$

Then (2.39) gives the S-matrix:

$$\mathcal{S}(\omega) = \prod_k \frac{i\lambda_k + \omega}{i\lambda_k - \omega} \times \prod_i \frac{iJ_i - \omega}{iJ_i + \omega} \quad (2.54)$$

In the upper half-plane, $\mathcal{S}(\omega)$ has poles at $\{i\lambda_k\}$ with residues

$$\text{Res } \mathcal{S}(\omega \rightarrow i\lambda_k) = (-i)\beta_k \quad (2.55)$$

with β_k defined in (1.2). In real space, the S-matrix $S(z)$ defined in (2.47) can be written as a sum over poles,

$$S(z) = \sum_i \beta_i e^{-\lambda_i z}, \quad z > 0 \quad (2.56)$$

We defer the remaining technical steps to section G, where we show that (2.49) combined with (2.56) reduces to (1.2)–(1.3).

Thus the parameters $\{i\lambda_k, \beta_k\}$ in (1.2)–(1.3) are determined entirely by the pole and residue data of the S-matrix. As shown in section E, one can also write an equivalent formula for $m\Omega(z)$ directly as a contour integral of $\mathcal{S}(\omega)$, using techniques familiar from giant graviton expansion in unitary matrix integral [31], without introducing $\{i\lambda_k, \beta_k\}$ explicitly:

$$m^2 \Omega(z)^2 = -\partial_z^2 \log \left[1 + \sum_{k=1}^{+\infty} G^{(k)}(z) \right] \quad (2.57)$$

$$G^{(k)}(z) := \frac{1}{(k!)^2} \int \prod_{i=1}^k \frac{d\omega_i}{2\pi} \frac{d\tilde{\omega}_i}{2\pi} \times \frac{\prod_{1 \leq i < j \leq k} (\omega_i - \omega_j)^2 (\tilde{\omega}_i - \tilde{\omega}_j)^2}{\prod_{1 \leq i, j \leq k} (\omega_i - \tilde{\omega}_j)^2} \times \prod_{i=1}^k e^{i2z(\omega_i - \tilde{\omega}_i)} \times \prod_{i=1}^k \frac{\mathcal{S}(\omega_i)}{\mathcal{S}(\tilde{\omega}_i)} \quad (2.58)$$

where the integral contour of ω_i is along $\int_{\mathbb{R}+i0^+}$, while $\tilde{\omega}_i$ along $\int_{\mathbb{R}-i0^+}$.

Finally, although the BOGC approach in section 2.2 and the inverse scattering approach here look different, they are closely related. In fact, Geronimo and Case [22] (1979) derived what is

now called the BOGC formula using inverse scattering ideas.

3 Curvature near horizon and AdS universality

In this section we use (1.2) and (1.3) to study the near-horizon geometry. From the perspective of entanglement renormalization [51], the deep bulk region $z \rightarrow +\infty$ probes IR physics of the boundary theory, where one may expect universality to emerge, independent of microscopic details. We focus on the near-horizon curvature R_h and its dependence on the boundary correlator $A(t, t')$.

Let's order $\{i\lambda_i, i \geq 0\}$, the zeros of $A(\omega)$ in the upper half plane, in increasing order of their real part: $0 < \text{Re } \lambda_0 \leq \text{Re } \lambda_1 \leq \text{Re } \lambda_2 \leq \dots$. Then, the formula (1.3) for conformal factor $\Omega(z)$ admits a near horizon expansion where the $\log \det[\mathbf{1} - B(z)^2]$ term is expanded into $-\sum_{k=1}^{+\infty} \frac{1}{k} \text{Tr}[B(z)^{2k}]$, further organized into a sum over the exponential decays in z ¹³:

$$m^2\Omega(z)^2 = 4\beta_0^2 e^{-4\lambda_0 z} + 8\beta_0\beta_1 e^{-2(\lambda_0+\lambda_1)z} + 2\frac{\beta_0^4}{\lambda_0^2} e^{-8\lambda_0 z} + (\text{subleading}) \quad (3.1)$$

The first two terms and the third term come from $\text{Tr}[B(z)^2]$ and $\text{Tr}[B(z)^4]$ respectively.

As a starting point, we first determine the temperature T_{bh} of this blackhole geometry, which only needs the first exponentially decaying term of $\Omega(z)$, controlled by λ_0 :

$$ds^2 = \Omega^2(z)(-dt^2 + dz^2), \quad m^2\Omega(z)^2 = 4\beta_0^2 e^{-4\lambda_0 z} + (\text{subleading}) \quad (3.2)$$

This immediately gives the Hawking temperature:

$$T_{\text{bh}} = \frac{\lambda_0}{\pi} \quad (3.3)$$

At this order, the geometry is Rindler. To extract the near-horizon curvature, we may either evaluate the exact Ricci scalar of the conformal metric (1.1),

$$R(z) = -\Omega(z)^{-2} \partial_z^2 [\log \Omega(z)^2] \quad (3.4)$$

and take the limit $z \rightarrow +\infty$, or equivalently, directly read off the horizon curvature after changing to Rindler coordinates,

$$\rho := e^{-2\lambda_0 z}, \quad \tilde{t} = 2\lambda_0 t \quad (3.5)$$

for which the metric becomes

$$ds^2 = \frac{\beta_0^2}{\lambda_0^2 m^2} \left[1 + \frac{2\beta_1}{\beta_0} \rho^{\lambda_1-1} + \frac{\beta_0^2}{2\lambda_0^2} \rho^2 + (\text{subleading}) \right] (-\rho^2 d\tilde{t}^2 + d\rho^2) \quad (3.6)$$

We compare this with a maximally symmetric (1 + 1)-dimensional spacetime of constant Ricci scalar R , written in Rindler coordinates as

$$ds_0^2 = \frac{-\rho^2 d\tilde{t}^2 + d\rho^2}{(1 + \frac{R}{8}\rho^2)^2} = \left[1 - \frac{R}{4}\rho^2 + (\text{subleading}) \right] (-\rho^2 d\tilde{t}^2 + d\rho^2) \quad (3.7)$$

¹³We further assume $\lambda_0, \lambda_1, \lambda_2$ are real and nondegenerate, with $0 < \lambda_0 < \lambda_1 < \lambda_2$.

The horizon curvature is therefore fixed by the coefficient of ρ^2 . Applying this to (3.6), we must determine whether the fractional-power term ρ^{λ_1-1} is subleading compared to, comparable to, or dominant over the ρ^2 term. This leads to three cases:

- **Case I (AdS universality):** $\lambda_1 > 3\lambda_0$. The near-horizon geometry is universally AdS, with dimensionless curvature $R_h/m^2 = -2$, independent of any microscopic details of boundary model:

$$R(z)/m^2 = -2 + (\text{subleading}) \quad (3.8)$$

- **Case II (tunable curvature):** $\lambda_1 = 3\lambda_0$. The near-horizon curvature approaches a tunable constant:

$$R(z)/m^2 = -2\left(1 + \frac{4\lambda_0^2\beta_1}{\beta_0^3}\right) + (\text{subleading}) \quad (3.9)$$

The sign and magnitude of R_h are tunable through the boundary correlator. In section 4.2 we construct a simple model with $\lambda_1 = 3\lambda_0$ and tune $R_h > 0$, yielding a de Sitter near-horizon region. Thus dS behavior is less generic than AdS, occupying a codimension-one locus in parameter space. In section 5 we will find that large- q SYK at any finite temperature satisfies $\lambda_1 = 3\lambda_0$ and exhibits a nontrivial temperature dependence of R_h via (3.9). For the “purely dissipative Gaussian Lindbladian” class later discussed in section 4.3, one can show that all β_i have the same sign, so the geometry remains AdS even in Case II.

A final comment is that the condition $\lambda_1 = 3\lambda_0$ need not represent fine tuning. For a broad class of models whose Wightman function $\mathcal{G}_W(\omega)$ has no zeros in the complex frequency plane, KMS implies $\mathcal{A}(\omega) = (1 + e^{\beta\omega})\mathcal{G}_W(\omega)$ (see section A), and the relation $\lambda_1 = 3\lambda_0$ follows automatically. More generally, this “no-zero” property [50] is a consequence of the geometry that is analytic at horizon to all order, for which the zeros of $\mathcal{A}(\omega)$ sit at $\lambda_n = (2n + 1)\lambda_0, n \in \mathbb{Z}_{\geq 0}$. See section F.3.

- **Case III (non-smooth horizon):** $\lambda_1 < 3\lambda_0$. The near-horizon curvature diverges:

$$R(z)/m^2 = -2\frac{\beta_1}{\beta_0^3}(\lambda_0 - \lambda_1)^2 e^{2(3\lambda_0 - \lambda_1)z} + (\text{subleading}) \quad (3.10)$$

From (3.6) the fractional-power term ρ^{λ_1-1} dominates over ρ^2 term, leading to divergent curvature. This divergence reflects non-analyticity of the metric. From (1.3), if the metric is analytic at horizon to all order, the set $\{\lambda_n, n \geq 0\}$ should satisfy that $\lambda_0 \in \mathbb{R}_+$ and $\{\lambda_n, n \geq 1\}$ being a subset (finite or infinite) of $(\mathbb{Z}_{>0} + \frac{1}{2})(2\lambda_0)$. For a generic set of $\{i\lambda_i\}$, the metric is generically non-analytic. The Ricci scalar can only detect possible non-analyticity from λ_1 , while higher-derivative geometric quantities will be sensitive to non-analyticity induced from $\lambda_2, \lambda_3, \dots$ etc.

As a final comment, whether R_h diverges to $+\infty$ or $-\infty$ depends on the relative signs of β_0 and β_1 . For the “purely dissipative Gaussian Lindbladian” class later discussed in section 4.3, one can show that all β_i share the same sign, implying $R_h \rightarrow -\infty$ in Case III.

4 Examples: finite QNMs

In this section we study boundary correlators $A(t, t')$ with finitely many (N_{qnm}) quasi-normal modes (QNMs) [34, 35]:

$$A(t, t') = \sum_{i=1}^{N_{\text{qnm}}} c_i e^{-J_i |t-t'|} \quad (4.1)$$

In frequency space, $\mathcal{A}(\omega)$ has N_{qnm} poles in the upper half-plane, at $\{iJ_i\}_{i=1}^{N_{\text{qnm}}}$:

$$\mathcal{A}(\omega) = \sum_{i=1}^{N_{\text{qnm}}} \frac{c_i J_i}{J_i^2 + \omega^2} \quad (4.2)$$

For generic parameters c_i, J_i , $\mathcal{A}(\omega)$ has $N_{\text{qnm}} - 1$ zeros in the upper half plane, at $\{i\lambda_k\}_{k=1}^{N_{\text{qnm}}-1}$.

The simplest case is $N_{\text{qnm}} = 1$, where $A(t, t')$ is a single exponential. In section D.2, we show that the dual bulk geometry has $m\Omega(z) = 0$ for all z , which we interpret as a massless Majorana fermion on the half-line $z \geq 0$. From a standard QFT perspective one might ask how a massless bulk theory can induce exponential decay in the boundary correlator. We address this in section F.4; the effect arises from the boundary condition (2.21) at $z = 0$.

In section 4.1, we study the simplest nontrivial case $N_{\text{qnm}} = 2$ and find that the metric is always constant-curvature AdS_2 . From the bulk-QFT perspective, these correspond to ‘discrete series’ representations of the AdS_2 isometry with integer mass; see section F.5.

To obtain geometries beyond AdS , in section 4.2 we study $N_{\text{qnm}} = 3$ and exhibit a family of boundary models with $R_{\text{h}}/m^2 > 0$, realizing a de Sitter near-horizon region.

Finally, in section 4.3 we show that finite-QNM spectral functions $A(t, t')$ can be realized by Gaussian Lindbladian dynamics, in particular we give an explicit family of boundary models realizing the $N_{\text{qnm}} = 3$ de Sitter example.

4.1 Two QNMs

For $N_{\text{qnm}} = 2$, the boundary anti-commutator is

$$A(t, t') = c_1 e^{-J_1 |t-t'|} + c_2 e^{-J_2 |t-t'|} \quad (4.3)$$

Using (1.2) and (1.3), we obtain a closed-form expression for the conformal factor:

$$m\Omega(z) = \frac{2\lambda_0}{\sinh[\lambda_0(2z + z_0)]}, \quad \lambda_0 := \sqrt{\frac{J_1 J_2 (c_2 J_1 + c_1 J_2)}{c_1 J_1 + c_2 J_2}}, \quad z_0 := -\frac{1}{2\lambda_0} \log \left[\frac{(J_1 - \lambda_0)^2 (J_2 - \lambda_0)^2}{(J_1 + \lambda_0)^2 (J_2 + \lambda_0)^2} \right] \quad (4.4)$$

where $i\lambda_0$ is the unique zero of $\mathcal{A}(\omega)$ in the upper half plane. This is the AdS_2 Rindler metric, with constant negative curvature:

$$R(z)/m^2 = -2 \quad (4.5)$$

For real parameters c_1, c_2, J_1, J_2 , the boundary correlator $A(t, t')$ decays monotonically, and the dual geometry naturally contains a horizon. A notable feature is that (4.4) also holds for complex parameters. Requiring $A(t, t')$ to remain real forces c_1, c_2 and J_1, J_2 to come in complex-

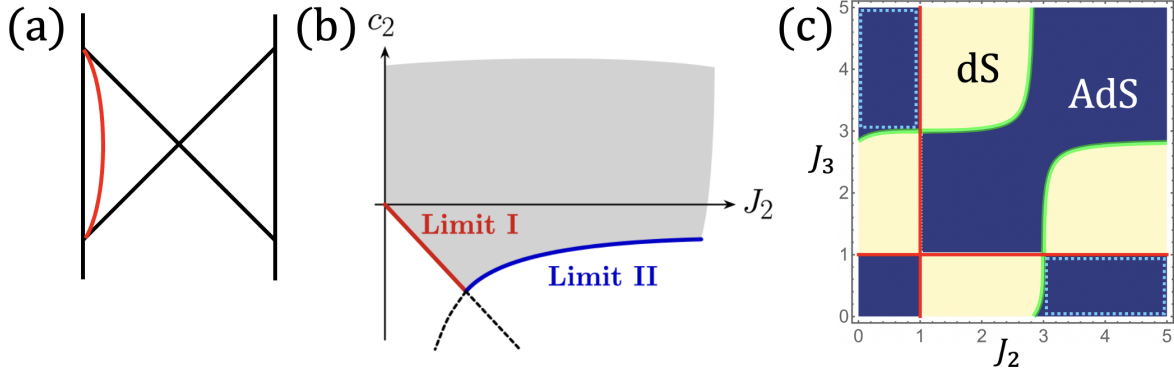


Figure 6: (a) For generic parameters, the boundary sits at finite radial location rather than at the asymptotic AdS_2 boundary. (b) Parameter-space “phase diagram” of the $N_{\text{qnm}} = 2$ model; the shaded region is physically allowed and its boundaries are discussed in the text. (c) Phase diagram of the $N_{\text{qnm}} = 3$ model of section 4.2 at $J_1 = 2$, showing the sign of R_h (4.12) (AdS in blue, dS in yellow). The green line marks $R_h = 0$ and the red line marks $R_h = \infty$. The region inside the dotted blue box has $c_i \geq 0$ and corresponds to purely dissipative Gaussian Lindbladian models.

conjugate pairs; then $A(t, t')$ is an exponentially decaying envelope modulated by oscillations¹⁴. Such modulated decay also yields a horizon.

Another key feature is that for all physical¹⁵ choices of parameters, one finds $z_0 \geq 0$. Thus the boundary at $z = 0$ does not lie at the asymptotic AdS_2 boundary (fig. 6(a)). Intuitively, a generic $A(t, t')$ does not exhibit conformal symmetry; conformal boundary models are special (e.g. SYK at low temperature [38, 39, 40] or conformal quantum mechanics [52, 53]). For generic parameters the construction naturally realizes finite-cutoff holography [10, 36, 37].

A natural question is when the boundary approaches the asymptotic AdS_2 boundary. For simplicity, we address this in the case of real c_1, c_2, J_1, J_2 .

For real parameters, decay requires $J_1, J_2 \geq 0$. Without loss of generality we set $J_1 = c_1 = 1$ to fix the time scale and normalize the Majorana operator. The remaining parameters c_2 and J_2 are constrained by positivity (footnote 15), which requires $\mathcal{A}(\omega) \geq 0$ for all real ω . This implies $c_2 \geq -J_2$ and $c_2 \geq -J_2^{-1}$; see fig. 6(b). We now study the two boundary limits of the allowed region:

- **Limit I, zero temperature blackhole.** We set $c_2 = -J_2 + J_2^{-1}\varepsilon^2$ with $0 < J_2 < 1$. Expand in $0 < \varepsilon \ll 1$, we find:

$$\lambda_0 = \frac{\varepsilon}{\sqrt{1 - J_2^2}} + O(\varepsilon^3), \quad z_0 = 2(1 + J_2^{-1}) + O(\varepsilon^2), \quad m\Omega(z) = \frac{1}{z + (1 + J_2^{-1})} \quad (4.6)$$

Since $\lambda_0 \rightarrow 0$ in this limit, (3.3) implies that the black hole temperature approaches zero. The metric approaches the Poincaré patch of AdS_2 , while the boundary ($z = 0$) remains at finite radial location.

¹⁴Let $c_1 = ce^{i\theta}, c_2 = ce^{-i\theta}, J_1 = J + i\nu, J_2 = J - i\nu$, with $c, \theta, J, \nu \in \mathbb{R}$. Then $A(t, t') = ce^{-J|t-t'|} \cos(\nu|t-t'| + \theta)$.

¹⁵Positivity of the Hilbert space requires $A(t, t')$, viewed as a matrix in (t, t') , to be positive semidefinite. This constrains its eigenvalues $A(\omega)$ to be nonnegative.

- **Limit II, asymptotic boundary.** We set $c_2 = -J_2^{-1} + J_2^{-1}\varepsilon^2$ with $J_2 > 1$. Expand in $0 < \varepsilon \ll 1$, we find:

$$\lambda_0 = \sqrt{J_2^2 - 1}\varepsilon^{-1} + O(\varepsilon), \quad z_0 = \frac{2}{J_2 - 1}\varepsilon^2 + O(\varepsilon^4) \quad (4.7)$$

Since λ_0 diverges, it is useful to rescale $z := \varepsilon\tilde{z}$ and $t := \varepsilon\tilde{t}$, keeping $\tilde{z}, \tilde{t} = O(1)$ as $\varepsilon \rightarrow 0^+$. Physically, because $\lambda_0 \rightarrow \infty$, the temperature measured in the original t coordinate diverges by (3.3); a finite limit requires zooming into time scales of order the inverse temperature. The rescaled coordinates probe the UV of the original variables, and the geometry approaches:

$$ds^2 = \tilde{\Omega}(\tilde{z})^2(-d\tilde{t}^2 + d\tilde{z}^2), \quad m\tilde{\Omega}(\tilde{z}) = \frac{2\sqrt{J_2^2 - 1}}{\sinh\left(2\sqrt{J_2^2 - 1}\tilde{z}\right)} \quad (4.8)$$

In these coordinates, the boundary at $\tilde{z} = 0$ lies at the asymptotic AdS₂ boundary.

Since the geometry is constant-curvature AdS₂, one might ask why the bulk QFT does not exhibit the usual infinite tower of QNMs of AdS₂ Rindler [35]. The reason is that the two-QNM model corresponds to a special mass. Using (4.5) to set units by the AdS length ℓ_{AdS} , one finds $m = 1$, i.e. an integer mass. Integer masses furnish discrete series representations of $\text{SL}(2, \mathbb{R})$ ¹⁶. Technically, the mode functions are hypergeometric functions for generic non-integer m ; at integer m the hypergeometric functions truncate to polynomials, leaving only finitely many poles. Equivalently, as one tunes m to an integer, most poles and zeros of $\mathcal{A}(\omega)$ collide and cancel, leaving finitely many uncanceled. More detailed discussion will be reserved to section F.5.

4.2 Three QNMs and a concrete de Sitter model

The goal of this section is to find an explicit $N_{\text{qnm}} = 3$ model whose near-horizon region is de Sitter, since we have seen that $N_{\text{qnm}} = 1, 2$ cannot realize $R_{\text{h}} > 0$.

The $N_{\text{qnm}} = 3$ ansatz has six boundary parameters $c_{1\sim 3}, J_{1\sim 3}$. In the upper half plane, $\mathcal{A}(\omega)$ has three poles $\{iJ_i\}_{i=1}^3$ and two zeros $\{i\lambda_0, i\lambda_1\}$. As discussed in section 3, avoiding AdS universality requires tuning $\lambda_1 = 3\lambda_0$. We therefore begin by extracting λ_0, λ_1 from the zeros of $\mathcal{A}(\omega)$:

$$\mathcal{A}(\omega) = \sum_{i=1}^3 \frac{c_i J_i}{J_i^2 + \omega^2} \equiv \frac{P(\omega)}{\prod_{i=1}^3 (J_i^2 + \omega^2)}, \quad P(\omega) := a_1 \omega^4 + a_2 \omega^2 + a_3 \quad (4.9)$$

$$\text{with: } a_1 := \left(\sum_{i=1}^3 c_i J_i\right), \quad a_2 := a_1 \left(\sum_{i=1}^3 J_i^2\right) - \left(\sum_{i=1}^3 c_i J_i^3\right), \quad a_3 := \left(\prod_{i=1}^3 J_i^2\right) \left(\sum_{i=1}^3 c_i J_i^{-1}\right) \quad (4.10)$$

The zeros of $P(\omega)$ give $\lambda_0^2 = \frac{a_2 - \sqrt{a_2^2 - 4a_1 a_3}}{2a_1}$ and $\lambda_1^2 = \frac{a_2 + \sqrt{a_2^2 - 4a_1 a_3}}{2a_1}$. Imposing $\lambda_1 = 3\lambda_0$ (with $\lambda_0 > 0$) yields $a_2 = 10a_1\lambda_0^2$ and $a_3 = 9a_1\lambda_0^4$. Without loss of generality we set $\lambda_0 = 1$ (fixing the time unit) and $a_1 = 1$ (fixing the Majorana operator normalization), so $a_2 = 10$ and $a_3 = 9$. We

¹⁶Strictly speaking, our finite cutoff at $z = 0$ breaks $\text{SL}(2, \mathbb{R})$ to time translations, so the single-particle Hilbert space is not organized into full $\text{SL}(2, \mathbb{R})$ irreps. Here “discrete series” refers to the corresponding theory on the full AdS₂ Rindler background.

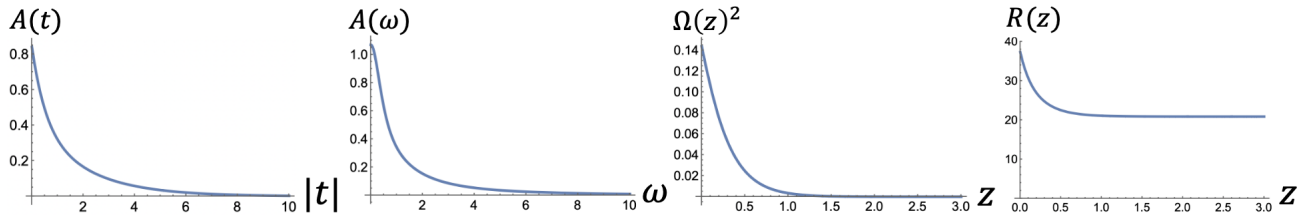


Figure 7: $A(t, t')$, $\mathcal{A}(\omega)$, $\Omega(z)^2$, and $R(z)$ for a representative $N_{\text{qnm}} = 3$ model with a de Sitter near-horizon region (parameters in (4.2)).

then take (J_1, J_2, J_3) as free dimensionless parameters, with c_i determined by (4.10):

$$c_i = \frac{(J_i^2 - 1)(J_i^2 - 9)}{J_i} \prod_{j=1, j \neq i}^3 \frac{1}{J_i^2 - J_j^2} \quad (4.11)$$

From (3.9), we obtain the curvature near horizon:

$$R_{\text{h}}/m^2 = -\frac{1}{2} \left[1 - \frac{3}{4} p(J_1)p(J_2)p(J_3) \right], \quad p(x) := \frac{(x-3)(x+1)^3}{(x+3)(x-1)^3} \quad (4.12)$$

We now identify parameters with $R_{\text{h}} > 0$. For simplicity we take $J_i \in \mathbb{R}_{>0}$. In fig. 6(c), we fix $J_1 = 2$ and plot the sign of R_{h} in the (J_2, J_3) plane: AdS (blue) and dS (yellow). The green curve marks $R_{\text{h}} = 0$, while the red curve marks a divergence of R_{h} . As a check, the region with $c_i \geq 0$ (inside the dashed light-blue box) corresponds to purely dissipative Gaussian Lindbladian models and is always AdS, as discussed in section 4.3.

Away from the horizon the full z -dependence is not particularly illuminating, but for completeness we record the explicit expression from (1.3):

$$m^2 \Omega(z)^2 = -\partial_z^2 \log \left[1 - \frac{\beta_0^2}{4} e^{-4z} - \frac{\beta_0 \beta_1}{8} e^{-8z} - \frac{\beta_1^2}{36} e^{-12z} + \frac{\beta_0^2 \beta_1^2}{2304} e^{-16z} \right] \quad (4.13)$$

with $\beta_0 = 4 \prod_{i=1}^3 \frac{J_i-1}{J_i+1}$ and $\beta_1 = -12 \prod_{i=1}^3 \frac{J_i-3}{J_i+3}$ from (1.2).

In fig. 7, we plot $A(t, t')$, $\mathcal{A}(\omega)$, $\Omega(z)^2$, $R(z)$ for a concrete de Sitter model near horizon, with parameters $J_1 = 2, J_2 = 2.9, J_3 = 0.5$. In the next section we construct an explicit boundary model that realizes this boundary two-point function.

4.3 A Gaussian Lindbladian boundary model

To provide some more physical motivation for the finite QNM model studied in this section, now we construct a simple Gaussian Lindbladian model that realizes a GFF whose two-point function decomposes into finitely many QNMs, as in (4.1).

Let's start with N_{qnm} Majorana fermions (with $2^{N_{\text{qnm}}/2}$ dimensional Hilbert space) with canon-

ical commutation $\{\chi_i, \chi_j\} = 2\delta_{ij}$. The operator dynamics is governed by Lindbladian equation¹⁷:

$$\frac{dO}{dt} = i[H, O] + \sum_a (-2L_a^\dagger O L_a - \{L_a^\dagger L_a, O\}) \quad (4.14)$$

with:

$$H = \frac{1}{4} \sum_{i,j} \chi_i h_{ij} \chi_j, \quad L_a = \frac{1}{2} \sum_i M_{ai} \chi_i \quad (4.15)$$

where h_{ij} is a purely imaginary anti-symmetric matrix, and M_{ai} is unconstrained. Choosing H quadratic in χ and L_a linear in χ keeps the dynamics Gaussian, so correlators satisfy Wick's theorem and the boundary fermion furnishes a GFF.

The finite-time evolution implied by (4.14) is

$$\chi_i(t) = \sum_{j=1}^{N_{\text{qnm}}} [e^{-\mathcal{L}t}]_{ij} \chi_j(0), \quad t > 0, \quad \text{with } \mathcal{L} := ih + \text{Re } M^\dagger M \quad (4.16)$$

Let's use a particular fermion component $\chi_1(t)$ to do bulk reconstruction. Thus the anti-commutator correlator is

$$A(t, t') := \frac{1}{2} 2^{-N/2} \text{Tr}(\{\chi_1(t), \chi_1(t')\}) = [e^{-\mathcal{L}|t-t'|}]_{11} = \sum_{i=1}^{N_{\text{qnm}}} V_{1i} (V^{-1})_{i1} e^{-J_i |t-t'|} \quad (4.17)$$

where we assume \mathcal{L} is diagonalizable and write $\mathcal{L} := V D V^{-1}$, with $D = \text{diag}(\{J_i\}_{i=1}^{N_{\text{qnm}}})$ and V invertible. This matches (4.1), with $c_i := V_{1i} (V^{-1})_{i1}$ (no sum).

A special case is $H = 0$, i.e. pure dissipation, which we call a ‘‘purely dissipative Gaussian Lindbladian model’’. Then $\mathcal{L} = \text{Re } M^\dagger M$ is real symmetric and positive semidefinite¹⁸, so its eigenvalues satisfy $J_i \geq 0$ and its eigenvectors form a real orthogonal matrix V , implying $c_i = V_{1i}^2 \geq 0$. We can then ask what $c_i \geq 0$ and $J_i \geq 0$ imply for the bulk geometry. From (4.2), one can show¹⁹ that the $N_{\text{qnm}} - 1$ zeros $\{i\lambda_k\}$ interlace with the poles: ordering J_i increasingly, one has $J_k < \lambda_k < J_{k+1}$. This ordering implies (via (1.2)) that all β_i have the same sign. Then the near-horizon curvature is negative in all three cases of section 3. Interestingly, purely dissipative Gaussian Lindbladians are always AdS near the horizon and cannot realize de Sitter near-horizon curvature.

Next, we proceed to construct an explicit Gaussian Lindbladian model that realizes the $N_{\text{qnm}} = 3$ de Sitter example of section 4.2 by finding a concrete matrix \mathcal{L} . Our procedure is randomized for two reasons: (i) for fixed $\{c_i, J_i\}$ there are generically many admissible \mathcal{L} , and it suffices to find one example; (ii) the physical constraint $\mathcal{L} + \mathcal{L}^\top = 2 \text{Re } M^\dagger M \succeq 0$ is nontrivial, so a simple generate-and-check strategy is effective. The algorithm is:

¹⁷We are interested in the case where O and L_a are fermionic. In this case, unlike usual Lindbladian equation where at least one of O, L_a is bosonic, the sign in front of $L_a^\dagger O L_a$ is minus, see [54].

¹⁸Write $M^\dagger M = \text{Re } M^\dagger M + i \text{Im } M^\dagger M$, with $\text{Im } M^\dagger M$ real antisymmetric. Then for all $x \in \mathbb{R}^N$, $x^\top (\text{Re } M^\dagger M) x = x^\top (M^\dagger M) x \geq 0$.

¹⁹We view $A(i\lambda) = \sum_{i=1}^{N_{\text{qnm}}} \frac{c_i J_i}{J_i^2 - \lambda^2}$ as a function of λ^2 , it will have $N_{\text{qnm}} - 1$ zeros in general. Since $A(\omega)$ is a real function on the imaginary axes, and notice that $A(i\lambda) \rightarrow -\infty$ as $\lambda^2 \rightarrow J_k^2 + 0^+$ and $A(i\lambda) \rightarrow +\infty$ as $\lambda^2 \rightarrow J_{k+1}^2 - 0^+$, so there must be at least one zero in the interval between J_k and J_{k+1} . Since the number of interval already equals the number of zeros, so there could be one and only one zero in each interval.

Pseudo-code. Given a set of $\{c_i, J_i\}_{i=1}^{N_{\text{qnm}}}$ (for simplicity we focus on real c_i and positive J_i), the code back-engineers a physical N_{qnm} dimensional matrix \mathcal{L} satisfying: (1), the spectrum of \mathcal{L} is $\{J_i\}$; (2) its decomposition $\mathcal{L} = VD V^{-1}$ satisfy $V_{1i}(V^{-1})_{i1} = c_i$; (3) its symmetric part $\mathcal{L} + \mathcal{L}^\top$ is positive semi-definite. It contains the following five steps.

- Input list of $\{J_i\}$ and $\{c_i\}$. Normalize $\{c_i\}$ such that $\sum_i c_i = 1$.
- Generate N_{qnm} non-zero random real numbers x_i and assemble into a column vector x , used as $V_{1i} := x_i$.
- Define a $N_{\text{qnm}} \times 1$ column vector $y_i = \frac{c_i}{V_{1i}}$. Define $N_{\text{qnm}} \times N_{\text{qnm}}$ projector $P = I - \frac{|y\rangle\langle y|}{\langle y|y\rangle}$.
- Generate an $(N_{\text{qnm}} - 1) \times N_{\text{qnm}}$ random real rectangular matrix Q . Then let $V := \begin{bmatrix} x^\top \\ QP \end{bmatrix}$, and let $\mathcal{L} := V \text{diag}(\{J_i\})V^{-1}$.
- Check if $\mathcal{L} + \mathcal{L}^\top$ is positive semi-definite. If yes, code ends and output \mathcal{L} ; if not, go back to the second step.

Running this algorithm on the concrete $N_{\text{qnm}} = 3$ de Sitter example of [section 4.2](#), with parameters (4.2) and coefficients $c_1 = 0.453515$, $c_2 = -0.0418932$, $c_3 = 0.428922$ (from (4.11)), we find one realization of \mathcal{L} :

$$\mathcal{L} = \begin{bmatrix} 1.18971 & -0.530428 & -0.984871 \\ -1.11738 & 1.31535 & -1.55849 \\ 0.143654 & -0.0742184 & 2.89494 \end{bmatrix} \quad (4.18)$$

Repeating the run yields many realizations.

5 Examples: large- q SYK

In this section we apply the above formalism to the bulk geometry of the large- q Sachdev–Ye–Kitaev (SYK) model [38, 39, 40, 41]. At zero temperature, SYK is dual to JT gravity on AdS_2 Rindler wedge [55, 56, 57, 58]. The dual geometry of the finite temperature SYK model has been discussed²⁰ but remains an open question. Here we use the reconstruction developed above to study the bulk geometry. Interestingly, we found that the near-horizon curvature has an unexpected temperature dependence.

5.1 General setup

We begin by recalling the basic aspects of SYK relevant for our purposes, following [40]. The model is $(0 + 1)\text{d}$ quantum mechanics of N Majorana fermions with $\{\chi_i, \chi_j\} = \delta_{ij}$, interacting via a q -local random Hamiltonian:

$$H_{\text{syk}} = i^{q/2} \sum_{i_1 < \dots < i_q} J_{i_1 \dots i_q} \chi_{i_1} \cdots \chi_{i_q}, \quad \overline{J_{i_1 \dots i_q}^2} = \frac{2^{q-1} \mathcal{J}^2 (q-1)!}{q N^{q-1}} \quad (5.1)$$

We set $\mathcal{J} \equiv 1$ to fix the energy scale.

In the large- N limit, connected correlators vanish and the fermions obey Wick’s theorem, so χ_i furnishes a GFF. In addition, if we take the large- q limit with $q \rightarrow \infty, q^2/N \rightarrow 0$, the

²⁰In the double scaled limit of SYK [59, 60], the model is conjectured [8, 61, 62, 63, 9, 64] to dual to de Sitter spacetime at finite or infinite temperature.

anti-commutator two-point function takes an analytic form [40]:

$$A(t, t') \equiv \frac{1}{N} \sum_{i=1}^N \langle \{\chi_i(t), \chi_i(t')\} \rangle = \text{Re} \left[\left(\frac{\cos \theta}{\cosh(i\theta + (t-t') \cos \theta)} \right)^{2\Delta} \right], \quad \beta_{\text{syk}} = \frac{2\theta}{\cos \theta}, \quad \Delta = \frac{1}{q} \quad (5.2)$$

Here $\theta \in (0, \pi/2)$ parametrizes the inverse temperature β_{syk} : $\theta = 0$ corresponds to infinite temperature and $\theta = \pi/2$ to zero temperature.

Unlike the finite-QNM examples of section 4, the SYK two-point function has infinitely many QNMs:

$$A(t, t') = \sum_{n=0}^{+\infty} c_n e^{-J_n |t-t'|} \quad (5.3)$$

$$\text{with: } c_n = (\cos \theta)^{-2\Delta} (-1)^n \frac{2^{2\Delta} \Gamma(2\Delta + n)}{n! \Gamma(2\Delta)} \cos[2\theta(\Delta + n)] \quad (5.4)$$

$$\text{and: } J_n = 2 \cos \theta (n + \Delta) = 2\pi T_{\text{fake}} (n + \Delta) \quad (5.5)$$

where T_{fake} is the ‘‘fake disk’’ temperature [40, 42], which controls the submaximal chaos exponent $\lambda_{\text{Lyapunov}} = 2\pi T_{\text{fake}}$ at finite temperature.

To extract the near-horizon data as in section 3, we work in Fourier space and determine the zeros of the spectral function:

$$\mathcal{A}(\omega) = \frac{(\cos \theta)^{-2\Delta-1} 2^{2\Delta-2}}{\Gamma(2\Delta)} \Gamma\left(\Delta + \frac{i\omega}{2 \cos \theta}\right) \Gamma\left(\Delta - \frac{i\omega}{2 \cos \theta}\right) \cosh\left(\frac{\theta\omega}{\cos \theta}\right) \quad (5.6)$$

The zeros of $\mathcal{A}(\omega)$ arise from the cosh factor and lie at $\{\pm i\lambda_k\}_{k \geq 0}$:

$$\lambda_k = \frac{\pi \cos \theta}{\theta} \left(k + \frac{1}{2}\right) = 2\pi T_{\text{syk}} \left(k + \frac{1}{2}\right), \quad k \geq 0 \quad (5.7)$$

Comparing (5.5) and (5.7), we see that the poles $\{iJ_n\}$ and zeros $\{i\lambda_k\}$ form equally spaced lattices on the imaginary axis, with spacings set by the fake and physical temperatures, respectively. Collisions between poles and zeros can therefore occur when the two spacings are incommensurate.

Next we perform the causal kernel decomposition of section 2.3.1. Using the Gamma function reflection formula, $\mathcal{A}(\omega)$ can be rewritten as:

$$\mathcal{A}(\omega) = A_0 \frac{\Gamma\left(\Delta + \frac{i\omega}{2 \cos \theta}\right) \Gamma\left(\Delta - \frac{i\omega}{2 \cos \theta}\right)}{\Gamma\left(\frac{1}{2} + \frac{i\theta\omega}{\pi \cos \theta}\right) \Gamma\left(\frac{1}{2} - \frac{i\theta\omega}{\pi \cos \theta}\right)}, \quad A_0 := \frac{\pi (\cos \theta)^{-2\Delta-1} 2^{2\Delta-2}}{\Gamma(2\Delta)} \quad (5.8)$$

From (2.37), the modulus of the future kernel on the real axis is

$$|\mathcal{K}^f(\omega)| = \sqrt{A_0} \left| \frac{\Gamma\left(\frac{1}{2} - \frac{i\theta\omega}{\pi \cos \theta}\right)}{\Gamma\left(\Delta - \frac{i\omega}{2 \cos \theta}\right)} \right| \quad (5.9)$$

Since the causal factorization requires both $\mathcal{K}^f(\omega)$ and $\mathcal{R}^f(\omega) = 1/\mathcal{K}^f(\omega)$ to be analytic in the

upper half plane, one might naively guess

$$\mathcal{K}_{\text{naive}}^f(\omega) = \sqrt{A_0} \frac{\Gamma(\frac{1}{2} - \frac{i\theta\omega}{\pi \cos \theta})}{\Gamma(\Delta - \frac{i\omega}{2 \cos \theta})} \quad (5.10)$$

which has no poles or zeros in the upper half-plane. However, this naive choice fails because the corresponding real-time kernel (or its inverse) is not causal: $K^f(t)$ and $R^f(t)$ do not vanish for $t < 0$. The obstruction is that at any nonzero temperature $\mathcal{K}_{\text{naive}}^f(\omega)$ grows factorially at large complex ω ²¹ so the Fourier contour cannot be closed in the upper half-plane, even though there are no poles. For example, at infinite temperature one finds

$$R_{\text{naive}}^f(t) = \int \frac{d\omega}{2\pi} e^{-i\omega t} \frac{1}{\sqrt{\pi A_0}} \Gamma(\Delta - \frac{i\omega}{2}) = \frac{2}{\sqrt{\pi A_0}} e^{-2\Delta t - e^{-2t}} \quad (5.11)$$

Thus $R_{\text{naive}}^f(t)$ is nonzero for $t < 0$, though doubly exponentially suppressed.

In fact, one can show that a strictly causal $R^f(t)$ does not exist at any finite temperature. The reason is that for large real ω one has exponential decay:

$$\log |\mathcal{R}^f(\omega)| = -\frac{|\omega|}{4} \left(\frac{1}{T_{\text{fake}}} - \frac{1}{T_{\text{syk}}} \right) - \left(\frac{1}{2} - \Delta \right) \log |\omega| + O(1) \quad (5.12)$$

It follows that $R^f(t)$ is analytic in the strip $|\text{Im } t| < \frac{1}{4} \left(\frac{1}{T_{\text{fake}}} - \frac{1}{T_{\text{syk}}} \right)$. By analyticity, if $R^f(t)$ vanished on an open interval $t < 0$, it would vanish identically in the strip. Physically, $R^f(t)$ is “too analytic” to support a sharp causal discontinuity at $t = 0$.

We expect the UV-sensitive behavior discussed above not to affect the near-horizon physics, which corresponds to IR physics on the boundary. We therefore evaluate the near-horizon geometry by introducing a UV regulator. To this end, define a regulated Gamma function by truncating the infinite lattice of poles of $\Gamma(z)$ to the first $(\Lambda + 1)$ poles:

$$\Gamma_{\Lambda}(z) := (\Lambda^z \Lambda!) P_{\Lambda}(z), \quad P_{\Lambda}(z) := \frac{1}{z(z+1)(z+2)\cdots(z+\Lambda)} \quad (5.13)$$

where Λ is a large positive integer. Note that

$$\lim_{\Lambda \rightarrow +\infty} \Gamma_{\Lambda}(z) = \Gamma(z) \quad (5.14)$$

The regulated spectral function is

$$\mathcal{A}_{\Lambda}(\omega) := A_0 \frac{\Gamma_{\Lambda}(\Delta + \frac{i\omega}{2 \cos \theta}) \Gamma_{\Lambda}(\Delta - \frac{i\omega}{2 \cos \theta})}{\Gamma_{\Lambda}(\frac{1}{2} + \frac{i\theta\omega}{\pi \cos \theta}) \Gamma_{\Lambda}(\frac{1}{2} - \frac{i\theta\omega}{\pi \cos \theta})} = (A_0 \Lambda^{2\Delta-1}) \frac{P_{\Lambda}(\Delta + \frac{i\omega}{2 \cos \theta}) P_{\Lambda}(\Delta - \frac{i\omega}{2 \cos \theta})}{P_{\Lambda}(\frac{1}{2} + \frac{i\theta\omega}{\pi \cos \theta}) P_{\Lambda}(\frac{1}{2} - \frac{i\theta\omega}{\pi \cos \theta})} \quad (5.15)$$

²¹Using Stirling’s formula, for (5.10) one finds at large ω that $\log \mathcal{K}_{\text{naive}}^f(\omega) = (1 - \eta)(i\nu) \log(i\nu) + (i\nu)(\eta - 1 - \eta \log \eta) + (\frac{1}{2} - \Delta) \log(i\nu) + O(1)$, with $\nu := \frac{\omega}{2\pi T_{\text{syk}}}$ and $\eta := \frac{T_{\text{syk}}}{T_{\text{fake}}} \geq 1$. At $T_{\text{syk}} = 0$ (so $\eta = 1$), the $O(\omega \log \omega)$ and $O(\omega)$ terms vanish and $\mathcal{K}_{\text{naive}}^f(\omega) \sim \omega^{\frac{1}{2} - \Delta}$.

Since $\mathcal{A}_\Lambda(\omega)$ is a finite product of the form (2.52), the corresponding kernel is well defined:

$$\mathcal{K}_\Lambda^f(\omega) := \sqrt{A_0 \Lambda^{2\Delta-1}} \frac{P_\Lambda(\frac{1}{2} - \frac{i\omega}{\pi \cos \theta})}{P_\Lambda(\Delta - \frac{i\omega}{2 \cos \theta})}, \quad \mathcal{R}_\Lambda^f(\omega) := 1/\mathcal{K}_\Lambda^f(\omega) \quad (5.16)$$

With this choice, the time-domain kernels $\mathcal{K}_\Lambda^f(t)$ and $\mathcal{R}_\Lambda^f(t)$ are causal. Using (2.39), the S-matrix is

$$\mathcal{S}_\Lambda(\omega) = \frac{P_\Lambda(\frac{1}{2} + \frac{i\omega}{\pi \cos \theta})}{P_\Lambda(\frac{1}{2} - \frac{i\omega}{\pi \cos \theta})} \frac{P_\Lambda(\Delta - \frac{i\omega}{2 \cos \theta})}{P_\Lambda(\Delta + \frac{i\omega}{2 \cos \theta})} = \Lambda^{\frac{i\omega}{\pi}(\frac{1}{T_{\text{syk}}} - \frac{1}{T_{\text{fake}}})} \widehat{\mathcal{S}}_\Lambda(\omega) \quad (5.17)$$

$$\text{with: } \widehat{\mathcal{S}}_\Lambda(\omega) := \frac{\Gamma_\Lambda(\frac{1}{2} + \frac{i\omega}{\pi \cos \theta})}{\Gamma_\Lambda(\frac{1}{2} - \frac{i\omega}{\pi \cos \theta})} \frac{\Gamma_\Lambda(\Delta - \frac{i\omega}{2 \cos \theta})}{\Gamma_\Lambda(\Delta + \frac{i\omega}{2 \cos \theta})} \quad (5.18)$$

where in the last step we rewrote $P_\Lambda(z)$ in terms of $\Gamma_\Lambda(z)$. Thus, up to the phase factor $\Lambda^{\frac{i\omega}{\pi}(\frac{1}{T_{\text{syk}}} - \frac{1}{T_{\text{fake}}})}$, the remaining factor $\widehat{\mathcal{S}}_\Lambda(\omega)$ has a finite limit as $\Lambda \rightarrow +\infty$.

We now extract the near-horizon geometry. Determining the geometry further requires the residues $\{\beta_{\Lambda,k}\}_{k \geq 0}$ defined in (2.55):

$$\beta_{\Lambda,k} = e^{-2(\alpha_0 \log \Lambda)\lambda_k} \widehat{\beta}_{\Lambda,k}, \quad \alpha_0 := \frac{1}{2\pi} \left(\frac{1}{T_{\text{syk}}} - \frac{1}{T_{\text{fake}}} \right) \quad (5.19)$$

$$\text{with: } \lim_{\Lambda \rightarrow +\infty} \widehat{\beta}_{\Lambda,k} := \beta_k = (2\pi T_{\text{syk}}) \frac{(-1)^k \Gamma[\Delta + \frac{\pi}{2\theta}(k + \frac{1}{2})]}{(k!)^2 \Gamma[\Delta - \frac{\pi}{2\theta}(k + \frac{1}{2})]} \quad (5.20)$$

For large but finite Λ , this is well behaved. A potential concern is that $\beta_{\Lambda,k}$ has no nonzero limit as $\Lambda \rightarrow +\infty$: while $\widehat{\beta}_{\Lambda,k}$ converges, the prefactor $e^{-2(\alpha_0 \log \Lambda)\lambda_k}$ drives all $\beta_{\Lambda,k} \rightarrow 0$.

As we now show, this does not affect near-horizon geometric quantities (e.g. the Ricci scalar), since they depend only on ratios of $\beta_{\Lambda,k}$. From (3.3) and (5.7), the black-hole temperature is independent of Λ :

$$T_{\text{bh}} = T_{\text{syk}} \quad (5.21)$$

To obtain the horizon curvature, note from section 3 that large- q SYK falls into Case II with $\lambda_1 = 3\lambda_0$. The near-horizon curvature is then given by (3.9), which we repeat for convenience:

$$R_{\text{h},\Lambda}/m^2 = -2\left(1 + \frac{4\lambda_0^2 \beta_{\Lambda,1}}{\beta_{\Lambda,0}^3}\right) = -2\left(1 + \frac{4\lambda_0^2 \widehat{\beta}_{\Lambda,1}}{\widehat{\beta}_{\Lambda,0}^3}\right) \quad (5.22)$$

In the last step, we used that in the combination $\beta_{\Lambda,1}/\beta_{\Lambda,0}^3$ the “un-wanted” exponential factors $e^{-2(\alpha_0 \log \Lambda)\lambda_k}$ cancel precisely because of $\lambda_1 = 3\lambda_0$. We therefore obtain a finite limit for horizon curvature,

$$R_{\text{h}}/m^2 = \lim_{\Lambda \rightarrow +\infty} R_{\text{h},\Lambda}/m^2 = -2\left(1 + \frac{4\lambda_0^2 \beta_1}{\beta_0^3}\right) \quad (5.23)$$

One may also ask whether the geometry at finite proper distance from the horizon admits a finite limit as $\Lambda \rightarrow +\infty$. It does. In (1.3), the residues $\beta_{\Lambda,k}$ always appear multiplied by $e^{-2\lambda_k z}$, so the extra factor $e^{-2(\alpha_0 \log \Lambda)\lambda_k}$ can be absorbed into a coordinate shift, $\tilde{z} := z + \alpha_0 \log \Lambda$. Working with the renormalized coordinate \tilde{z} , only $\widehat{\beta}_{\Lambda,k}$ appears in (1.3), and it has a finite limit given by (5.20). This yields a well-defined limit of geometry, $ds^2 = \Omega(\tilde{z})^2(-dt^2 + d\tilde{z}^2)$.

We now discuss the zero and finite temperature cases.

5.2 Zero temperature limit

In the zero temperature limit, we don't need Λ -regularization and the causality of $K^{p,f}(t), R^{p,f}(t)$ works just fine. The relevant coefficients to extract geometry behave as

$$\beta_0 = -(2\pi T_{\text{syk}})\left(\frac{1}{2} - \Delta\right) + O(T_{\text{syk}}^2), \quad \beta_1 = -(2\pi T_{\text{syk}})\left(\frac{1}{2} + \Delta\right)\left(\frac{1}{2} - \Delta\right)\left(\frac{3}{2} - \Delta\right) + O(T_{\text{syk}}^2) \quad (5.24)$$

Since $\lambda_0, \beta_0,$ and β_1 are all $O(T_{\text{syk}})$, (5.22) implies that R_h remains $O(1)$ as $T_{\text{syk}} \rightarrow 0$:

$$R_h/m^2 = -\frac{2}{\left(\frac{1}{2} - \Delta\right)^2}, \quad \text{when } T_{\text{syk}} = 0 \quad (5.25)$$

Writing the curvature as $R_h = -2\ell_{\text{AdS}}^{-2}$, the fermion mass is $m = \left(\frac{1}{2} - \Delta\right)\ell_{\text{AdS}}^{-1}$, matching the standard AdS_2 relation between mass and scaling dimension for a Majorana field.

One can in fact reconstruct the full geometry, not just the near-horizon expansion. Using (1.2) and (1.3), one finds²² that the conformal factor is:

$$m\Omega(z) = \frac{\frac{1}{2} - \Delta}{\sinh\left[(2\pi T_{\text{syk}})z\right]} \quad (5.26)$$

This reproduces AdS_2 Rindler, with the boundary $z = 0$ at the asymptotic boundary.

5.3 Finite temperature geometry

We first record the explicit horizon-curvature formula obtained from (5.22) and (5.20):

$$R_h/m^2 = (-2) \left[1 - \pi^2 \frac{\sin\left(\pi\left(\Delta - \frac{3}{2}\eta\right)\right)}{\sin^3\left(\pi\left(\Delta - \frac{1}{2}\eta\right)\right)} \frac{\Gamma\left(\Delta + \frac{3}{2}\eta\right)\Gamma\left(1 - \Delta + \frac{3}{2}\eta\right)}{\Gamma\left(\Delta + \frac{1}{2}\eta\right)^3\Gamma\left(1 - \Delta + \frac{1}{2}\eta\right)^3} \right], \quad \eta := \frac{T_{\text{syk}}}{T_{\text{fake}}} \quad (5.27)$$

We have used the reflection formula to ensure that the arguments of the Gamma functions are positive. Therefore, possible divergences of R_h arise from the sine factor in the denominator, i.e. from $\beta_0 = 0$. This corresponds to a collision between the first pole $i\lambda_0$ and one of the zeros $\{iJ_n\}$ due to the incommensurability of the physical and fake temperature lattices. Explicitly, the divergences occur at:

$$\frac{T_{\text{syk}}}{T_{\text{fake}}} = 2\Delta + 2n \implies T_{\text{syk}} = \frac{2}{\pi}(n + \Delta) \cos\left(\frac{\pi/4}{n + \Delta}\right) \quad n = 0, 1, 2, 3, \dots \quad (5.28)$$

At high temperature, T_{fake} approaches the constant π^{-1} , so the curvature diverges almost peri-

²²One first notice that in zero temperature, β_k can be expressed in terms of elementary functions as $\beta_k = (2\pi T_{\text{syk}}) \frac{(-1)^k}{(k!)^2} \prod_{j=0}^{2k} \left(\Delta - k - \frac{1}{2} + j\right)$. Also, notice that since λ_k are integer spaced, then from (1.3), Ω^2 can be written as Taylor series of $\varepsilon := e^{-(2\pi T_{\text{syk}})2z}$, since no fractional power. Of course, the $B(z)$ matrix in (1.3) is infinite dimensional, so we used Mathematica to obtain its first twenty Taylor coefficients, and find that it satisfy $\frac{1}{4}m^2\Omega(z)^2 = \left(\frac{1}{2} - \Delta\right)^2(\varepsilon + 2\varepsilon^2 + 3\varepsilon^3 + 4\varepsilon^4 + 5\varepsilon^5 + 6\varepsilon^6 + \dots)$. Therefore, though we cannot prove it, it is convincing to believe that the full answer is $\frac{1}{4}m^2\Omega(z)^2 = \left(\frac{1}{2} - \Delta\right)^2 \sum_{n=1}^{+\infty} n\varepsilon^n$, which leads to (5.26).

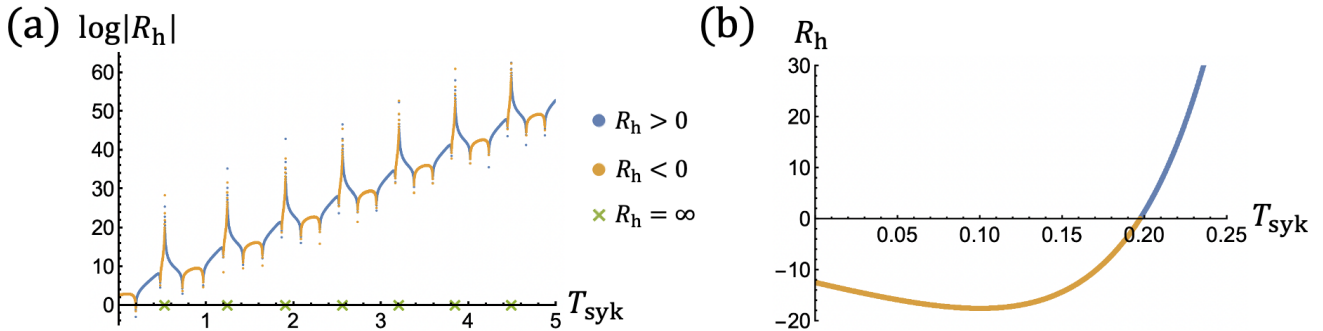


Figure 8: **(a)** The horizon curvature from (5.27) as a function of temperature for large- q ($\Delta = 1/10$) SYK. Colors indicate the sign of R_h . **(b)** Zoom into low temperature regime of (a).

odically at $T_{\text{syk}} \approx \frac{2}{\pi}(\Delta + n)$. The infinite-temperature limit [65] of the reconstructed geometry is therefore not manifestly well-defined in our set up. Using Stirling’s approximation, the ratio of Gamma functions grows as $\sim e^{(3 \log 3) \frac{T_{\text{syk}}}{T_{\text{fake}}}} \sim e^{(3\pi \log 3) T_{\text{syk}}}$, so $|R_h|$ grows exponentially with temperature. As shown in fig. 8, the sign of R_h alternates, so AdS and dS near-horizon behavior appear almost periodically as T_{syk} increases. At low but nonzero temperature, the near-horizon region remains AdS.

6 Algebra near the horizon

Recent progress in AdS/CFT has emphasized that the appropriate notion of a “subregion” in QFT/gravity is an operator algebra rather than a tensor factor, with modular theory providing the intrinsic dynamics [66, 67, 68, 69]. In particular, the large- N algebra program [70, 71, 72] and related crossed-product/observer viewpoints [73, 74, 75, 7, 76, 77, 78, 79] clarify how semiclassical N^{-1} effects can promote a strictly type-III structure to a type-I or type-II setting, in which generalized entropy and reconstruction admit a precise algebraic formulation. These developments are largely structural: the relevant generators are typically specified abstractly (via their automorphism action or universal properties) rather than constructed explicitly from boundary operators.

Here we take a step towards a constructive realization by giving boundary expressions for an approximate algebra, generated by two null translations and a boost, which becomes exact when acting on the modes at the bifurcate horizon.

In a maximally symmetric $(1+1)$ d spacetime, there are three generators: null translations P^\pm and a boost B . They obey $[B, P^\pm] = \pm i P^\pm$ and $[P^-, P^+] \propto -i R B$, with the algebra closing to $\mathfrak{sl}(2, \mathbb{R})$, $\mathfrak{so}(1, 2)$, or the Poincaré algebra depending on the sign of the Ricci scalar R .

In a general $(1+1)$ d spacetime with metric (1.1), only B is an exact isometry. Nevertheless, one can define “null translations” P^\pm in a natural way so that $[B, P^\pm] = \pm i P^\pm$ holds exactly. While $[P^-, P^+]$ is not proportional to $-i R B$ when R varies, we will show that $[P^-, P^+] \propto -i R_h B$ still holds when acting on fields at the bifurcate horizon, where R_h is the local horizon curvature; see (6.13).

We first introduce Kruskal coordinates near the horizon. Using the leading near-horizon

behavior $e^{-4\lambda_0 z}$ in (3.1), we define (U, V) by:

$$ds^2 = \frac{4\beta_0^2}{m^2} \tilde{\Omega}^2 \times e^{-4\lambda_0 z} (-dt^2 + dz^2) = \frac{\beta_0^2 \tilde{\Omega}^2}{m^2 \lambda_0^2} (-dU dV) \quad (6.1)$$

$$\text{with: } U := e^{2\lambda_0 u} \geq 0, \quad V := -e^{-2\lambda_0 v} \leq 0, \quad \text{and } \tilde{\Omega}^2 := m^2 \Omega^2 e^{4\lambda_0 z} / (4\beta_0^2) \quad (6.2)$$

Next we define P^\pm and B on the past/future horizons. Using the horizon modes in (2.33), define the rescaled fields $\Upsilon^p(V)$ and $\Upsilon^f(U)$ on the horizons:

$$\Upsilon^f(U) := \frac{1}{\sqrt{2\lambda_0 U}} \Psi^f(u), \quad \Upsilon^p(V) := \frac{1}{\sqrt{-2\lambda_0 V}} \Psi^p(v) \quad (6.3)$$

The rescale factor is chosen so that the canonical anti-commutators are preserved under coordinate change from (u, v) to (U, V) :

$$\{\Upsilon^f(U), \Upsilon^f(U')\} = (2\pi)\delta(U - U'), \quad \{\Upsilon^p(V), \Upsilon^p(V')\} = (2\pi)\delta(V - V') \quad (6.4)$$

The mixed anti-commutator between Υ^f and Υ^p is controlled by the S-matrix:

$$\tilde{S}(U, V) := \{\Upsilon^f(U), \Upsilon^p(V)\} = \frac{1}{2\lambda_0 \sqrt{-UV}} S(u, v) \quad (6.5)$$

Equivalently, the future mode can be expanded in the past modes as:

$$\Upsilon^f(U) = \frac{1}{2\pi} \int dV \tilde{S}(U, V) \Upsilon^p(V) \quad (6.6)$$

With these preparations, we define P^+ (null translation along V), P^- (null translation along U), and the boost B on the horizons:

$$\begin{aligned} P^+ &:= \frac{i}{4\pi} \int dV \Upsilon^p(V) \partial_V \Upsilon^p(V) \\ P^- &:= \frac{i}{4\pi} \int dU \Upsilon^f(U) \partial_U \Upsilon^f(U) \\ B &:= -\frac{i}{4\pi} \int dV \Upsilon^p(V) V \partial_V \Upsilon^p(V) \equiv \frac{i}{4\pi} \int dU \Upsilon^f(U) U \partial_U \Upsilon^f(U) \end{aligned} \quad (6.7)$$

The equivalence of the two expressions for B follows from unitarity of the S-matrix:

$$\int dU \tilde{S}(U, V_1) \tilde{S}(U, V_2) = (2\pi)^2 \delta(V_1 - V_2) \quad (6.8)$$

By construction, these generators act on the horizon fields as translations and boosts:

$$[iP^+, \Upsilon^p(V)] = \partial_V \Upsilon^p(V), \quad [iP^-, \Upsilon^f(U)] = \partial_U \Upsilon^f(U) \quad (6.9)$$

$$[iB, \Upsilon^p(V)] = \left(-\frac{1}{2} - V \partial_V\right) \Upsilon^p(V), \quad [iB, \Upsilon^f(U)] = \left(\frac{1}{2} + U \partial_U\right) \Upsilon^f(U) \quad (6.10)$$

The factor $\frac{1}{2}$ reflects the fermion scaling dimension. Their action on $\Psi_{L/R}(u, v)$ away from the

horizon follows from the equations of motion.

In [section H.1](#), we will benchmark that the definition in [\(6.7\)](#) matches the exact $\mathfrak{sl}(2, \mathbb{R})$ generator of AdS₂-Rindler wedge with massive Majorana fermion, whose boundary is at asymptotic boundary with usual normalizable boundary condition.

We now examine the commutators. From [\(6.7\)](#), one checks directly that

$$[B, P^\pm] = \pm i P^\pm \tag{6.11}$$

The remaining commutator $[P^-, P^+]$ is:

$$[P^-, P^+] = \frac{1}{16\pi^3} \int dV_1 dV_2 \Upsilon^p(V_1) \Upsilon^p(V_2) \left[\int dU \cdot \tilde{S}(U, V_1) \partial_U \partial_{V_2} \tilde{S}(U, V_2) - (V_1 \leftrightarrow V_2) \right] \tag{6.12}$$

Even on the past horizon, $[P^-, P^+]$ maps a local operator $\Upsilon^p(V)$ to a nonlocal one, so it is not generally a geometric flow. In special cases—notably AdS₂-Rindler ([section H.2.3](#))—the kernel becomes local and $[P^-, P^+]$ is exactly proportional to B .

Nevertheless, in [section H](#) we show that the action of $[P^-, P^+]$ on the bifurcate-horizon modes $\mathcal{O} \in \{\Upsilon^f(0), \Upsilon^p(0)\}$ is local and related to the boost generator as expected:

$$[[P^-, P^+], \mathcal{O}] = -i \frac{\beta_0^2}{(2\lambda_0)^2} (R_h/m^2) \times [B, \mathcal{O}] \tag{6.13}$$

This provides an algebraic interpretation of the near-horizon curvature studied in [section 3](#). It also suggests an emergent IR symmetry for any boundary system.

We should comment that, even away from the bifurcate horizon, the Majorana fermion dynamics along the horizon is universal if the boundary is in a thermal state [\[17\]](#). In this work, we focused on bulk reconstruction from the fermion anti-commutator two-point function $\mathcal{A}(\omega)$, which is sufficient to determine the bulk geometry. To identify which quantum state in the QFT Hilbert space the bulk fermions occupy, one needs additional input, namely the fermion commutator two-point function $\mathcal{G}_C(\omega)$; see [section A](#). Assuming the Kubo–Martin–Schwinger (KMS) condition holds, $\mathcal{G}_C(\omega)$ is related to $\mathcal{A}(\omega)$ in a universal way; see [\(A.4\)](#). Therefore, the bulk quantum state is the two-sided thermofield-double state. The commutator of the horizon modes satisfies universal CFT₂ behaviour [\[17\]](#).

7 Discussion

In this paper, building on [\[17\]](#), we obtained an explicit analytic formula for the semiclassical bulk geometry dual to an arbitrary boundary Majorana generalized free field. We derived the formula in two complementary ways: via unitary matrix integral techniques and via inverse scattering. We then used it to study the near-horizon curvature as a probe of IR universality of boundary theory. For generic boundary data, the near-horizon region is AdS. For correlators with finitely many QNMs, the $N_{\text{qnm}} = 2$ case yields AdS₂ Rindler, while $N_{\text{qnm}} = 3$ admits families with de Sitter near-horizon curvature realizable by Lindbladian boundary dynamics. We also applied the construction to large- q SYK, recovering AdS₂ Rindler at zero temperature and finding an unusual, nearly periodic pattern of sign changes and divergences in the near-horizon curvature at finite temperature, driven by the incommensurability between the physical and “fake” temperatures. Finally, we constructed boundary expressions for an approximate algebra

generated by null translations and a boost, which becomes exact acting on bifurcate-horizon modes.

We conclude with a list of open questions and directions:

- *Scalar field.* Here we focused on Majorana fields. It would be natural to study scalar fields as an even simpler testbed. Ref. [17] discussed that there is a scalar analogue of the bulk quantum circuit, where each $\text{SO}(2)$ gate is replaced by a symplectic matrix, describing the discrete evolution of a scalar GFF.
- *Higher dimensions.* Our analysis focused on the duality between $(1+1)\text{d}$ bulk and $(0+1)\text{d}$ boundary. A higher-dimensional extension should be straightforward under (say) spherical symmetry of the transverse geometry, where reconstruction can be performed in each angular-momentum sector and reduced to an effective two-dimensional problem. Scalar fields would again be a natural starting point, since fermions acquire additional components in higher dimensions.
- *Euclidean version.* Our approach reconstructs a Lorentzian bulk geometry from real-time boundary data. It would be interesting to start instead from the Euclidean two-point function on the thermal circle and reconstruct a Euclidean disk geometry with $\text{U}(1)$ -symmetric metric $ds^2 = d\rho^2 + G(\rho)^2 d\theta^2$. A preliminary step was performed in [80, 81]. A technical obstacle to this approach is the absence of a direct Euclidean analogue of the Nebabu–Qi circuit, since Euclidean signature lacks causal structure. One possible route is to work directly in the continuum and formulate the corresponding inverse scattering problem.
- *Relation to large-mass expansions*²³. Our relation between the S-matrix $\mathcal{S}(\omega)$ and the conformal factor $\Omega(z)$ is organized as a small-mass expansion (e.g. (2.48)). In the opposite large-mass limit, boundary correlators are often approximated by a worldline action dominated by a (possibly complex) geodesic anchored at the boundary, so geometric data can in principle be inferred from the dependence of geodesic length on boundary endpoints [80, 81]. This viewpoint is closely related to differential entropy and kinematic space [82, 83, 84]. It would be interesting to connect these approaches.
- *A more microscopic de Sitter model.* We found de Sitter near-horizon curvature in a class of dissipative Gaussian Lindbladian boundary models. An unsatisfactory aspect is that the effective Lindbladian dynamics is non-unitary, describing an open subsystem coupled to a Markovian bath (if one include the bath, the infinitely large whole system is still unitary though). It would be preferable to find a fully microscopic unitary model whose large- N limit yields positive near-horizon curvature.
- *Entanglement entropy.* We used only boundary anti-commutators to reconstruct the bulk geometry, but did not determine the bulk quantum state. The bulk quantum state is determined by the commutator of fermion $\chi(t)$ on the boundary [17]. It would be interesting to compute bulk entanglement entropy in this framework.
- *Relation to Krylov space.* Krylov space and Krylov complexity [85, 86], which encode two-point-function data, provide a useful diagnostic of chaos and scrambling. Recent work by Dodelson [87, 88] proposes a putative asymptotic “bulk geometry” dual to Krylov space

²³We thank Henry Lin for asking this question.

as an intermediate structure for computing QNMs and complex-time analyticity. It would be interesting to relate that proposal to our reconstructed bulk geometry. In the main text, the continuum limit (2.8) keeps both space and time continuous while preserving a 45° lightcone, yielding a relativistic theory. By contrast, Krylov space is obtained by a nonrelativistic limit of the Nebabu–Qi circuit, in which time becomes continuous while space remains discrete:

$$\Delta t \rightarrow 0 \text{ and } \mathfrak{t} \rightarrow \infty, \text{ while } (\mathfrak{t}\Delta t) \rightarrow t \in \mathbb{R}, \text{ and } \mathbf{z} := n \in \mathbb{Z}_+ \text{ fixed.} \quad (7.1)$$

The discrete spatial coordinate \mathbf{z} is identified with the Krylov lattice index n . One then finds that the gate angle $\theta(\mathbf{z})$ is related to the Krylov coefficient b_n by:

$$\lim_{\Delta t \rightarrow 0 \text{ as (7.1)}} \frac{\theta(\mathbf{z} = n)}{\Delta t} = b_n \quad (7.2)$$

We will report these results and further details on the dual geometry of Krylov space in future work.

- *Fluctuations of geometry.* Our reconstruction assumes a boundary GFF, i.e. a strict large- N limit. It would be interesting to include perturbative N^{-1} corrections. Since connected four-point functions can be viewed as fluctuations of two-point data, and two-point data maps to geometry, one expects the connected four-point function to determine the bulk metric fluctuations.
- *More on algebras.* Our discussion of bulk algebras focused on the bifurcate horizon. Recent developments in von Neumann algebra methods suggest many further structures to explore, including subregion algebras [69, 68, 89], algebras of local Lorentz symmetry in the bulk, and half-sided modular inclusions.
- *Puzzles at finite-temperature large- q SYK.* In section 5, the reconstructed horizon curvature exhibits an unusual temperature dependence. What is its physical interpretation? Our derivation used a subtle Λ -regularization to enforce causality of the inverse kernel; one might instead advocate using the naive (noncausal) inverse kernel, suggesting that the minimal ansatz of a local Majorana field coupled to a metric is insufficient. The correct bulk description might be nonlocal or receive “stringy” corrections [90] or higher derivative corrections, as expected for submaximal chaos [90, 42]. One hint is that at finite temperature the S-matrix $\mathcal{S}(\omega)$ grows factorially at high energy for complex ω , which is unusual for particle scattering. It is also possible that the correct dual theory does not have a sharp lightcone.
- *Physical origin of AdS universality.* In section 3, we found that AdS behavior is generic near the horizon over a large region of boundary parameter space. Is this tied to an IR universality class of the boundary theory? We do not yet have a satisfactory answer.
- *Distinguishing chaos from dissipation.* Finite-QNM correlators are naturally realized by dissipative boundary dynamics (section 4), while SYK provides a unitary example (section 5). Both can reconstruct bulk geometries with horizons. The horizon indicates information loss in the space of simple operators, but does not by itself distinguish dissipation

(operators leak into a bath) from chaos (operators scramble into complex ones). Is there a bulk criterion that differentiates the two mechanisms?

- *Horizonless geometries.* Although all examples in this paper have horizons, the construction does not require them. The scattering problem remains well defined as long as $\Omega(z) \rightarrow 0$ as $z \rightarrow +\infty$; horizons correspond to exponential decay. What boundary properties lead to horizonless geometries?
- *A new scaling limit of unitary matrix integrals.* In [section 2.2](#), we identified a scaling limit in which all subleading eigenvalue-instanton contributions enter at the same order due to the additional parameter Δt , with $N \rightarrow \infty$, $\Delta t \rightarrow 0$, and $N\Delta t \rightarrow z = \text{const}$. Effectively, the discrete large parameter N is traded for a continuous parameter $z > 0$. It would be interesting to study this limit directly from the matrix model perspective.
- *“Measuring” the bulk geometry from boundary experiments.* We provided an explicit formula showing that the dual bulk geometry is determined by boundary two-point functions. Since two-point functions are among the simplest observables accessible experimentally (compared to, e.g., entanglement entropies or out-of-time-ordered correlators [[91](#), [92](#), [93](#)], which may require multiple copies or post-selection), it would be interesting to propose concrete experimental protocols and estimate the precision required in measuring the two-point function to reliably reconstruct the bulk geometry.

Acknowledgements

We thank Shoaib Akhtar, Yiming Chen, Matthew Dodelson, Anatoly Dymarsky, Dan Eniceicu, Jonah Kudler-Flam, Nima Lashkari, Albert Law, Hong Liu, Hideo Mabuchi, Juan Maldacena, Steve Shenker, Douglas Stanford, Xinyu Sun, and Zimo Sun for helpful discussions. We thank the LITP lunch for feedback. HT especially thanks Yiming Chen for valuable comments and encouragement during the long development of this work, Matthew Dodelson for pointing out relevant literature, and Dan Eniceicu for illuminating discussions on unitary matrix integral. Part of this work was completed while XLQ and HT were visiting the Institute for Advanced Study, and we thank IAS for hospitality. This work is supported by the Shoucheng Zhang Graduate Fellowship Program (HT), the Simons Foundation (TN, XLQ), the Eric and Wendy Schmidt AI in Science (TN), and Knight-Hennessy Scholars (HW).

A Convention for the Fourier transformation

Here we collect our Fourier transform conventions for the boundary fermion $\chi(t)$; the bulk horizon modes $\Psi^f(u), \Psi^p(v)$; the bulk-to-boundary kernels $K^{p,f}(t)$ and their inverses $R^{p,f}(t)$; the spectral

function $A(t, t')$; and the S-matrix $S(z)$:

$$\begin{aligned}
\chi(t) &:= \int d\omega e^{i\omega t} \chi(\omega) \\
\Psi^f(u) &:= \int d\omega e^{i\omega u} \Psi^f(\omega), \quad \Psi^p(v) := \int d\omega e^{i\omega v} \Psi^p(\omega) \\
K^p(t) &:= \int \frac{d\omega}{2\pi} e^{-i\omega t} \mathcal{K}^p(\omega), \quad K^f(t) := \int \frac{d\omega}{2\pi} e^{-i\omega t} \mathcal{K}^f(\omega) \\
R^p(t) &:= \int \frac{d\omega}{2\pi} e^{-i\omega t} \mathcal{R}^p(\omega), \quad R^f(t) := \int \frac{d\omega}{2\pi} e^{-i\omega t} \mathcal{R}^f(\omega) \\
A(t, t') &:= \int d\omega e^{i\omega(t-t')} \mathcal{A}(\omega) \\
S(z) &= \int \frac{d\omega}{2\pi} e^{i\omega z} \mathcal{S}(\omega)
\end{aligned} \tag{A.1}$$

We also record the relations among the Wightman function $G_W(t)$, the two-sided correlator $G_{12}(t)$, the spectral function $G_A(t)$, and the commutator $G_C(t)$:

$$\begin{aligned}
G_W(t) &= \text{Tr}[e^{-\beta H} O(t) O(0)] \\
G_{12}(t) &= \text{Tr}[e^{-\frac{\beta H}{2}} O(t) e^{-\frac{\beta H}{2}} O(0)] \\
G_A(t) &= \text{Tr}[e^{-\beta H} \{O(t), O(0)\}] \\
G_C(t) &= \text{Tr}(e^{-\beta H} [O(t), O(0)])
\end{aligned} \tag{A.2}$$

The KMS condition is $G_W(t - i\beta) = G_W(-t)$. We use the same Fourier-transform convention for all four: $G_{\dots}(t) = \int d\omega e^{i\omega t} \mathcal{G}_{\dots}(\omega)$. Their Fourier-space relations are:

$$\mathcal{G}_A(\omega) = (1 + e^{\beta\omega}) \mathcal{G}_W(\omega), \quad \mathcal{G}_C(\omega) = (1 - e^{\beta\omega}) \mathcal{G}_W(\omega), \quad \mathcal{G}_{12}(\omega) = e^{\frac{\beta\omega}{2}} \mathcal{G}_W(\omega) \tag{A.3}$$

In particular, these KMS relation imply that the commutator two-point function is related to anti-commutator two-point function in a universal way:

$$\mathcal{G}_C(\omega) = -\tanh\left(\frac{\beta\omega}{2}\right) \mathcal{G}_A(\omega) \tag{A.4}$$

B Determinant formula for multi-flavor fermions

In this appendix, we generalize the determinant formula (2.18) to the case in which the fermions $\chi_\alpha(t)$ carry an additional flavor index $\alpha \in \{1, \dots, N_f\}$.

The anticommutator two-point function is

$$A(\alpha, t, \alpha', t') = \langle \{\chi_\alpha(t), \chi_{\alpha'}(t')\} \rangle \tag{B.1}$$

with the normalization $A(\alpha, t, \alpha', t) = \delta_{\alpha\alpha'}$. We follow the vector notation of section 2.2.1 and use the same setup as in fig. 3(a), additionally assuming that there are N_B time points in region B . We use $|\chi_D\rangle$ and $|\chi_C\rangle$ to represent the N_f fermions in regions D and C (each corresponding to a single time point but containing N_f flavors), and similarly $|\chi_B\rangle$ to represent the $N_B N_f$ fermions

in region B .

Following [section 2.2.1](#), we use A_B to denote the $N_B N_f \times N_B N_f$ submatrix of $A(\alpha, \mathbf{t}, \alpha', \mathbf{t}')$ whose indices lie in region B ; similarly, A_D and A_C are $N_f \times N_f$ matrices, A_{DB} and A_{BC} are $(N_f + N_B N_f) \times (N_f + N_B N_f)$ matrices, and A_{DBC} is a $(2N_f + N_B N_f) \times (2N_f + N_B N_f)$ matrix. For convenience, we parametrize these matrices in terms of four intermediate matrices $W_{1\sim 4}$:

$$A_{DBC} = \begin{bmatrix} \mathbf{1} & W_2^\top & W_4 \\ W_2 & W_1 & W_3 \\ W_4^\top & W_3^\top & \mathbf{1} \end{bmatrix}, \quad A_{DB} = \begin{bmatrix} \mathbf{1} & W_2^\top \\ W_2 & W_1 \end{bmatrix}, \quad A_{BC} = \begin{bmatrix} W_1 & W_3 \\ W_3^\top & \mathbf{1} \end{bmatrix}, \quad A_B = W_1 \quad (\text{B.2})$$

In [fig. 3](#), the circuit implements a step-by-step orthonormalization: $|\psi_3\rangle$ is the component of $|\chi_D\rangle$ orthonormal to $|\chi_B\rangle$, while $|\psi_1\rangle$ is the component of $|\chi_C\rangle$ orthonormal to $|\chi_B\rangle$. We denote by $|\tilde{\psi}_3\rangle$ and $|\tilde{\psi}_1\rangle$ the corresponding unnormalized vectors,

$$|\tilde{\psi}_3\rangle = |\chi_D\rangle - W_2^\top W_1^{-1} |\chi_B\rangle, \quad |\tilde{\psi}_1\rangle = |\chi_C\rangle - W_3^\top W_1^{-1} |\chi_B\rangle \quad (\text{B.3})$$

which are fixed by the orthogonality conditions $\langle \tilde{\psi}_3 | \chi_B \rangle = 0$ and $\langle \tilde{\psi}_1 | \chi_B \rangle = 0$. The inner-product matrix of $|\tilde{\psi}_3\rangle$, $|\chi_B\rangle$, and $|\tilde{\psi}_1\rangle$ is then

$$\tilde{A}_{DBC} = \begin{bmatrix} \mathbf{1} - W_2^\top W_1^{-1} W_2 & 0 & W_4 - W_2^\top W_1^{-1} W_3 \\ 0 & W_1 & 0 \\ W_4^\top - W_3^\top W_1^{-1} W_2 & 0 & \mathbf{1} - W_3^\top W_1^{-1} W_3 \end{bmatrix} \quad (\text{B.4})$$

Note that \tilde{A}_{DBC} can be obtained from A_{DBC} by Gaussian elimination: add $[(-W_3 W_1^{-1}) \times (2^{\text{nd}} \text{ row})]$ to the third row and add $[(-W_2 W_1^{-1}) \times (2^{\text{nd}} \text{ row})]$ to the first row, and similarly for the corresponding columns. Therefore, \tilde{A}_{DBC} and A_{DBC} have the same determinant,

$$\det(A_{DBC}) = \det(\tilde{A}_{DBC}) \quad (\text{B.5})$$

To obtain $|\psi_{1,3}\rangle$ from $|\tilde{\psi}_{1,3}\rangle$, we only need to normalize them. Define

$$\Lambda_3 \Lambda_3^\top := \mathbf{1} - W_2^\top W_1^{-1} W_2, \quad \Lambda_1 \Lambda_1^\top := \mathbf{1} - W_3^\top W_1^{-1} W_3 \quad (\text{B.6})$$

so that

$$|\psi_3\rangle = \Lambda_3^{-1} |\tilde{\psi}_3\rangle, \quad |\psi_1\rangle = \Lambda_1^{-1} |\tilde{\psi}_1\rangle \quad (\text{B.7})$$

For later use, we compute the inner product between ψ_3 and ψ_1 :

$$\langle \psi_3 | \psi_1 \rangle = \Lambda_3^{-1} (W_4 - W_2^\top W_1^{-1} W_3) \Lambda_1^{-\top} \quad (\text{B.8})$$

Each gate in the circuit is an $\text{SO}(2N_f)$ matrix. For the specific gate U in [fig. 3\(a\)](#), we write

$$\begin{bmatrix} \psi_3 \\ \psi_4 \end{bmatrix} = \begin{bmatrix} U_{31} & U_{32} \\ U_{41} & U_{42} \end{bmatrix} \begin{bmatrix} \psi_1 \\ \psi_2 \end{bmatrix} \quad (\text{B.9})$$

where each block U_{ij} is an $N_f \times N_f$ matrix. It follows that

$$\langle \psi_3 | \psi_1 \rangle = U_{31}^\top \quad (\text{B.10})$$

Combining (B.2)–(B.10) and using standard determinant identities for block matrices, one finds

$$\begin{aligned}\det(A_{DBC}) &= \det(\Lambda_1)^2 \det(\Lambda_3)^2 \det(A_B) \det(\mathbf{1} - U_{31}U_{31}^\dagger) \\ \det(A_{DB}) &= \det(\Lambda_3)^2 \det(A_B) \\ \det(A_{BC}) &= \det(\Lambda_1)^2 \det(A_B)\end{aligned}\tag{B.11}$$

Eliminating $\det(\Lambda_{1,3})$, we obtain

$$\det(\mathbf{1} - U_{31}U_{31}^\dagger) = \frac{\det(A_{DBC}) \det(A_B)}{\det(A_{DB}) \det(A_{BC})}\tag{B.12}$$

This is a direct generalization of (2.18). Indeed, when $N_f = 1$, $U_{31} = \cos\theta$ is a scalar, and $\det(\mathbf{1} - U_{31}U_{31}^\dagger)$ reduces to $\sin^2\theta$.

To elucidate the physical meaning of the factor $\det(\mathbf{1} - U_{31}U_{31}^\dagger)$, we adopt an ansatz for the bulk QFT. For multi-flavor fermions, the bulk theory naturally admits the action

$$S = \frac{1}{4\pi} \int dt dz \cdot i\Psi_L^\alpha \partial_t \Psi_L^\alpha + i\Psi_R^\alpha \partial_t \Psi_R^\alpha - i\Psi_L^\alpha \partial_z \Psi_L^\alpha + i\Psi_R^\alpha \partial_z \Psi_R^\alpha + 2i\widehat{m}_{\alpha\beta}(z, t)\Omega(z, t)\Psi_L^\alpha \Psi_R^\beta\tag{B.13}$$

which is a direct generalization of (2.9). Here $\widehat{m}(z, t)$ is an $N_f \times N_f$ real symmetric matrix.

We next relate the discrete-circuit gate data to the bulk QFT. From (2.12), for $N_f = 1$ and in the small- Δt limit we have $\cos\theta \approx (\Delta t)\frac{1}{2}m\Omega(z)$. The corresponding multi-flavor generalization is

$$U_{31} \approx (\Delta t)\frac{1}{2}\widehat{m}(z, t)\Omega(z, t)\tag{B.14}$$

which implies

$$\log \det(\mathbf{1} - U_{31}U_{31}^\dagger) = \text{Tr} \log(\mathbf{1} - U_{31}U_{31}^\dagger) \approx -\frac{1}{4}(\Delta t)^2 \text{Tr}(\widehat{m}(z, t)^2)\Omega(z, t)^2\tag{B.15}$$

As in section 2.2.1, let $A_{[t_1, t_2]}$ denote the submatrix of $A(\alpha, \mathbf{t}, \alpha', \mathbf{t}')$ with indices $\mathbf{t}, \mathbf{t}' \in [t_1, t_2]$ (a time band). In the continuum limit, this becomes $A_{[t_1, t_2]}$. Moreover, a boundary time band $[t_1, t_2]$ determines a bulk point with lightcone coordinates (u, v) via $t_1 = u$ and $t_2 = v$, and we therefore also write $A_{[t_1, t_2]} \equiv A_{[u, v]}$. In this notation, the matrices $A_{DBC}, A_{DB}, A_{BC}, A_B$ become

$$A_B \equiv A_{[u, v]}, \quad A_{DB} \equiv A_{[u, v+\Delta t]}, \quad A_{BC} \equiv A_{[u-\Delta t, v]}, \quad A_{DBC} \equiv A_{[u-\Delta t, v+\Delta t]}\tag{B.16}$$

Consequently,

$$\log \left[\frac{\det(A_{DBC}) \det(A_B)}{\det(A_{DB}) \det(A_{BC})} \right] \approx -(\Delta t)^2 \partial_u \partial_v \log \det(A_{[u, v]})\tag{B.17}$$

Combining this with (B.15), we obtain in the continuum limit the determinant formula

$$\text{Tr}(\widehat{m}(z, t)^2)\Omega(z, t)^2 = 4\partial_u \partial_v \log \det(A_{[u, v]})\tag{B.18}$$

This is consistent with (1.3), since when $N_f = 1$ and the setup is time-translation invariant, we have $4\partial_u \partial_v = -\partial_z^2$.

An interesting question is under what conditions one can obtain a spacetime-independent mass matrix, $\widehat{m}(z, t) \equiv \widehat{m}$. Only in this case does it make sense to interpret $\Omega(z, t)$ as a geometry

that is experienced universally by all fermion flavors (and only then is “geometry” a meaningful notion). This requires the matrix $U_{31}U_{31}^\top$ to be proportional across different spacetime locations. It would be interesting to translate this requirement into a condition on the boundary fermions’ anticommutator $A(\alpha, t, \alpha', t')$.

C Technical details of applying BOGC formula

In this appendix we record the details of applying the BOGC formula (2.26) to obtain (2.27). We first restate the formula:

Theorem. (Borodin–Okounkov–Geromino–Case) [21, 22]. *Given a $N \times N$ real symmetric Toeplitz matrix A_N , with matrix element $(A_N)_{ij} := f_{|i-j|}$, $i, j = 1, \dots, N$. View $\{f_n\}$ as Fourier coefficient of $f(\theta) := \sum_{n \in \mathbb{Z}} f_n e^{in\theta}$. Assume $g(\theta) := \log f(\theta)$ exist everywhere on $\theta \in (0, 2\pi]$, with $\{g_n\}$ its Fourier coefficient given by $g(\theta) = \sum_{n \in \mathbb{Z}} g_n e^{in\theta}$. Further define $g_+(\theta) := \sum_{n=1}^{+\infty} g_n e^{in\theta}$, $g_-(\theta) := \sum_{n=-\infty}^{-1} g_n e^{in\theta}$, and $b^-(\theta) := e^{g_-(\theta) - g_+(\theta)}$, with Fourier coefficient $\{b_n^-\}$ given by $b^-(\theta) = \sum_{n \in \mathbb{Z}} b_n^- e^{in\theta}$. Now, define a Hankel matrix B_N on half infinite lattice $L^2(\mathbb{Z}_{\geq 0})$ via $(B_N)_{ij} := b_{i+j+N+1}^-$, $i, j \geq 0$. We then have:*

$$\log \det A_N = Ng_0 + \left(\sum_{k=1}^{\infty} k g_k g_{-k} \right) + \log \det [\mathbf{1} - (B_N)^2] \quad (\text{C.1})$$

Since this appendix is very technical, we summarize the procedure as follows:

- **Step one**, factorize $f(\theta)$ into $e^{g_0} e^{g_+(\theta)} e^{g_-(\theta)}$.
- **Step two**, calculate $b^-(\theta)$ and extract its Fourier coefficient $\{b_n^-\}$.
- **Step three**, evaluate $\text{Tr}(B_N^{2m})$, since in $\log \det[\mathbf{1} - (B_N)^2] = -\sum_{m=1}^{\infty} \frac{1}{m} \text{Tr}(B_N^{2m})$, we only need the information of trace of the moment of B_N .
- **Step four**, take continuous limit of $\log \det[\mathbf{1} - (B_N)^2]$, following (2.22), and obtain (2.27).

As a preparation, recall that around (1.2), we assume the anti-commutator two-point function of GFF $A(t, t')$ in upper half frequency plane $\mathcal{A}(\omega)$ have simple poles at $\{iJ_k\}$. Further assume time reversal symmetry, then $\mathcal{A}(\omega)$ can be written as:

$$\mathcal{A}(\omega) = \sum_k \frac{c_k J_k}{J_k^2 + \omega^2} \quad (\text{C.2})$$

where the coefficients $\{c_k\}$ encode the residues. For notational convenience we assume finitely many poles $\{iJ_k\}_{k=1}^{N_{\text{qnm}}}$; the case of infinitely many poles can be recovered by taking $N_{\text{qnm}} \rightarrow \infty$ at the end.

In the time domain, $A(t, t')$ admits the quasi-normal-mode (QNM) expansion:

$$A(t, t') = \sum_{k=1}^{N_{\text{qnm}}} c_k e^{-J_k |t-t'|} \quad (\text{C.3})$$

Recall that $A_N := A_{[t, t+(N-1)\Delta t]}$ is defined by discretizing time; its Toeplitz entries $(A_N)_{ij} := f_{|i-j|}$ are:

$$f_n = \sum_{k=1}^{N_{\text{qnm}}} c_k e^{-J_k(\Delta t)n} := \sum_{k=1}^{N_{\text{qnm}}} c_k r_k^n, \quad r_k := e^{-J_k \Delta t} \quad (\text{C.4})$$

where we introduced r_k for notational simplicity.

• **Step one.** View $\{f_n\}$ as the Fourier coefficients of $f(\theta) = \sum_{n \in \mathbb{Z}} f_n e^{in\theta}$. It is convenient to use the complex variable $\xi := e^{i\theta}$:

$$f(\xi) := \sum_{n \in \mathbb{Z}} f_n \xi^n = \sum_{i=1}^{N_{\text{qnm}}} \frac{c_i(1-r_i^2)}{(1-r_i\xi)(1-r_i\xi^{-1})} = \frac{\sum_{i=1}^{N_{\text{qnm}}} c_i(1-r_i^2) \prod_{j \neq i} (1+r_j^2 - r_j(\xi + \xi^{-1}))}{\prod_{i=1}^{N_{\text{qnm}}} (1-r_i\xi)(1-r_i\xi^{-1})} \quad (\text{C.5})$$

The next step is to factorize $f(\theta)$ as $e^{g_0} e^{g_+(\theta)} e^{g_-(\theta)}$, equivalently to factorize $f(\xi)$ as:

$$f(\xi) = f_0 f_+(\xi) f_-(\xi), \quad \text{with } g_0 = \log f_0, \quad g_{\pm} = \log f_{\pm} \quad (\text{C.6})$$

where $f_+(\xi) - 1$ contains only non-negative powers of ξ and $f_-(\xi) - 1$ contains only non-negative powers of ξ^{-1} . In our case, the symmetry $f(\xi) = f(\xi^{-1})$ implies $f_-(\xi) = f_+(\xi^{-1})$. To determine $f_+(\xi)$, we factorize the numerator of (C.5) as a polynomial $P(x)$ in $x := \frac{1}{2}(\xi + \xi^{-1})$:

$$P(x) := \sum_{i=1}^{N_{\text{qnm}}} c_i(1-r_i^2) \prod_{j \neq i} (1+r_j^2 - 2r_j x) \quad (\text{C.7})$$

Then for generic choice of parameter, $P(x)$ is an $(N_{\text{qnm}} - 1)$ degree polynomial of x , with roots $\{x_i\}_{i=1}^{N_{\text{qnm}}-1}$. Therefore $P = C_1 \prod_{i=1}^{N_{\text{qnm}}-1} (x - x_i)$ with C_1 some constant. Now, we can further factorize $(x - x_i)$ into $-(2s_i)^{-1}(1 - s_i\xi)(1 - s_i\xi^{-1})$ with

$$s_i := x_i - \sqrt{x_i^2 - 1}. \quad (\text{C.8})$$

Finally, we obtain a factorized re-writing of $f(\xi)$:

$$f(\xi) = f_0 \times \frac{\prod_{i=1}^{N_{\text{qnm}}-1} (1 - s_i\xi)}{\prod_{i=1}^{N_{\text{qnm}}} (1 - r_i\xi)} \times \frac{\prod_{i=1}^{N_{\text{qnm}}-1} (1 - s_i\xi^{-1})}{\prod_{i=1}^{N_{\text{qnm}}} (1 - r_i\xi^{-1})} \quad (\text{C.9})$$

$$\text{with: } f_0 := \left(\prod_{i=1}^{N_{\text{qnm}}-1} s_i^{-1} \right) \left(\prod_{i=1}^{N_{\text{qnm}}} r_i \right) \left(\sum_{i=1}^{N_{\text{qnm}}} c_i(1-r_i^2)r_i^{-1} \right) \quad (\text{C.10})$$

Comparing with (C.6) determines $f_{\pm}(\xi)$.

• **Step two.** Compute $b^-(\xi) := f_-(\xi)/f_+(\xi)$ and its Laurent coefficients $\{b_n^-\}$:

$$b^-(\xi) = \sum_{n \in \mathbb{Z}} b_n^- \xi^n \quad (\text{C.11})$$

One finds:

$$b^-(\xi) = \prod_{i=1}^{N_{\text{qnm}}-1} \frac{1-s_i\xi^{-1}}{1-s_i\xi} \times \prod_{j=1}^{N_{\text{qnm}}} \frac{1-r_j\xi}{1-r_j\xi^{-1}} = - \left[\frac{\prod_{j=1}^{N_{\text{qnm}}} r_j}{\prod_{i=1}^{N_{\text{qnm}}-1} s_i} \right] \xi + \sum_{i=1}^{N_{\text{qnm}}-1} \frac{\alpha_i}{1-s_i\xi} + \sum_{j=1}^{N_{\text{qnm}}} \frac{\tilde{\alpha}_j}{\xi-r_j} \quad (\text{C.12})$$

with:

$$\alpha_i = (1-s_i^2) \prod_{k=1, k \neq i}^{N_{\text{qnm}}-1} \frac{1-s_k s_i}{1-s_k s_i^{-1}} \times \prod_{j=1}^{N_{\text{qnm}}} \frac{1-r_j s_i^{-1}}{1-r_j s_i} \quad (\text{C.13})$$

Since $(B_N)_{ij} = b_{i+j+N+1}^-$ with $i, j \geq 0$ and $N \geq 1$, we only need b_n^- for $n \geq 2$. Expanding $\frac{1}{1-s_i\xi} = \sum_{n \geq 0} s_i^n \xi^n$ contains only nonnegative powers, while $\frac{1}{\xi-r_j} = -\sum_{n \geq 0} r_j^n \xi^{-n-1}$ contains only negative powers. Hence, in (C.12) only the second term contributes to b_n^- for $n \geq 2$:

$$b_n^- = \sum_{i=1}^{N_{\text{qnm}}-1} \alpha_i s_i^n, \quad n \geq 2 \quad (\text{C.14})$$

• **Step three.** Construct the Hankel matrix B_N on $L^2(\mathbb{Z}_{\geq 0})$ with entries $(B_N)_{ij} := b_{i+j+N+1}^-$ for $i, j \geq 0$. It is convenient to use the orthonormal basis $\{|i\rangle\}_{i=0}^{\infty}$ with $\langle i|j\rangle = \delta_{ij}$. Then:

$$(B_N)_{ij} = \sum_k^{N_{\text{qnm}}-1} \alpha_k s_k^{N+1} s_k^{i+j} \longrightarrow B_N = \sum_{k=1}^{N_{\text{qnm}}-1} \alpha_k s_k^{N+1} |u_k\rangle \langle u_k|, \quad \text{with } |u_k\rangle := \sum_{i=0}^{+\infty} s_k^i |i\rangle \quad (\text{C.15})$$

To compute $\text{Tr}(B_N^{2m})$, define the $(N_{\text{qnm}}-1) \times (N_{\text{qnm}}-1)$ Gram matrix G of $\{|u_k\rangle\}$:

$$G_{kl} := \langle u_k | u_l \rangle = \sum_{i=0}^{+\infty} s_k^i s_l^i = \frac{1}{1-s_k s_l} \quad (\text{C.16})$$

Also define the diagonal matrix Λ of the same dimension:

$$\Lambda_{kl} := \alpha_k s_k^{N+1} \delta_{kl} \quad (\text{C.17})$$

Then:

$$\text{Tr}(B_N^{2m}) = \text{Tr}[(G\Lambda)^{2m}] \quad (\text{C.18})$$

It is therefore convenient to define the finite matrix \tilde{B}_N :

$$(\tilde{B}_N)_{kl} := (G\Lambda)_{kl} = \frac{\alpha_l s_l^{N+1}}{1-s_k s_l} \quad (\text{C.19})$$

Then we have:

$$\log \det[\mathbf{1} - (B_N)^2] = \log \det[\mathbf{1} - (\tilde{B}_N)^2] \quad (\text{C.20})$$

• **Step four.** We now take the continuum limit (2.22) of \tilde{B}_N . We first solve for the roots of

$P(x)$ at small Δt . It is convenient to parametrize $x := e^{\frac{1}{2}\lambda^2(\Delta t)^2}$. To leading order in Δt :

$$P(x) = 2(\Delta t)^{2N_{\text{qnm}}-1} \times \prod_{i=1}^{N_{\text{qnm}}} (J_i^2 - \lambda^2) \times \left[\sum_{i=1}^{N_{\text{qnm}}} \frac{c_i J_i}{J_i^2 - \lambda^2} \right] + O((\Delta t)^{2N_{\text{qnm}}}) \quad (\text{C.21})$$

Comparing with (C.2), the roots of $P(x)$ are determined by the zeros of $\mathcal{A}(\omega \equiv i\lambda)$. Thus, if $\mathcal{A}(\omega)$ has zeros $\{i\lambda_k\}_{k=1}^{N_{\text{qnm}}-1}$ in the upper half-plane, then (C.7) and (C.13) imply:

$$s_i = 1 - \lambda_i \Delta t + O((\Delta t)^2), \quad \alpha_i = (\Delta t) \times 2\lambda_i \times \prod_{k=1, k \neq i}^{N_{\text{qnm}}-1} \frac{\lambda_k + \lambda_i}{\lambda_k - \lambda_i} \times \prod_{j=1}^{N_{\text{qnm}}} \frac{J_j - \lambda_i}{J_j + \lambda_i} + O((\Delta t)^2) \quad (\text{C.22})$$

Therefore, using (C.19), \tilde{B}_N has a finite continuum limit:

$$B(z)_{ij} := \lim_{(2.22)} (\tilde{B}_N)_{ij} = \frac{\beta_j e^{-\lambda_j 2z}}{\lambda_i + \lambda_j} \quad (\text{C.23})$$

which reproduces (1.2) and (1.3). Together with (C.20), this yields (2.27).

D An elementary calculation of determinants in one and two QNM models

In section C we used the BOGC formula to evaluate Toeplitz determinants. Here we benchmark that computation in simple cases, $N_{\text{qnm}} = 1$, $N_{\text{qnm}} = 2$ and $N_{\text{qnm}} = 3$ in (C.3), and show that the BOGC result (section D.1) agrees with a direct elementary computation of determinant (section D.2).

D.1 BOGC evaluation of determinant

Example: $N_{\text{qnm}} = 1$. This case is particularly simple. From (C.5) we have the factorization $f(\xi) = c_1(1 - r_1^2)(1 - r_1\xi)^{-1}(1 - r_1\xi^{-1})^{-1}$, from which f_0 and $f_{\pm}(\xi)$ follow via (C.6). The Fourier coefficients satisfy $g_k = g_{-k} = \frac{1}{k}r_1^k$ for $k > 0$. Since there is no subleading $\log \det [\mathbf{1} - (\tilde{B}_N)^2]$ term when $N_{\text{qnm}} = 1$, (2.26) yields:

$$\det A_N = [c_1(1 - r_1^2)]^N (1 - r_1^2)^{-1} \quad (\text{D.1})$$

As a check, for $N = 1$ this gives $\det A_1 = c_1$, as expected.

Using (2.20), one finds $\sin^2 \theta_N = 1$ for all $N \geq 2$, i.e. all gates beyond the first layer are exact SWAPs. Then (2.12) implies that in the continuum limit the conformal factor satisfies $m\Omega(z) \equiv 0$.

Example: $N_{\text{qnm}} = 2$. In this case there is a single root s_1 . It is convenient to introduce two intermediate quantities Q_1 and Q_2 :

$$Q_2 = c_1(1 - r_1^2)(1 + r_2^2) + c_2(1 - r_2^2)(1 + r_1^2), \quad Q_1 = c_1(1 - r_1^2)r_2 + c_2(1 - r_2^2)r_1 \quad (\text{D.2})$$

Then:

$$s_1 = \frac{Q_2 - \sqrt{Q_2^2 - 4Q_1^2}}{2Q_1} \quad (\text{D.3})$$

We also record the following intermediate relations:

$$f_0 = s_1^{-1}Q_1, \quad g_k = g_{-k} = \frac{1}{k}(r_1^k + r_2^k - s_1^k), \quad k > 0 \quad (\text{D.4})$$

When $N_{\text{qnm}} = 2$, \tilde{B}_N is a one-dimensional matrix, so $\log \det \left[\mathbf{1} - (\tilde{B}_N)^2 \right] = \log \left(1 - \tilde{B}_N^2 \right)$. Substituting these expressions, we find:

$$\det A_N = \frac{(1 - r_1 s_1)^2 (1 - r_2 s_1)^2 \eta_+^N - (1 - r_1 s_1^{-1})^2 (1 - r_2 s_1^{-1})^2 s_1^2 \eta_-^N}{(1 - r_1^2)(1 - r_2^2)(1 - r_1 r_2)^2 (1 - s_1^2)}, \quad \eta_{\pm} := \frac{Q_2 \pm \sqrt{Q_2^2 - 4Q_1^2}}{2} \quad (\text{D.5})$$

A quick check is to evaluate $N = 1, 2$ and verify (e.g. in Mathematica) agreement with the elementary results $\det A_1 = c_1 + c_2$ and $\det A_2 = (c_1 + c_2)^2 - (c_1 r_1 + c_2 r_2)^2$.

Example: $N_{\text{qnm}} = 3$. In this case there are two roots, s_1 and s_2 . It is convenient to introduce three intermediate quantities Q_1, Q_2, Q_3 :

$$\begin{aligned} Q_3 &:= (r_1 r_2 r_3) \left(\sum_{i=1}^3 c_i (1 - r_i^2) r_i^{-1} \right) \\ Q_2 &:= -c_1 (1 - r_1^2) (r_2 + r_3) (1 + r_2 r_3) - c_2 (1 - r_2^2) (r_1 + r_3) (1 + r_1 r_3) - c_3 (1 - r_3^2) (r_1 + r_2) (1 + r_1 r_2) \\ Q_1 &:= 2Q_3 + \left(\prod_{i=1}^3 1 + r_i^2 \right) \left(\sum_{i=1}^3 \frac{c_i (1 - r_i^2)}{1 + r_i^2} \right) \end{aligned} \quad (\text{D.6})$$

Then (C.7) reduces to a quadratic polynomial $P(x) = 4Q_3 x^2 + 2Q_2 x + Q_1 - 2Q_3$, with roots x_1 and x_2 . Using (E.8) we then obtain s_1 and s_2 , and from (C.10) we read off $f_0 = s_1^{-1} s_2^{-1} Q_3$. For $N_{\text{qnm}} = 3$, \tilde{B}_N is a two-dimensional matrix. Collecting these results and applying the BOGC formula (2.26), we find

$$\det A_N = \sum_{i=0}^4 \mathbf{a}_i \eta_i^N \quad (\text{D.7})$$

with

$$\eta_i \in \{f_0, f_0 s_1 s_2, f_0 s_1^2 s_2^2, f_0 s_1^3, f_0 s_2^3\}. \quad (\text{D.8})$$

Here \mathbf{a}_i are coefficients independent of N . Equivalently, $\det A_N$ is a sum of five terms, each exponential in N . Later we will match these exponents η_i against a direct (elementary) computation of the determinant.

D.2 Elementary evaluation of determinant

Example: $N_{\text{qnm}} = 1$ case. The matrix A_N is explicitly

$$A_{N+1} = c_1^{N+1} \times \begin{bmatrix} 1 & r_1 & r_1^2 & \cdots & r_1^N \\ r_1 & 1 & r_1 & \cdots & r_1^{N-1} \\ r_1^2 & r_1 & 1 & \cdots & r_1^{N-2} \\ \vdots & \vdots & \vdots & \ddots & \vdots \\ r_1^N & r_1^{N-1} & r_1^{N-2} & \cdots & 1 \end{bmatrix}_{N+1}, \quad r_1 := e^{-J_1 \Delta t} \quad (\text{D.9})$$

The subindex $[\cdots]_{N+1}$ on the matrix bracket serves as a reminder of the dimension of that matrix. Using the identity

$$\det \begin{bmatrix} 1 & r_1 & r_1^2 & \cdots & r_1^N \\ r_1 & 1 & r_1 & \cdots & r_1^{N-1} \\ r_1^2 & r_1 & 1 & \cdots & r_1^{N-2} \\ \vdots & \vdots & \vdots & \ddots & \vdots \\ r_1^N & r_1^{N-1} & r_1^{N-2} & \cdots & 1 \end{bmatrix}_{N+1} = \det \begin{bmatrix} 1 - r_1^2 & r_1 & r_1^2 & \cdots & r_1^N \\ 0 & 1 & r_1 & \cdots & r_1^{N-1} \\ 0 & r_1 & 1 & \cdots & r_1^{N-2} \\ \vdots & \vdots & \vdots & \ddots & \vdots \\ 0 & r_1^{N-1} & r_1^{N-2} & \cdots & 1 \end{bmatrix}_{N+1} \quad (\text{D.10})$$

obtained by adding $[(-r_1) \times 2^{\text{nd}} \text{ column}]$ to the 1st column (which does not change the determinant by multilinearity), we obtain the recursion

$$\det A_{N+1} = c_1(1 - r_1^2) \det A_N. \quad (\text{D.11})$$

Matching the initial condition at $N = 1$, this recursion reproduces the BOGC result (D.1).

Example: $N_{\text{qnm}} = 2$ case. Similarly, we reduce the determinant as follows:

$$\begin{aligned} \det(A_{N+1}) &= \det \begin{bmatrix} f_0 & f_1 & f_2 & \cdots & f_N \\ f_1 & f_0 & f_1 & \cdots & f_{N-1} \\ f_2 & f_1 & f_0 & \cdots & f_{N-2} \\ \vdots & \vdots & \vdots & \ddots & \vdots \\ f_N & f_{N-1} & f_{N-2} & \cdots & f_0 \end{bmatrix}_{N+1} \stackrel{(1)}{=} \det \begin{bmatrix} Q_3 & f_1 & f_2 & \cdots & f_N \\ Q_1 & f_0 & f_1 & \cdots & f_{N-1} \\ 0 & f_1 & f_0 & \cdots & f_{N-2} \\ \vdots & \vdots & \vdots & \ddots & \vdots \\ 0 & f_{N-1} & f_{N-2} & \cdots & f_0 \end{bmatrix}_{N+1} \\ &\stackrel{(2)}{=} \det \begin{bmatrix} Q_2 & Q_1 & 0 & \cdots & 0 \\ Q_1 & f_0 & f_1 & \cdots & f_{N-1} \\ 0 & f_1 & f_0 & \cdots & f_{N-2} \\ \vdots & \vdots & \vdots & \ddots & \vdots \\ 0 & f_{N-1} & f_{N-2} & \cdots & f_0 \end{bmatrix}_{N+1} \end{aligned} \quad (\text{D.12})$$

In step (1) we add $[(-d_1) \times 2^{\text{nd}} \text{ column} + (-d_2) \times 3^{\text{rd}} \text{ column}]$ to the 1st column, where d_1, d_2 are to be determined. In step (2) we add $[(-d_1) \times 2^{\text{nd}} \text{ row} + (-d_2) \times 3^{\text{rd}} \text{ row}]$ to the 1st row. The quantities Q_1, Q_2, Q_3 are given by $Q_3 = f_0 - d_1 f_1 - d_2 f_2$, $Q_1 = f_1 - d_1 f_0 - d_2 f_1$, and $Q_2 = Q_3 - d_1 Q_1$.

The coefficients d_1, d_2 are fixed by

$$f_k = d_1 f_{k-1} + d_2 f_{k-2}, \quad \forall k > 0. \quad (\text{D.13})$$

For $N_{\text{qnm}} = 2$ with f_k given in (C.4), we find

$$d_1 = r_1 + r_2, \quad d_2 = -r_1 r_2. \quad (\text{D.14})$$

Moreover, Q_1 and Q_2 coincide with the intermediate quantities introduced in the BOGC derivation, (D.2).

We now evaluate the determinant in the second line of (D.12):

$$\det(A_{N+1}) = Q_2 \det \begin{bmatrix} f_0 & f_1 & \cdots & f_{N-1} \\ f_1 & f_0 & \cdots & f_{N-1} \\ \vdots & \vdots & & \vdots \\ f_{N-1} & f_{N-2} & \cdots & f_0 \end{bmatrix}_N - Q_1 \det \begin{bmatrix} Q_1 & 0 & \cdots & 0 \\ f_1 & f_0 & \cdots & f_{N-1} \\ \vdots & \vdots & & \vdots \\ f_{N-1} & f_{N-2} & \cdots & f_0 \end{bmatrix}_N. \quad (\text{D.15})$$

This yields the recursion

$$\det(A_{N+1}) = Q_2 \det(A_N) - Q_1^2 \det(A_{N-1}). \quad (\text{D.16})$$

The characteristic roots are η_{\pm} defined in (D.5). Matching the initial conditions at $N = 1, 2$, the solution of this recursion agrees with the BOGC result (D.5).

Example: the $N_{\text{qnm}} = 3$ case. Using the same procedure as above, we reduce the determinant to a finitely banded matrix:

$$\begin{aligned} \det(A_{N+1}) &= \det \begin{bmatrix} f_0 & f_1 & f_2 & \cdots & f_N \\ f_1 & f_0 & f_1 & \cdots & f_{N-1} \\ f_2 & f_1 & f_0 & \cdots & f_{N-2} \\ \vdots & \vdots & \vdots & & \vdots \\ f_N & f_{N-1} & f_{N-2} & \cdots & f_0 \end{bmatrix}_{N+1} \stackrel{(1)}{=} \det \begin{bmatrix} Q_4 & f_1 & f_2 & \cdots & f_N \\ Q_5 & f_0 & f_1 & \cdots & f_{N-1} \\ Q_3 & f_1 & f_0 & \cdots & f_{N-2} \\ \vdots & \vdots & \vdots & & \vdots \\ 0 & f_{N-1} & f_{N-2} & \cdots & f_0 \end{bmatrix}_{N+1} \\ &\stackrel{(2)}{=} \det \begin{bmatrix} Q_1 & Q_5 & Q_3 & & & \\ Q_5 & f_0 & f_1 & \cdots & f_{N-1} & \\ Q_3 & f_1 & f_0 & \cdots & f_{N-2} & \\ & \vdots & \vdots & & \vdots & \\ & f_{N-1} & f_{N-2} & \cdots & f_0 & \end{bmatrix}_{N+1} \stackrel{(3)}{=} \det \begin{bmatrix} Q_1 & Q_2 & Q_3 & & & \\ Q_2 & Q_1 & Q_5 & Q_3 & & \\ Q_3 & Q_5 & f_0 & f_1 & f_2 & \cdots & f_{N-2} \\ & Q_3 & f_1 & f_0 & f_1 & \cdots & f_{N-3} \\ & & f_2 & f_1 & f_0 & \cdots & f_{N-4} \\ & & \vdots & \vdots & \vdots & & \vdots \\ & & f_{N-2} & f_{N-3} & f_{N-4} & \cdots & f_0 \end{bmatrix}_{N+1} \\ &= \cdots = \det \begin{bmatrix} Q_1 & Q_2 & Q_3 & & & & \\ Q_2 & Q_1 & Q_2 & Q_3 & & & \\ Q_3 & Q_2 & \ddots & \ddots & \ddots & & \\ & Q_3 & \ddots & & & & \\ & & \ddots & & & & \\ & & & Q_1 & Q_2 & Q_3 & \\ & & & Q_2 & Q_1 & Q_5 & Q_3 \\ & & & Q_3 & Q_5 & f_0 & f_1 & f_2 \\ & & & & Q_3 & f_1 & f_0 & f_1 \\ & & & & & f_2 & f_1 & f_0 \end{bmatrix}_{N+1} \end{aligned} \quad (\text{D.17})$$

In step (1), we add $[(-d_1) \times 2^{\text{nd}} \text{ column} + (-d_2) \times 3^{\text{rd}} \text{ column} + (-d_3) \times 4^{\text{th}} \text{ column}]$ to the 1st column, where d_1, d_2, d_3 are parameters to be fixed. In step (2), we add $[(-d_1) \times 2^{\text{nd}} \text{ row} + (-d_2) \times 3^{\text{rd}} \text{ row} + (-d_3) \times 4^{\text{th}} \text{ row}]$ to the 1st row. These operations set most entries in the first row and first column to zero. In step (3), we iterate the same column and row operations to eliminate most entries in the second row and second column. Repeating this procedure reduces the matrix to a five-banded form. The coefficients d_1, d_2, d_3 are determined by the following relation:

$$f_k = d_1 f_{k-1} + d_2 f_{k-2} + d_3 f_{k-3}, \forall k \quad (\text{D.18})$$

For the three-QNM case, using f_k defined in (C.4), we find:

$$d_1 = r_1 + r_2 + r_3, \quad d_2 = -r_1 r_2 - r_1 r_3 - r_2 r_3, \quad d_3 = r_1 r_2 r_3 \quad (\text{D.19})$$

The five parameters $Q_{1\sim 5}$ are given by:

$$\begin{aligned} Q_4 &= f_0 - d_1 f_1 - d_2 f_2 - d_3 f_3, & Q_5 &= f_1 - d_1 f_0 - d_2 f_1 - d_3 f_2 \\ Q_3 &= f_2 - d_1 f_1 - d_2 f_0 - d_3 f_1, & Q_2 &= Q_5 - d_1 Q_3, & Q_1 &= Q_4 - d_1 Q_5 - d_2 Q_3 \end{aligned} \quad (\text{D.20})$$

In what follows, we will only need $Q_{1,2,3}$, since they determine the determinant recursion relation. One can directly verify that $Q_{1,2,3}$ defined in (D.20) agree with the intermediate variables in (D.6) used in the BOGC method.

We are now ready to derive the determinant recursion relation for the five-banded matrix in the last line of (D.17):

$$\begin{aligned} \det A_{N+1} &= \det \begin{bmatrix} Q_1 & Q_2 & Q_3 & & & & \\ Q_2 & Q_1 & Q_2 & Q_3 & & & \\ Q_3 & Q_2 & Q_1 & Q_2 & Q_3 & & \\ & Q_3 & Q_2 & Q_1 & Q_2 & Q_3 & \\ & & & & \ddots & & \\ & & & & & & \ddots & \end{bmatrix}_{N+1} \\ &= Q_1 \det A_N - Q_2 \det \begin{bmatrix} Q_2 & Q_3 & & & & & \\ Q_2 & Q_1 & Q_2 & Q_3 & & & \\ Q_3 & Q_2 & Q_1 & Q_2 & Q_3 & & \\ & Q_3 & Q_2 & Q_1 & Q_2 & Q_3 & \\ & & & & \ddots & & \end{bmatrix}_N + Q_3 \det \begin{bmatrix} Q_2 & Q_3 & & & & & \\ Q_1 & Q_2 & Q_3 & & & & \\ Q_3 & Q_2 & Q_1 & Q_2 & Q_3 & & \\ & Q_3 & Q_2 & Q_1 & Q_2 & Q_3 & \\ & & Q_3 & Q_2 & Q_1 & Q_2 & Q_3 \\ & & & & \ddots & & \end{bmatrix}_N \\ &:= Q_1 \det A_N - Q_2 \det E_N^{(1)} + Q_3 \det E_N^{(2)} \end{aligned} \quad (\text{D.21})$$

In the last line, we introduced two new matrices $E_N^{(1)}$ and $E_N^{(2)}$ as intermediate variables. Note that the matrix subscripts match the corresponding matrix dimensions. We next derive two

additional relations for $E_N^{(1)}$ and $E_N^{(2)}$:

$$\begin{aligned}
\det E_N^{(1)} &= \det \begin{bmatrix} Q_2 & Q_3 & & & & & \\ Q_2 & Q_1 & Q_2 & Q_3 & & & \\ Q_3 & Q_2 & Q_1 & Q_2 & Q_3 & & \\ & Q_3 & Q_2 & Q_1 & Q_2 & Q_3 & \\ & & & & & & \ddots \\ & & & & & & & Q_3 \end{bmatrix}_N = Q_2 \det A_{N-1} - Q_3 \det \begin{bmatrix} Q_2 & Q_2 & Q_3 & & & & \\ Q_3 & Q_1 & Q_2 & Q_3 & & & \\ & Q_2 & Q_1 & Q_2 & Q_3 & & \\ & Q_3 & Q_2 & Q_1 & Q_2 & Q_3 & \\ & & Q_3 & Q_2 & Q_1 & Q_2 & Q_3 \\ & & & & & & \ddots \\ & & & & & & & Q_3 \end{bmatrix}_{N-1} \\
&= Q_2 \det A_{N-1} - Q_3 \det E_{N-1}^{(1)\top} \\
&= Q_2 \det A_{N-1} - Q_3 \det E_{N-1}^{(1)}
\end{aligned} \tag{D.22}$$

and:

$$\begin{aligned}
\det E_N^{(2)} &= \det \begin{bmatrix} Q_2 & Q_3 & & & & & \\ Q_1 & Q_2 & Q_3 & & & & \\ Q_3 & Q_2 & Q_1 & Q_2 & Q_3 & & \\ & Q_3 & Q_2 & Q_1 & Q_2 & Q_3 & \\ & & Q_3 & Q_2 & Q_1 & Q_2 & Q_3 \\ & & & & & & \ddots \\ & & & & & & & Q_3 \end{bmatrix}_N \\
&= Q_2 \det \begin{bmatrix} Q_2 & Q_3 & & & & & \\ Q_2 & Q_1 & Q_2 & Q_3 & & & \\ Q_3 & Q_2 & Q_1 & Q_2 & Q_3 & & \\ & Q_3 & Q_2 & Q_1 & Q_2 & Q_3 & \\ & & & & & & \ddots \\ & & & & & & & Q_3 \end{bmatrix}_{N-1} - Q_3 \det \begin{bmatrix} Q_1 & Q_3 & & & & & \\ Q_3 & Q_1 & Q_2 & Q_3 & & & \\ & Q_2 & Q_1 & Q_2 & Q_3 & & \\ & Q_3 & Q_2 & Q_1 & Q_2 & Q_3 & \\ & & & & & & \ddots \\ & & & & & & & Q_3 \end{bmatrix}_{N-1} \\
&= Q_2 \det E_{N-1}^{(1)} - Q_3(Q_1 \det A_{N-2} - Q_3^2 \det A_{N-3})
\end{aligned} \tag{D.23}$$

To summarize, we obtain the following coupled recursion relation:

$$\begin{aligned}
\det A_{N+1} &= Q_1 \det A_N - Q_2 \det E_N^{(1)} + Q_3 \det E_N^{(2)} \\
\det E_N^{(1)} &= Q_2 \det A_{N-1} - Q_3 \det E_{N-1}^{(1)} \\
\det E_N^{(2)} &= Q_2 \det E_{N-1}^{(1)} - Q_3(Q_1 \det A_{N-2} - Q_3^2 \det A_{N-3})
\end{aligned} \tag{D.24}$$

We first use the third equation to eliminate $\det E_N^{(2)}$, and then use the second equation to eliminate $\det A_N$. This yields a recursion relation involving only $\det E_N^{(1)}$:

$$\begin{aligned}
\det E_{N+1}^{(1)} &= (Q_1 - Q_3) \det E_N^{(1)} + (Q_1 Q_3 - Q_2^2) \det E_{N-1}^{(1)} \\
&\quad + (Q_2^2 Q_3 - Q_1 Q_3^2) \det E_{N-2}^{(1)} + (Q_3^4 - Q_1 Q_3^3) \det E_{N-3}^{(1)} + Q_3^5 \det E_{N-4}^{(1)}
\end{aligned} \tag{D.25}$$

The characteristic equation yields five roots $\eta_{0,1,2,3,4}$, given by:

$$\begin{aligned}\eta_0 &= Q_3 \\ \eta_{1\sim 4} &= \frac{1}{4} \left(Q_1 - 2Q_3 \pm \sqrt{(Q_1 - 2Q_2 + 2Q_3)(Q_1 + 2Q_2 + 2Q_3)} \right. \\ &\quad \left. - \sqrt{2} \sqrt{Q_1^2 - 2Q_2^2 - 4Q_3^2 \pm (Q_1 - 2Q_3) \sqrt{(Q_1 - 2Q_2 + 2Q_3)(Q_1 + 2Q_2 + 2Q_3)}} \right)\end{aligned}\tag{D.26}$$

A symbolic computation in Mathematica confirms that these five roots η_i coincide with those obtained via the BOGC method in (D.8).

E An alternative inverse formula via contour integral of S-matrix

In this appendix we derive (2.57) and (2.58), which rewrite the inversion formula (1.3) directly in terms of contour integrals of the S-matrix. We follow techniques developed by Eniceicu [31], in the context of giant graviton expansion of unitary matrix integral, where an equivalent reformulation of the BOGC formula is obtained via contour integrals:

Corollary. (Eniceicu) [31]. *We use the same set up and notation as in BOGC formula (2.26). The subleading part of determinant can be re-written in terms of contour integral:*

$$\log \det [\mathbf{1} - (B_N)^2] = \log \left[1 + \sum_{k=1}^{+\infty} G_N^{(k)} \right]\tag{E.1}$$

$$G_N^{(k)} = \frac{(-1)^k}{(k!)^2} \oint \prod_{i=1}^k \frac{dp_i}{2\pi i} \frac{d\tilde{p}_i}{2\pi i} \times \frac{\prod_{1 \leq i < j \leq k} (p_i - p_j)^2 (\tilde{p}_i - \tilde{p}_j)^2}{\prod_{1 \leq i, j \leq k} (p_i - \tilde{p}_j)^2} \times \prod_{i=1}^k \left(\frac{p_i}{\tilde{p}_i} \right)^N \times \prod_{i=1}^k \frac{b_-(\tilde{p}_i)}{b_-(p_i)}\tag{E.2}$$

where the integral contour for $\{p_i\}$ is a counter-clockwise circle slightly smaller than unit circle and for $\{\tilde{p}_i\}$ is a counter-clockwise circle slightly larger than unit circle.

As in section C, we now take the scaling limit (2.22). Recalling $b^-(\xi)$ from (C.12) together with $s_k = 1 - \Delta t \lambda_k$ and $r_k = e^{-J_k \Delta t}$, and parametrizing $\xi = e^{i\Delta t \omega}$, one finds that the continuum limit of $b^-(\xi)$ becomes precisely the S-matrix in (2.54):

$$b^-(\xi) = \prod_i \frac{1 - s_i \xi^{-1}}{1 - s_i \xi} \times \prod_j \frac{1 - r_j \xi}{1 - r_j \xi^{-1}} = \prod_k \frac{\lambda_k + i\omega}{\lambda_k - i\omega} \times \prod_n \frac{J_n - i\omega}{J_n + i\omega} := [\mathcal{S}(\omega)]^{-1}\tag{E.3}$$

Next set $p_i := e^{i\Delta t \omega_i}$ and $\tilde{p}_i := e^{i\Delta t \tilde{\omega}_i}$. Then (2.22) gives $(p_i/\tilde{p}_i)^N = e^{i2z(\omega_i - \tilde{\omega}_i)}$, so the N -dependence becomes z -dependence. The remaining Δt factors cancel: the Jacobian contributes $(i\Delta t)^{2k}$, the Vandermonde in the numerator gives $(i\Delta t)^{4 \frac{k(k-1)}{2}}$, and the denominator gives $(i\Delta t)^{2k^2}$.

Thus $G_N^{(k)}$ has a finite $O(1)$ continuum limit as $\Delta t \rightarrow 0$, which we denote by $G^{(k)}(z)$:

$$G^{(k)}(z) := \frac{1}{(k!)^2} \int \prod_{i=1}^k \frac{d\omega_i}{2\pi} \frac{d\tilde{\omega}_i}{2\pi} \times \frac{\prod_{1 \leq i < j \leq k} (\omega_i - \omega_j)^2 (\tilde{\omega}_i - \tilde{\omega}_j)^2}{\prod_{1 \leq i, j \leq k} (\omega_i - \tilde{\omega}_j)^2} \times \prod_{i=1}^k e^{i2z(\omega_i - \tilde{\omega}_i)} \times \prod_{i=1}^k \frac{\mathcal{S}(\omega_i)}{\mathcal{S}(\tilde{\omega}_i)} \quad (\text{E.4})$$

where the contours for ω_i and $\tilde{\omega}_i$ are inherited from those of p_i and \tilde{p}_i . This reproduces (2.58).

As a check, we can extract the leading contribution to $m\Omega(z)$ from (2.57):

$$m^2\Omega(z)^2 \approx -\partial_z^2 G^{(1)}(z) \quad (\text{E.5})$$

with:

$$G^{(1)}(z) = \int \frac{d\omega}{2\pi} \frac{d\tilde{\omega}}{2\pi} \frac{e^{i2z(\omega - \tilde{\omega})}}{(\omega - \tilde{\omega})^2} \frac{\mathcal{S}(\omega)}{\mathcal{S}(\tilde{\omega})} \quad (\text{E.6})$$

Therefore:

$$-\partial_z^2 G^{(1)}(z) = \left[\int \frac{d\omega}{2\pi} e^{i2z\omega} \mathcal{S}(\omega) \right] \times \left[\int \frac{d\tilde{\omega}}{2\pi} e^{-i2z\tilde{\omega}} \mathcal{S}(-\tilde{\omega}) \right] = S(2z) \times S(2z) \quad (\text{E.7})$$

with $S(z)$ being S-matrix in real space defined in (2.47). This predicts:

$$m\Omega(z) \approx S(2z) \quad (\text{E.8})$$

which is indeed the first term in the ‘zig-zag’ formula (2.48) describing forward scattering.

One can further check the equivalence between (1.3) and (2.57)–(2.58) by expanding both sides:

$$\begin{cases} \log \det[\mathbf{1} - B(z)^2] = -\text{Tr}[B(z)^2] - \frac{1}{2}\text{Tr}[B(z)^4] + \dots \\ \log[1 + \sum_{k=1}^{+\infty} G^{(k)}(z)] = G^{(1)}(z) + G^{(2)}(z) - \frac{1}{2}G^{(1)}(z)G^{(1)}(z) + \dots \end{cases} \quad (\text{E.9})$$

At leading order, one finds $G^{(1)}(z) = -\text{Tr}[B(z)^2]$. This follows directly from (E.6) by evaluating the frequency integrals via residues:

$$G^{(1)}(z) = - \sum_{i,j} \frac{\beta_i \beta_j e^{-(\lambda_i + \lambda_j)2z}}{(\lambda_i + \lambda_j)^2} \quad (\text{E.10})$$

which matches $-\text{Tr}[B(z)^2]$ by the definition of $B(z)$ in (1.3). At next-to-leading order, one similarly verifies $G^{(1)}(z)G^{(1)}(z) - 2G^{(2)}(z) = \text{Tr}[B(z)^4]$ by evaluating the contour integral for $G^{(2)}(z)$:

$$G^{(2)}(z) = \frac{1}{4} \sum_{ijkl} \frac{(\lambda_i - \lambda_j)^2 (\lambda_k - \lambda_l)^2 \beta_i \beta_j \beta_k \beta_l e^{-(\lambda_i + \lambda_j + \lambda_k + \lambda_l)2z}}{(\lambda_i + \lambda_k)^2 (\lambda_j + \lambda_l)^2 (\lambda_i + \lambda_l)^2 (\lambda_j + \lambda_k)^2} \quad (\text{E.11})$$

Plug in the expression of $G^{(1)}, G^{(2)}$, one can indeed check their combination gives $\text{Tr}[B(z)^4]$:

$$\text{Tr}[B(z)^4] = \sum_{ijkl} \frac{\beta_i \beta_j \beta_k \beta_l e^{-(\lambda_i + \lambda_j + \lambda_k + \lambda_l)2z}}{(\lambda_i + \lambda_k)(\lambda_j + \lambda_l)(\lambda_i + \lambda_l)(\lambda_j + \lambda_k)} \quad (\text{E.12})$$

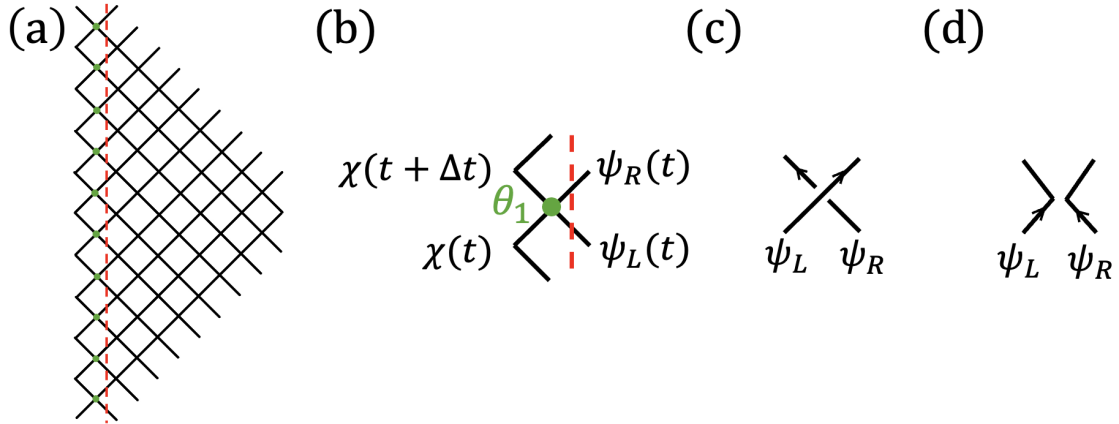


Figure 9: **(a)** An illustration of the Nebabu–Qi circuit near the boundary. The first-layer gates are marked by green dots. The red dashed line indicates the location immediately after the first layer; this corresponds to $z = 0$ in the continuum limit. **(b)** Zoom-in on a representative first-layer gate from panel (a). **(c)** An almost-SWAP gate. **(d)** A gate that almost reflects an incoming left/right mover.

F Match with bulk QFT

In this appendix we discuss several aspects of the bulk QFT of a (1+1)d Majorana field in the geometry (1.1). In section F.1 we derive the bulk QFT boundary condition from the Nebabu–Qi circuit. In section F.2 we provide an alternative derivation of the causal-kernel decomposition discussed in section 2.3.1. Using canonical quantization, we relate the causal kernel to the Jöst function [48, 49, 50]. Finally, in section F.5 we address the question raised in section 4.1: why the AdS_2 –Rindler two-QNM geometry admits a bulk solution with only finitely many quasinormal modes.

F.1 Boundary condition

From the relation between the gate angle and the conformal factor in (2.12), gates in the bulk approach SWAP with $\theta_N \sim \frac{\pi}{2} - O(\Delta t)$. Thus ψ_L and ψ_R interact only weakly and essentially pass through each other; see fig. 9(c). This statement holds for gates starting from the second layer ($N \geq 2$). The first-layer gate (green dots in fig. 9(a)) is special: its angle scales as $\theta_1 \sim O(\sqrt{\Delta t})$, so the incoming ψ_L and ψ_R are almost reflected; see fig. 9(d). The bulk field immediately after the first layer (red dashed line in fig. 9(a)) sets the boundary condition for the bulk QFT, which we now derive.

Consider the region near the first-layer gate in fig. 9(b). From the definition of the gate matrix in (2.3),

$$\psi_L(t) = (\cot \theta_1)\chi(t) - (\sin \theta_1)^{-1}\chi(t + \Delta t), \quad \psi_R(t) = -(\cot \theta_1)\chi(t + \Delta t) + (\sin \theta_1)^{-1}\chi(t) \quad (\text{F.1})$$

The angle θ_1 is fixed by requiring that $\psi_R(t)$ is normalized and orthogonal to $\chi(t + \Delta t)$, which gives

$$\theta_1 = \sqrt{2\mu\Delta t} + O(\Delta t), \quad \text{with: } \mu := -\left. \frac{\partial_t A(0, t)}{A(0, 0)} \right|_{t \rightarrow 0^+} > 0 \quad (\text{F.2})$$

Expanding at small Δt , we find

$$\psi_L = \sqrt{\frac{\Delta t}{2\mu}}(-\partial_t - \mu)\chi, \quad \psi_R = \sqrt{\frac{\Delta t}{2\mu}}(-\partial_t + \mu)\chi \quad (\text{F.3})$$

Using the relation between the circuit fermions ψ_a and the bulk-QFT fermions Ψ_a in (2.10), we obtain

$$\Psi_L = \frac{1}{\sqrt{2\mu}}(-\partial_t - \mu)\chi, \quad \Psi_R = \frac{1}{\sqrt{2\mu}}(-\partial_t + \mu)\chi \quad (\text{F.4})$$

Eliminating χ , we arrive at the boundary condition for Ψ at $z = 0$:

$$(\partial_t - \mu)\Psi_L = (\partial_t + \mu)\Psi_R, \quad z = 0 \quad (\text{F.5})$$

F.2 Causal kernel decomposition from bulk QFT

In this section we canonically quantize the massive (1+1)d Majorana field in the background (1.1), with action (2.9). For convenience, we repeat the action:

$$S = \frac{1}{4\pi} \int dt dz \cdot i\Psi_L \partial_t \Psi_L + i\Psi_R \partial_t \Psi_R - i\Psi_L \partial_z \Psi_L + i\Psi_R \partial_z \Psi_R + 2im\Omega(z)\Psi_L \Psi_R \quad (\text{F.6})$$

We use the Fourier transform $\Psi(t, z) = \int d\omega e^{i\omega t} \Psi(\omega, z)$ with reality condition $\Psi_a^\dagger(\omega, z) = \Psi_a(-\omega, z)$. The equation of motion in frequency space is

$$\begin{bmatrix} \partial_z & -m\Omega(z) \\ m\Omega(z) & -\partial_z \end{bmatrix} \begin{bmatrix} \Psi_L \\ \Psi_R \end{bmatrix} = i\omega \begin{bmatrix} \Psi_L \\ \Psi_R \end{bmatrix} \quad (\text{F.7})$$

There are two linearly independent mode solutions. We denote the incoming branch by $\phi(\omega, z)$; the outgoing branch is fixed by symmetry to be $\sigma_1 \phi(-\omega, z)$, where σ_1 is the Pauli- X matrix. We normalize these modes near the horizon as

$$\phi(\omega, z) \stackrel{z \rightarrow \pm\infty}{\cong} \begin{bmatrix} e^{i\omega z} \\ 0 \end{bmatrix}, \quad \sigma_1 \phi(-\omega, z) \stackrel{z \rightarrow \pm\infty}{\cong} \begin{bmatrix} 0 \\ e^{-i\omega z} \end{bmatrix} \quad (\text{F.8})$$

A normalized physical solution $\varphi(\omega, z)$ is a linear combination of incoming/outgoing modes,

$$\varphi(\omega, z) = \mathcal{C}_+(\omega)\phi(\omega, z) + \mathcal{C}_-(\omega)\sigma_1\phi(-\omega, z) \quad (\text{F.9})$$

By symmetry of the Majorana equation (F.7), solutions satisfy a reality condition (e.g. $\phi(\omega, z)^* = \phi(-\omega, z)$, and similarly for φ), which implies

$$\mathcal{C}_\pm(\omega)^* = \mathcal{C}_\pm(-\omega) \quad (\text{F.10})$$

The ratio of $\mathcal{C}_\pm(\omega)$ is fixed by the boundary condition (F.5):

$$\begin{bmatrix} \mathcal{C}_+(\omega) \\ \mathcal{C}_-(\omega) \end{bmatrix} = \begin{bmatrix} \phi_L(-\omega, 0) & -\phi_R(-\omega, 0) \\ -\phi_R(\omega, 0) & \phi_L(\omega, 0) \end{bmatrix} \begin{bmatrix} \varphi_L(\omega, 0) \\ \varphi_R(\omega, 0) \end{bmatrix} \quad (\text{F.11})$$

Here we used that the Wronskian $W(z) := \phi_L(\omega, z)\phi_L(-\omega, z) - \phi_R(\omega, z)\phi_R(-\omega, z)$ is z -independent

by the equations of motion, and evaluating it at $z \rightarrow +\infty$ gives $W(z) = 1$.

The overall normalization of $\mathcal{C}_\pm(\omega)$ is fixed by the canonical anti-commutator

$$\{\Psi_a(t, z), \Psi_b(t, z')\} = (2\pi)\delta_{ab}\delta(z - z') \quad (\text{F.12})$$

We expand the field operator in this mode basis as

$$\Psi(t, z) = \int d\omega e^{i\omega t} \Psi(\omega, z) := \int d\omega e^{i\omega t} c_\omega \varphi(\omega, z), \quad \text{with: } c_\omega^\dagger = c_{-\omega}, \{c_\omega, c_{\omega'}\} = \delta(\omega + \omega') \quad (\text{F.13})$$

Requiring (F.12) implies the completeness/normalization condition

$$\int d\omega \varphi_a(\omega, z) \varphi_b(-\omega, z') = (2\pi)\delta_{ab}\delta(z - z') \quad (\text{F.14})$$

Evaluating this at $z, z' \rightarrow \infty$ yields

$$\mathcal{C}_\pm(\omega)\mathcal{C}_\pm(-\omega) = 1 \quad (\text{F.15})$$

Together with (F.10), this implies that $\mathcal{C}_\pm(\omega)$ are pure phases for real ω .

We now compute the boundary correlator $\{\chi(t), \chi(t')\}$. Rewriting (F.4) in frequency space gives

$$\Psi(\omega, 0) = \left[\begin{array}{c} \frac{1}{\sqrt{2\mu}}(-i\omega - \mu) \\ \frac{1}{\sqrt{2\mu}}(-i\omega + \mu) \end{array} \right] \chi(\omega) := a(\omega)\chi(\omega), \quad \text{with: } \chi(t) = \int d\omega e^{i\omega t} \chi(\omega) \quad (\text{F.16})$$

The boundary condition (F.5) can be written as

$$\frac{\varphi_L(\omega, 0)}{a_L(\omega)} = \frac{\varphi_R(\omega, 0)}{a_R(\omega)} = \mathcal{R}(\omega) \quad (\text{F.17})$$

where $\mathcal{R}(\omega)$ inherits the reality property of $\varphi(\omega, z)$, i.e. $\mathcal{R}(\omega)^* = \mathcal{R}(-\omega)$ for real ω . Hence, from (F.16) we find

$$\chi(\omega) = \mathcal{R}(\omega)c_\omega \quad (\text{F.18})$$

and therefore the boundary two-point function is

$$\{\chi(t), \chi(t')\} = \int d\omega e^{i\omega(t-t')} \mathcal{R}(\omega)\mathcal{R}(-\omega), \quad (\text{F.19})$$

so that

$$\mathcal{A}(\omega) = \mathcal{R}(\omega)\mathcal{R}(-\omega). \quad (\text{F.20})$$

From (F.21) and (F.17) we also obtain

$$\left[\begin{array}{c} \mathcal{C}_+(\omega) \\ \mathcal{C}_-(\omega) \end{array} \right] = \mathcal{R}(\omega) \left[\begin{array}{cc} \phi_L(-\omega, 0) & -\phi_R(-\omega, 0) \\ -\phi_R(\omega, 0) & \phi_L(\omega, 0) \end{array} \right] \left[\begin{array}{c} a_L(\omega) \\ a_R(\omega) \end{array} \right] := \mathcal{R}(\omega) \left[\begin{array}{c} -\mathcal{J}(-\omega) \\ \mathcal{J}(\omega) \end{array} \right] \quad (\text{F.21})$$

where $\mathcal{J}(\omega)$ is the Jöst function [48, 49, 50] (in analogy with the scalar case). In the last equality we used $a_L(\omega) = -a_R(-\omega)$ from (F.16). Note that $\mathcal{J}(\omega)^* = \mathcal{J}(-\omega)$ for real ω . The scattering

amplitude is

$$\mathcal{S}(\omega) := -\frac{\mathcal{C}_+(\omega)}{\mathcal{C}_-(\omega)} = \frac{\mathcal{J}(-\omega)}{\mathcal{J}(\omega)} \quad (\text{F.22})$$

For real ω , write $\mathcal{J}(\omega) = \rho_{\mathcal{J}}(\omega)e^{i\theta_{\mathcal{J}}(\omega)}$ with $\rho_{\mathcal{J}}(-\omega) = \rho_{\mathcal{J}}(\omega)$ and $\theta_{\mathcal{J}}(-\omega) = -\theta_{\mathcal{J}}(\omega)$, and similarly $\mathcal{R}(\omega) = \rho_{\mathcal{R}}(\omega)e^{i\theta_{\mathcal{R}}(\omega)}$. Using (F.15) gives $\rho_{\mathcal{R}}(\omega) = [\rho_{\mathcal{J}}(\omega)]^{-1}$. Thus the boundary spectral function and scattering phase are determined by the Jöst function:

$$\mathcal{A}(\omega) = \frac{1}{\rho_{\mathcal{J}}(\omega)^2}, \quad \mathcal{S}(\omega) = e^{-2i\theta_{\mathcal{J}}(\omega)} \quad (\text{F.23})$$

The phase $\theta_{\mathcal{R}}(\omega)$ is not fixed by physical data. In section 2.3.1 we identified a preferred choice from the causal-kernel decomposition: one demands that $\mathcal{K}^f(\omega) = \frac{1}{\mathcal{R}^f(\omega)}$ is analytic in the upper half-plane.

In section F.3 we will show that, under the condition

$$\int_0^{+\infty} dz \cdot \Omega(z) < \infty, \quad (\text{F.24})$$

the Jöst function $\mathcal{J}(\omega)$ is analytic in the upper half-plane. In this situation the causal kernel exists and can be chosen as $\mathcal{R}^f(\omega) = \frac{1}{\mathcal{J}(\omega)}$, with

$$\mathcal{A}(\omega) = \frac{1}{\mathcal{J}(\omega)\mathcal{J}(-\omega)} \quad (\text{F.25})$$

F.3 Analytic property of Jöst function

In this section we establish the following statements under the condition (F.27):

- (1). The incoming solution $\phi(\omega, z)$ is analytic in the upper half ω -plane. Consequently, the Jöst function $\mathcal{J}(\omega)$ is analytic in the upper half-plane.
- (2). In the upper half-plane and at high energy ($\text{Im } \omega \rightarrow +\infty$), $\phi(\omega, z)$ approaches the free solution.
- (3). Zeros of the Jöst function $\mathcal{J}(\omega)$ in the upper half-plane correspond to bound states.
- (4). For an analytic metric with temperature (3.3), $\mathcal{J}(\omega)$ has simple poles at the fermionic Matsubara frequencies $\{-i(2n+1)\lambda_0 = -i(n+\frac{1}{2})\beta \mid n = 0, 1, 2, \dots\}$ and is otherwise analytic. As a corollary, using (F.25) and (A.3), the Wightman function $\mathcal{G}_W(\omega)$ has no zeros.
- (5). The (unnormalized) physical solution $\tilde{\varphi}(\omega, z)$ is analytic on the entire complex ω -plane and approaches the free physical solution at high energy.
- (6). At high energy the S-matrix obeys $\mathcal{S}(\omega) \rightarrow -1$ as $|\text{Im } \omega| \rightarrow +\infty$.

These properties are used in deriving the inverse-scattering formula and related analyticity statements in the frequency plane.

(1). We first recall the definition of the Jöst function from (F.21):

$$\mathcal{J}(\omega) = \phi_L(\omega, 0)a_R(\omega) - \phi_R(\omega, 0)a_L(\omega) \quad (\text{F.26})$$

From (F.16), $a_{L,R}(\omega)$ are analytic on the whole ω -plane, so it suffices to show that $\phi(\omega, 0)$ is analytic in the upper half-plane. In fact, we can prove the stronger statement that $\phi(\omega, z)$ is analytic in the upper half-plane for any $z \geq 0$.

Theorem. *The incoming wavefunction $\phi(\omega, z)$ is bounded for all $\text{Im } \omega \geq 0$ and all $z \geq 0$, provided that*

$$C_0 := \int_0^{+\infty} dz \cdot \Omega(z) < \infty. \quad (\text{F.27})$$

Proof. The incoming solution obeys the Volterra equation

$$\phi(\omega, z) = \begin{bmatrix} e^{i\omega z} \\ 0 \end{bmatrix} - \int_z^{+\infty} dz' \begin{bmatrix} 0 & e^{i\omega(z-z')} \\ e^{-i\omega(z-z')} & 0 \end{bmatrix} m\Omega(z')\phi(\omega, z') \quad (\text{F.28})$$

which can be solved iteratively as

$$\phi(\omega, z) := \sum_{n=0}^{+\infty} \phi^{(n)}(\omega, z), \quad (\text{F.29})$$

with

$$\phi^{(0)}(\omega, z) = \begin{bmatrix} e^{i\omega z} \\ 0 \end{bmatrix}, \quad \phi^{(n)}(\omega, z) = - \int_z^{+\infty} dz' \begin{bmatrix} 0 & e^{i\omega(z-z')} \\ e^{-i\omega(z-z')} & 0 \end{bmatrix} m\Omega(z')\phi^{(n-1)}(\omega, z'), \quad n \geq 1. \quad (\text{F.30})$$

We bound $|\phi(\omega, z)|$ using the Euclidean norm. For any vector v and matrix M , $|Mv| \leq \|M\|_2|v| = \sqrt{\max\text{-eigval}(M^\dagger M)}|v|$. Writing $\nu := \text{Im } \omega$, we obtain

$$|\phi^{(n)}(\omega, z)| \leq \int_z^{+\infty} dz' m\Omega(z') e^{|\nu|(z'-z)} |\phi^{(n-1)}(\omega, z')|. \quad (\text{F.31})$$

It is convenient to define $\tilde{\phi}^{(n)}(\omega, z) := e^{|\nu|z}\phi^{(n)}(\omega, z)$. Iterating the bound gives

$$\begin{aligned} |\tilde{\phi}^{(n)}(\omega, z)| &\leq \int_z^{+\infty} dz_1 \int_{z_1}^{+\infty} dz_2 \cdots \int_{z_{n-1}}^{+\infty} dz_n \cdot \prod_{k=1}^n [m\Omega(z_k)] \cdot e^{(|\nu|-\nu)z_n} \\ &= e^{(|\nu|-\nu)z} \int_z^{+\infty} dz_1 \int_{z_1}^{+\infty} dz_2 \cdots \int_{z_{n-1}}^{+\infty} dz_n \cdot \prod_{k=1}^n [m\Omega(z_k)] \cdot e^{(|\nu|-\nu)(z_n-z)} \\ &\leq e^{(|\nu|-\nu)z} \int_z^{+\infty} dz_1 \int_{z_1}^{+\infty} dz_2 \cdots \int_{z_{n-1}}^{+\infty} dz_n \cdot \prod_{k=1}^n [m\Omega(z_k) e^{(|\nu|-\nu)(z_k-z)}] \\ &= e^{(|\nu|-\nu)z} \frac{1}{n!} \left[\int_z^{+\infty} dz' \cdot m\Omega(z') e^{(|\nu|-\nu)(z'-z)} \right]^n \end{aligned} \quad (\text{F.32})$$

Since $|\tilde{\phi}^{(0)}(\omega, z)| = e^{(|\nu|-\nu)z}$ and $1 \leq e^{(|\nu|-\nu)(z_k-z)}$ (because $(|\nu|-\nu)(z_k-z) \geq 0$), we obtain

$$|\phi(\omega, z)| \leq e^{-\nu z} \exp \left[\int_z^{+\infty} dz' \cdot m\Omega(z') e^{(|\nu|-\nu)(z'-z)} \right]. \quad (\text{F.33})$$

For $\nu \geq 0$ we have $|\nu| - \nu = 0$, so this simplifies to

$$|\phi(\omega, z)| \leq e^{-\nu z} \exp \left[\int_z^{+\infty} dz' \cdot m\Omega(z') \right] \leq e^{-\nu z} e^{mC_0}, \quad \text{Im } \omega \geq 0. \quad (\text{F.34})$$

This proves the claim. \square

In fact, using the asymptotic behavior $\Omega(z) \sim e^{-2\lambda_0 z}$, one can show a stronger statement: $|\phi(\omega, z)|$ is bounded as long as $\text{Im } \omega > -\lambda_0$.

(2). As a corollary, we can bound the deviation from the free solution:

$$\begin{aligned} |\phi(\omega, z) - \phi^{(0)}(\omega, z)| &\leq \int_z^{+\infty} dz' e^{|\nu|(z'-z)} m\Omega(z') |\phi(\omega, z')| \\ &\leq \int_z^{+\infty} dz' e^{|\nu|(z'-z)} m\Omega(z') e^{-\nu z'} e^{mC_0} \\ &\leq e^{-\nu z} mC_0 e^{mC_0}, \quad \text{Im } \omega \geq 0 \end{aligned} \quad (\text{F.35})$$

where the first step uses the Volterra equation (F.28). Thus, for finite C_0 , the incoming solution approaches the free solution in the upper half-plane.

(3). As another corollary of (F.34), we show that zeros of the Jöst function in the upper half-plane correspond to bound states. Suppose $\mathcal{J}(\omega_0) = 0$ with $\text{Im } \omega_0 > 0$. By (F.26), the incoming solution $\phi(\omega_0, z)$ by itself satisfies the boundary condition (F.17) and is therefore physical. The factor $e^{-(\text{Im } \omega_0)z}$ in (F.34) implies exponential decay toward the horizon, so this mode is a bound state.

(4). Next, consider a conformal factor $\Omega(z)$ that is analytic to all orders near the horizon, with temperature (3.3). Equivalently, after passing to local Rindler coordinates, the metric admits a Taylor expansion with no fractional powers. The most general such conformal factor can be written as the ansatz

$$m\Omega(z) := \sum_{n=0}^{+\infty} a_n e^{-2(2n+1)\lambda_0 z} \quad (\text{F.36})$$

This follows by combining the leading exponential $e^{-4\lambda_0 z}(-dt^2 + dz^2)$ with the local Rindler coordinate $-\rho^2 dt^2 + d\rho^2$, where $\rho := e^{-2\lambda_0 z}$. The remaining factor $\tilde{\Omega}(\rho)$ is a Taylor series in ρ with only even powers; hence $\Omega(\rho) \propto \rho \tilde{\Omega}(\rho)$ contains only odd powers of ρ .

We claim that $\phi(\omega, z)$ has poles only at $\{-i(2n+1)\lambda_0 \mid n = 1, 2, 3, \dots\}$. This is straightforward to see by tracking the ω -dependence in each term of the iterative solution (F.30). A low-order example is:

$$\phi^{(2)}(\omega, z) = \begin{bmatrix} e^{i\omega z} \\ 0 \end{bmatrix} \sum_{n_1, n_2=0}^{+\infty} \frac{a_{n_1} a_{n_2} e^{-2\lambda_0(m_1+m_2)z}}{(-4i\lambda_0)(\omega + im_1\lambda_0)(m_1 + m_2)}, \quad m_i := 2n_i + 1 \quad (\text{F.37})$$

The general expression for even number of iteration is:

$$\phi^{(2k)}(\omega, z) = \begin{bmatrix} e^{i\omega z} \\ 0 \end{bmatrix} \left(\prod_{i=1}^{2k} \sum_{n_i=0}^{+\infty} \right) \frac{(\prod_{i=1}^{2k} a_{n_i}) e^{-2\lambda_0(\sum_{i=1}^{2k} m_i)z}}{(-4i\lambda_0)^k \prod_{i=1}^k [(\omega + i\lambda_0(\sum_{j=1}^{2i-1} m_j))(\sum_{j=1}^{2i} m_j)]}, \quad m_i := 2n_i + 1 \quad (\text{F.38})$$

Thus the poles lie at $\omega = -i(2n+1)\lambda_0$, and they are all simple. A more careful discussion of convergence can be found in [33]; see also Appendix C of [50].

Using (F.25) and (A.3), the Wightman function is

$$\mathcal{G}_W(\omega) = \frac{1}{(1 + e^{\beta\omega})\mathcal{J}(\omega)\mathcal{J}(-\omega)}, \quad (\text{F.39})$$

so zeros of $(1 + e^{\beta\omega})$ cancel the poles of $\mathcal{J}(\omega)\mathcal{J}(-\omega)$ at fermionic Matsubara frequencies. Hence $\mathcal{G}_W(\omega)$ has no zeros.

(5). For later convenience, we define an unnormalized physical solution $\tilde{\varphi}(\omega, z)$ that satisfies a Volterra equation analogous to (F.28):

$$\tilde{\varphi}(\omega, z) = \tilde{\varphi}^{(0)}(\omega, z) + \int_0^z dz' \begin{bmatrix} 0 & e^{i\omega(z-z')} \\ e^{-i\omega(z-z')} & 0 \end{bmatrix} m\Omega(z')\tilde{\varphi}(\omega, z'), \quad \tilde{\varphi}^{(0)}(\omega, z) = \begin{bmatrix} a_L(\omega)e^{i\omega z} \\ a_R(\omega)e^{-i\omega z} \end{bmatrix} \quad (\text{F.40})$$

where $\tilde{\varphi}^{(0)}(\omega, z)$ is the free solution. Since $\tilde{\varphi}(\omega, 0) = \tilde{\varphi}^{(0)}(\omega, 0)$, $\tilde{\varphi}$ satisfies the boundary condition (F.17) with the choice $\mathcal{R}(\omega) = 1$. Thus $\varphi(\omega, z) = \mathcal{R}(\omega)\tilde{\varphi}(\omega, z)$. We can also expand $\tilde{\varphi}$ in the incoming/outgoing basis using (F.21):

$$\tilde{\varphi}(\omega, z) = -\mathcal{J}(-\omega)\phi(\omega, z) + \mathcal{J}(\omega)\sigma_1\phi(-\omega, z) \quad (\text{F.41})$$

Proceeding as in (F.32), we obtain the bound

$$|\tilde{\varphi}(\omega, z)| \leq e^{|\text{Im}\omega|z} \sqrt{\mu^{-1} [(\text{Re}\omega)^2 + (|\text{Im}\omega| + \mu)^2]} \exp \left[\int_0^z dz' m\Omega(z') \right] \quad (\text{F.42})$$

valid for any complex ω and $z \geq 0$. In particular, $\tilde{\varphi}(\omega, z)$ is analytic on the entire complex ω -plane. Its deviation from the free solution $\tilde{\varphi}^{(0)}$ can be bounded by

$$|\tilde{\varphi}(\omega, z) - \tilde{\varphi}^{(0)}(\omega, z)| \leq e^{|\text{Im}\omega|z} mC_0 e^{mC_0} \sqrt{\mu^{-1} [(\text{Re}\omega)^2 + (|\text{Im}\omega| + \mu)^2]} \quad (\text{F.43})$$

for any complex ω and $z \geq 0$.

(6). Finally, we comment on the high-energy behavior of the S-matrix. If $\Omega(z)$ is regular, then at sufficiently high energy we may neglect the mass term and study massless Majorana fermions. The only scatterer is then the boundary at $z = 0$, with boundary condition (F.5), which yields

$$\mathcal{S}^{(0)}(\omega) = \frac{a_R(-\omega)}{a_R(\omega)} = \frac{i\omega + \mu}{-i\omega + \mu} \quad (\text{F.44})$$

and therefore

$$\mathcal{S}_\infty = \mathcal{S}_\infty^{(0)} = -1 \quad (\text{F.45})$$

F.4 One QNMs model from bulk QFT

In this appendix we address a question raised in [section 4](#). There we found that the dual bulk geometry of the one-QNM model has conformal factor $m\Omega(z) = 0$ for all z , i.e. it corresponds to a massless fermion on the (1+1)d half-space ($z \geq 0$). From the bulk-QFT perspective, one may then ask how the boundary two-point function can nevertheless decay exponentially. The answer is that the exponential decay is induced by the boundary condition [\(F.5\)](#) at $z = 0$.

From [\(F.26\)](#) we obtain the Jöst function

$$\mathcal{J}(\omega) = \frac{1}{\sqrt{2\mu}}(i\omega + \mu) \quad (\text{F.46})$$

Quasinormal modes are defined as zeros of $-\mathcal{J}(-\omega)$ in the upper half-plane; this yields a single QNM at $\omega = i\mu$. Using [\(F.22\)](#) and [\(F.25\)](#), the spectral function and S-matrix are

$$\mathcal{A}(\omega) = \frac{2\mu}{\omega^2 + \mu^2}, \quad \mathcal{S}(\omega) = \frac{i\omega + \mu}{-i\omega + \mu} \quad (\text{F.47})$$

We can also compute the bulk two-point function:

$$\{\Psi_a(u, v), \Psi_b(u', v')\} = 2\pi \begin{bmatrix} \delta(v - v') & g(u' - v) \\ g(u - v') & \delta(u - u') \end{bmatrix}, \quad g(z) := \delta(z) - 2\mu e^{-\mu z} \Theta(z) \quad (\text{F.48})$$

In the off-diagonal left/right correlator, the $\delta(z)$ term corresponds to the usual boundary reflection. The second term $2\mu e^{-\mu z}$ encodes imperfect reflection at the boundary.

F.5 Two QNMs model from bulk QFT

Here we re-derive, purely from the bulk QFT, the S-matrix of the two-QNM model discussed in [section 4.1](#). The punchline is that the “finite number of QNMs” is not in tension with the fact that the background has constant AdS curvature: the usual AdS₂–Rindler analysis assumes the boundary sits at the asymptotic boundary with standard normalizable boundary conditions, which indeed gives an infinite tower [\[34\]](#). Once we move the boundary to a finite radial position (as dictated by the circuit), most of that tower disappears.

We start from the geometry [\(4.4\)](#):

$$m\Omega(z) = \frac{2\lambda_0}{\sinh[\lambda_0(2z + z_0)]}, \quad 0 < z_0 < z < +\infty \quad (\text{F.49})$$

It is convenient to use

$$y := \lambda_0(2z + z_0), \quad 0 < y < +\infty, \quad (\text{F.50})$$

so that $\Omega(y) = 1/\sinh y$. We keep the mass m general for the moment (the two-QNM model corresponds to $m = 1$ in AdS units). In terms of y , the Majorana equation [\(F.7\)](#) becomes:

$$\begin{bmatrix} \partial_y & -m\Omega(y) \\ m\Omega(y) & -\partial_y \end{bmatrix} \begin{bmatrix} \Psi_L \\ \Psi_R \end{bmatrix} = i\tilde{\omega} \begin{bmatrix} \Psi_L \\ \Psi_R \end{bmatrix}, \quad \tilde{\omega} := \frac{\omega}{2\lambda_0}, \quad \Omega(y) = \frac{1}{\sinh y}, \quad y > 0 \quad (\text{F.51})$$

Next, introduce the coordinate x such that $x = 0$ is the horizon and $x = 1$ is the asymptotic

boundary:

$$x := e^{-2y}, \quad x \in (0, 1), \quad (\text{F.52})$$

In terms of x , the Majorana equation becomes hypergeometric. It is useful to organize solutions by their near-horizon and near-boundary behavior. We take Ψ_1 and Ψ_2 to be the incoming/outgoing solutions, normalized near the horizon as

$$\Psi_1 \rightarrow \begin{bmatrix} x^{-\frac{i\tilde{\omega}}{2}} \\ 0 \end{bmatrix} = \begin{bmatrix} e^{i\tilde{\omega}y} \\ 0 \end{bmatrix}, \quad \Psi_2 \rightarrow \begin{bmatrix} 0 \\ x^{\frac{i\tilde{\omega}}{2}} \end{bmatrix} = \begin{bmatrix} 0 \\ e^{-i\tilde{\omega}y} \end{bmatrix}, \quad \text{as } x \rightarrow 0^+. \quad (\text{F.53})$$

We also define Ψ_3 and Ψ_4 as the normalizable and non-normalizable solutions, respectively, characterized by their behavior near the asymptotic boundary:

$$\Psi_3 \rightarrow \begin{bmatrix} (1-x)^m \\ (1-x)^m \end{bmatrix} = \begin{bmatrix} (2y)^m \\ (2y)^m \end{bmatrix}, \quad \Psi_4 \rightarrow \begin{bmatrix} (1-x)^{-m} \\ -(1-x)^{-m} \end{bmatrix} = \begin{bmatrix} (2y)^{-m} \\ -(2y)^{-m} \end{bmatrix}, \quad \text{as } x \rightarrow 1^- \quad (\text{F.54})$$

We will first record the result of mode functions:

$$\begin{aligned} \Psi_1(\omega, y) &= \begin{bmatrix} x^{-\frac{i\tilde{\omega}}{2}} (1-x)^{-m} {}_2F_1(-m, \frac{1}{2} - m - i\tilde{\omega}, \frac{1}{2} - i\tilde{\omega}, x) \\ \frac{-m}{\frac{1}{2} - i\tilde{\omega}} x^{\frac{1}{2} - \frac{i\tilde{\omega}}{2}} (1-x)^{-m} {}_2F_1(1 - m, \frac{1}{2} - m - i\tilde{\omega}, \frac{3}{2} - i\tilde{\omega}, x) \end{bmatrix} \\ \Psi_2(\omega, y) &= \begin{bmatrix} \frac{-m}{\frac{1}{2} + i\tilde{\omega}} x^{\frac{1}{2} + \frac{i\tilde{\omega}}{2}} (1-x)^{-m} {}_2F_1(1 - m, \frac{1}{2} - m + i\tilde{\omega}, \frac{3}{2} + i\tilde{\omega}, x) \\ x^{\frac{i\tilde{\omega}}{2}} (1-x)^{-m} {}_2F_1(-m, \frac{1}{2} - m + i\tilde{\omega}, \frac{1}{2} + i\tilde{\omega}, x) \end{bmatrix} \\ \Psi_3(\omega, y) &= \begin{bmatrix} x^{-\frac{i\tilde{\omega}}{2}} (1-x)^m {}_2F_1(m, \frac{1}{2} + m - i\tilde{\omega}, 1 + 2m, 1 - x) \\ x^{\frac{i\tilde{\omega}}{2}} (1-x)^m {}_2F_1(m, \frac{1}{2} + m + i\tilde{\omega}, 1 + 2m, 1 - x) \end{bmatrix} \\ \Psi_4(\omega, y) &= \begin{bmatrix} x^{-\frac{i\tilde{\omega}}{2}} (1-x)^{-m} {}_2F_1(-m, \frac{1}{2} - m - i\tilde{\omega}, 1 - 2m, 1 - x) \\ -x^{\frac{i\tilde{\omega}}{2}} (1-x)^{-m} {}_2F_1(-m, \frac{1}{2} - m + i\tilde{\omega}, 1 - 2m, 1 - x) \end{bmatrix} \end{aligned} \quad (\text{F.55})$$

The outgoing and incoming solutions are related by the symmetry that exchanges $\Psi_L \leftrightarrow \Psi_R$ and simultaneously sends $\tilde{\omega} \rightarrow -\tilde{\omega}$. The normalizable and non-normalizable solutions are related by $m \rightarrow -m$ together with $\Psi_R \rightarrow -\Psi_R$.

Using hypergeometric connection formulas [?], for non-integer m one can expand the normalizable and non-normalizable solutions in the incoming/outgoing basis:

$$\Psi_3 = C_{31}(\omega)\Psi_1 + C_{32}(\omega)\Psi_2, \quad C_{31}(\omega) = \frac{\Gamma(1+2m)\Gamma(\frac{1}{2} + i\tilde{\omega})}{\Gamma(1+m)\Gamma(\frac{1}{2} + m + i\tilde{\omega})}, \quad C_{32}(\omega) = \frac{\Gamma(1+2m)\Gamma(\frac{1}{2} - i\tilde{\omega})}{\Gamma(1+m)\Gamma(\frac{1}{2} + m - i\tilde{\omega})} \quad (\text{F.56})$$

$$\Psi_4 = C_{41}(\omega)\Psi_1 + C_{42}(\omega)\Psi_2, \quad C_{41}(\omega) = \frac{\Gamma(1-2m)\Gamma(\frac{1}{2} + i\tilde{\omega})}{\Gamma(1-m)\Gamma(\frac{1}{2} - m + i\tilde{\omega})}, \quad C_{42}(\omega) = -\frac{\Gamma(1-2m)\Gamma(\frac{1}{2} - i\tilde{\omega})}{\Gamma(1-m)\Gamma(\frac{1}{2} - m - i\tilde{\omega})} \quad (\text{F.57})$$

As a warm-up, place the boundary at the asymptotic boundary and impose the usual normalizability condition. Then Ψ_3 is the physical mode.

To extract QNMs, we look at the near-horizon decomposition into ingoing/outgoing waves. In our conventions, the ingoing piece is Ψ_2 (it depends on $t - z$), while the outgoing piece is Ψ_1 . A quasinormal mode is a solution that is purely ingoing at the future horizon and decays in time; with time dependence $e^{i\omega t}$ this means $\text{Im } \omega > 0$ and the coefficient of Ψ_1 vanishes. Anti-QNMs

are the time-reversed modes (purely outgoing at the past horizon).

For the asymptotic-boundary problem, the QNM condition is $C_{31}(\omega) = 0$ with $\text{Im } \omega > 0$, giving $\omega = i(2\lambda_0)(n + m + \frac{1}{2})$ for $n = 0, 1, 2, \dots$, and similarly $C_{32}(\omega) = 0$ gives the anti-QNMs at $\omega = -i(2\lambda_0)(n + m + \frac{1}{2})$. This is the familiar infinite tower along the imaginary axis.

The corresponding S-matrix²⁴ is

$$\mathcal{S}(\omega) = -\frac{C_{31}(\omega)}{C_{32}(\omega)} = -\frac{\Gamma(\frac{1}{2} + i\tilde{\omega}) \Gamma(\frac{1}{2} + m - i\tilde{\omega})}{\Gamma(\frac{1}{2} - i\tilde{\omega}) \Gamma(\frac{1}{2} + m + i\tilde{\omega})} \quad (\text{F.58})$$

and indeed its zeros (poles) in the upper (lower) half-plane reproduce the QNM (anti-QNM) spectrum.

Now comes the key point. When m is a positive integer, the analytic structure collapses: many of the Gamma-function poles that generate the infinite tower are paired up between numerator and denominator and cancel. Equivalently (and more geometrically), at integer m the hypergeometric functions appearing in the mode solutions truncate to polynomials.

Concretely, ${}_2F_1(a, b, c, x)$ becomes a polynomial of degree $n \in \mathbb{Z}_{\geq 0}$ whenever one of $a, b, c - a, c - b$ equals $-n$ [94]. For example, if $a = -n$ then

$${}_2F_1(-n, b, c, x) = \sum_{k=0}^n (-1)^k \binom{n}{k} \frac{(b)_k}{(c)_k} x^k, \quad (b)_n := b(b+1)(b+2)\dots(b+n-1), \quad n \in \mathbb{Z}_{\geq 0} \quad (\text{F.59})$$

The other truncation cases follow from the usual symmetry and connection identities of ${}_2F_1$. In our problem, the frequency ω enters only through the remaining hypergeometric parameters (and hence through finite Pochhammer symbols). As a result, the mode functions—and therefore the Jöst function—become rational functions of ω of finite degree, so only finitely many poles/zeros (and hence QNMs) remain.

To be more explicit, we now specialize to $m = 1$, which corresponds to the two-QNM model studied in the main text. The mode functions become

$$\Psi_1(\omega, y) = \left[\begin{array}{c} x^{-\frac{i\tilde{\omega}}{2}} (1-x)^{-1} \left(1 - x \left(\frac{\tilde{\omega} - \frac{i}{2}}{\tilde{\omega} + \frac{i}{2}} \right) \right) \\ \frac{i}{-\tilde{\omega} - \frac{i}{2}} x^{\frac{1}{2} - \frac{i\tilde{\omega}}{2}} (1-x)^{-1} \end{array} \right], \quad \Psi_2(\omega, y) = \left[\begin{array}{c} \frac{i}{\tilde{\omega} - \frac{i}{2}} x^{\frac{1}{2} + \frac{i\tilde{\omega}}{2}} (1-x)^{-1} \\ x^{\frac{i\tilde{\omega}}{2}} (1-x)^{-1} \left(1 - x \left(\frac{-\tilde{\omega} - \frac{i}{2}}{-\tilde{\omega} + \frac{i}{2}} \right) \right) \end{array} \right] \quad (\text{F.60})$$

$$\Psi_3 = \frac{-2i}{\tilde{\omega} - \frac{i}{2}} \Psi_1 + \frac{2i}{\tilde{\omega} + \frac{i}{2}} \Psi_2, \quad \Psi_4 = \frac{\tilde{\omega} + \frac{i}{2}}{2i} \Psi_1 + \frac{\tilde{\omega} - \frac{i}{2}}{2i} \Psi_2 \quad (\text{F.61})$$

If the boundary is placed at the asymptotic boundary, we must choose the normalizable mode Ψ_3 as the physical solution. In this case there are no QNMs, since $C_{31}(\omega) = \frac{-2i}{\tilde{\omega} - \frac{i}{2}}$ has no zeros in the upper half-plane.

We now move the boundary to a finite location $x_0 = e^{-2\lambda z_0}$. Using the definition of the Jöst function in (F.26), we obtain

$$\mathcal{J}(\omega) = -ie^{i\omega \frac{z_0}{2}} \frac{\omega^2 + ib_1\omega + b_0}{\sqrt{2\mu}(\omega + i\lambda_0)}, \quad b_1 := \mu + \frac{1 + \sqrt{x_0}}{1 - \sqrt{x_0}} \lambda, \quad b_2 = -\frac{1 - \sqrt{x_0}}{1 + \sqrt{x_0}} \lambda \mu \quad (\text{F.62})$$

²⁴In some literature one subtracts a ‘‘Rindler background’’ factor $\Gamma(\frac{1}{2} + i\tilde{\omega})/\Gamma(\frac{1}{2} - i\tilde{\omega})$ when discussing the density of states for real ω and static-patch thermodynamics. For our purpose—reconstructing geometry from the full S-matrix—we keep the full expression. HT thanks Albert Law and Zimo Sun for discussions of this point.

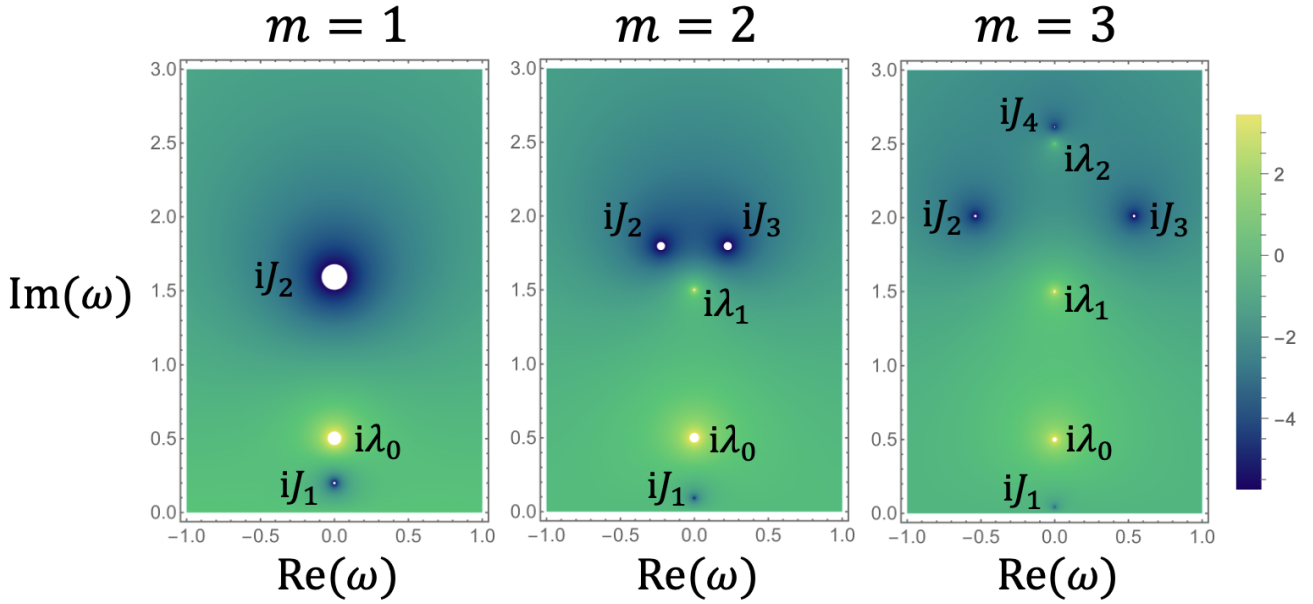


Figure 10: We numerically plot an example of $\log|\mathcal{S}(\omega)|$ on the upper half plane for several integer $m = 1, 2, 3$, and label their poles (yellow dots) and residue (blue dots). The boundary location is set at $x = 0.05$ (see (F.52) for definition of coordinate x) with boundary condition parameter $\mu = 1$.

Since the numerator is a quadratic polynomial in ω , $\mathcal{J}(\omega)$ has two zeros. Substituting the relations from (4.4) and (F.2) to express z_0, λ_0, μ in terms of $\{c_i, J_i\}_{i=1}^2$, the Jöst function takes the factorized form

$$\mathcal{J}(\omega) = -ie^{i\omega\frac{z_0}{2}} \frac{(\omega + iJ_1)(\omega + iJ_2)}{\sqrt{2\mu}(\omega + i\lambda_0)} \quad (\text{F.63})$$

QNMs are zeros of $-\mathcal{J}(-\omega)$ in the upper half-plane, so we find two QNMs at $\{iJ_1, iJ_2\}$. The boundary spectral function and S-matrix then follow from (F.22) and (F.25):

$$\mathcal{A}(\omega) = (2\mu) \frac{(\omega^2 + \lambda_0^2)}{(\omega^2 + J_1^2)(\omega^2 + J_2^2)}, \quad \mathcal{S}(\omega) = e^{i\omega z_0} \times \frac{i\lambda_0 + \omega}{i\lambda_0 - \omega} \times \prod_{i=1}^2 \frac{iJ_i - \omega}{iJ_i + \omega} \quad (\text{F.64})$$

This agrees with the boundary computation in (2.52) and (2.54). The extra phase factor $e^{i\omega z_0}$ arises because the near-horizon normalization in (F.53) differs from that in (F.8): near the horizon, $e^{\pm i\tilde{\omega}y} = e^{\pm i\omega z} e^{\pm i\omega\frac{z_0}{2}}$.

Finally, we comment on the generic structure at integer mass m in AdS₂–Rindler. In the bulk description the tunable parameters are λ_0, μ, z_0 : λ_0 sets the AdS length scale, while μ and z_0 fix the boundary condition and the boundary location. The Jöst function can be written as $\mathcal{J}(\omega) = \Psi_{1,L}(\omega, z_0)a_R(\omega) - \Psi_{1,R}(\omega, z_0)a_L(\omega)$, so its poles can arise only from the mode function $\Psi_1(\omega, z)$. Using (F.55) together with the integer-mass truncation property (F.59), one finds that poles can occur only at $\omega \in i(2\lambda_0)\{-\frac{1}{2}, -\frac{3}{2}, \dots, -m + \frac{1}{2}\}$. The zeros of $\mathcal{J}(\omega)$ must in general be found numerically; one typically obtains $m + 1$ zeros. Accordingly, the Jöst function has the schematic form

$$\mathcal{J}(\omega) \propto e^{i\omega\frac{z_0}{2}} \frac{\prod_{k=1}^{m+1}(\omega + iJ_k)}{\prod_{n=0}^{m-1}(\omega + i\lambda_n)}, \quad \lambda_n := 2\lambda_0(n + \frac{1}{2}) \quad (\text{F.65})$$

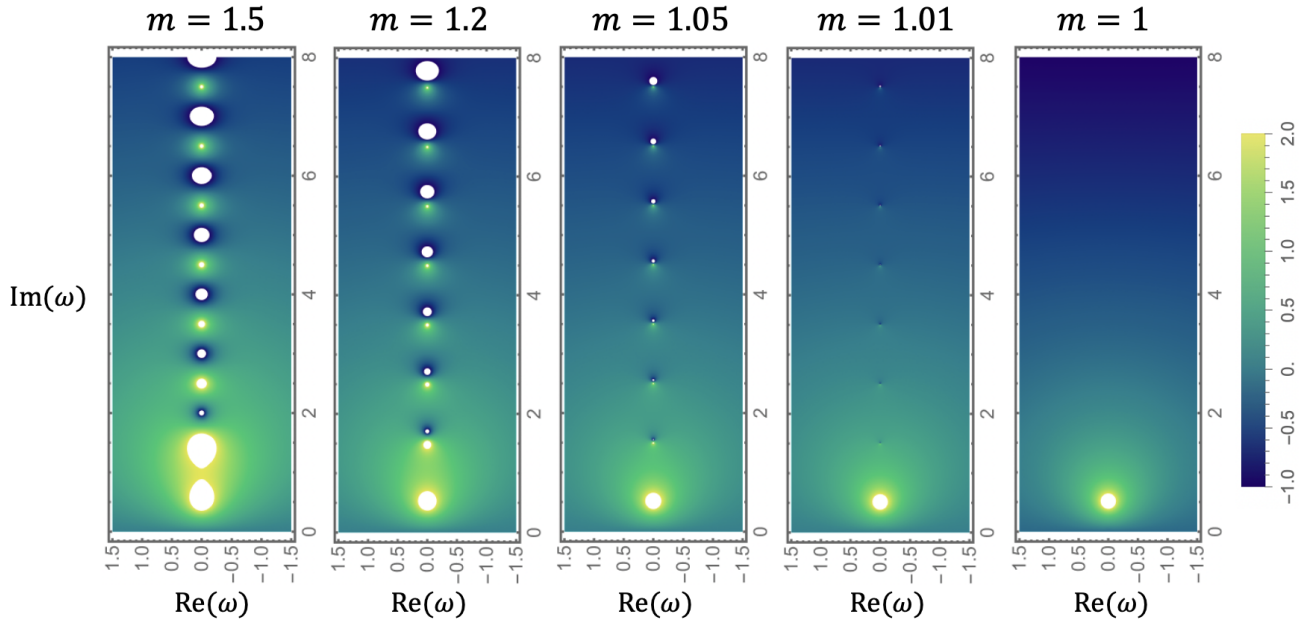


Figure 11: We numerically plot an example of $\log|\mathcal{S}(\omega)|$ on the upper half plane, gradually tuning mass m from non-integer ($m = 1.5, 1.2, 1.05, 1.01$) to integer ($m = 1$), and label their poles (yellow dots) and residue (blue dots). The boundary location is set at $x = 0.9$ (see (F.52) for definition of coordinate x) with boundary condition parameter $\mu = 1$.

In fig. 10 we plot $\log|\mathcal{S}(\omega)|$ on the upper half-plane for several integer values of m . We observe poles at $\{i\lambda_n\}_{n=0}^{m-1}$ and zeros at $\{iJ_k\}_{k=1}^{m+1}$.

In fig. 11 we fix the remaining parameters and continuously tune m from non-integer to integer. For non-integer m , there are infinitely many poles and zeros, with poles on the half-integer lattice $\{i\lambda_n\}_{n=0}^{+\infty}$. As m approaches an integer, most poles and zeros collide and cancel, leaving only finitely many.

G Technical detail of deriving inverse scattering formula

In this appendix we provide the derivation of the inverse-scattering formula (2.49), which inverts the forward-scattering relation (2.48). We then show how (2.49) reduces to the main results (1.2) and (1.3). The derivation uses the bulk-QFT setup developed in section F, and throughout we assume (F.27).

Rather than attempting a direct inversion of (2.48), we follow the standard Marchenko inverse-scattering route, adapted to the Majorana system. Our steps closely parallel the scalar-field treatment in Chapter 20 of [33].

We start from the Majorana equation (F.7). The incoming solution $\phi(\omega, z)$ satisfies the Volterra equation (F.28), which we repeat for convenience:

$$\phi(\omega, z) = \begin{bmatrix} e^{i\omega z} \\ 0 \end{bmatrix} - \int_z^{+\infty} dz' \begin{bmatrix} 0 & e^{i\omega(z-z')} \\ e^{-i\omega(z-z')} & 0 \end{bmatrix} m\Omega(z')\phi(\omega, z') \quad (\text{G.1})$$

This Volterra equation admits an iterative expansion around the free solution

$$\phi^{(0)}(\omega, z) := \begin{bmatrix} e^{i\omega z} \\ 0 \end{bmatrix} \quad (\text{G.2})$$

Equivalently, one can package the interaction with $m\Omega(z)$ into a (retarded) kernel along the z direction:

$$\phi(\omega, z) = \phi^{(0)}(\omega, z) + \int_z^{+\infty} dz' \begin{bmatrix} C_1(z, z') \\ C_2(z, z') \end{bmatrix} e^{i\omega z'} \quad (\text{G.3})$$

where $C_{1,2}(z, z')$ are supported only for $z < z'$. Plugging this ansatz into the Majorana equation (F.7) gives the kernel equations

$$(\partial_z + \partial_{z'})C_1(z, z') = m\Omega(z)C_2(z, z'), \quad (\partial_z - \partial_{z'})C_2(z, z') = m\Omega(z)C_1(z, z'), \quad m\Omega(z) = -2C_2(z, z) \quad (\text{G.4})$$

Setting $z' = z$ in the first equation yields $\partial_z C_1(z, z) = m\Omega(z)C_2(z, z)$. Using the third relation to eliminate C_2 gives

$$m^2\Omega(z)^2 = -2\partial_z C_1(z, z) \quad (\text{G.5})$$

To determine $C_1(z, z')$, we now take an inverse Fourier transform:

$$\begin{aligned} \begin{bmatrix} C_1(z, z') \\ C_2(z, z') \end{bmatrix} &= \int_{-\infty}^{+\infty} \frac{d\omega}{2\pi} e^{-i\omega z'} [\phi(\omega, z) - \phi^{(0)}(\omega, z)] \\ &= \int_{-\infty}^{+\infty} \frac{d\omega}{2\pi} e^{i\omega z'} [\phi(-\omega, z) - \phi^{(0)}(-\omega, z)] \\ &= \int_{-\infty}^{+\infty} \frac{d\omega}{2\pi} e^{i\omega z'} \left[\mathcal{S}(\omega)\sigma_1\phi(\omega, z) + \frac{\sigma_1\tilde{\varphi}(\omega, z)}{\mathcal{J}(\omega)} - \phi^{(0)}(-\omega, z) \right] \end{aligned} \quad (\text{G.6})$$

where in the first step we relabeled the dummy variable $\omega \rightarrow -\omega$, and in the last step we used (F.9) and (F.22).

Using (F.41) to rewrite $\phi(-\omega, z)$ in terms of $\tilde{\varphi}(\omega, z)$, it is convenient to split the integrand into four pieces:

$$\begin{aligned} &\left[\mathcal{S}(\omega)\sigma_1\phi(\omega, z) + \frac{\sigma_1\tilde{\varphi}(\omega, z)}{\mathcal{J}(\omega)} - \phi^{(0)}(-\omega, z) \right] = \\ &\underbrace{[\mathcal{S}(\omega) - \mathcal{S}_\infty]\sigma_1 [\phi(\omega, z) - \phi^{(0)}(\omega, z)]}_{\text{(I)}} + \underbrace{[\mathcal{S}(\omega) - \mathcal{S}_\infty]\sigma_1\phi^{(0)}(\omega, z)}_{\text{(II)}} \\ &+ \underbrace{\mathcal{S}_\infty\sigma_1 [\phi(\omega, z) - \phi^{(0)}(\omega, z)]}_{\text{(III)}} + \underbrace{\sigma_1 \left\{ \frac{\tilde{\varphi}(\omega, z)}{\mathcal{J}(\omega)} - [-\mathcal{S}_\infty\sigma_1\phi^{(0)}(\omega, z) + \phi^{(0)}(-\omega, z)] \right\}}_{\text{(IV)}} \end{aligned} \quad (\text{G.7})$$

The key simplification is that (III) and (IV) do not contribute once we do the ω contour integral. For (III), using the bound (F.35) we have $|e^{i\omega z'}(\phi(\omega, z) - \phi^{(0)}(\omega, z))| \sim e^{-(\text{Im}\omega)(z+z')}$ for $\text{Im}\omega > 0$. We can therefore close the contour in the upper half-plane, and analyticity of $\phi(\omega, z)$ there (cf. (F.34)) implies

$$\int_{-\infty}^{+\infty} \frac{d\omega}{2\pi} e^{i\omega z'} \text{(III)} = 0. \quad (\text{G.8})$$

Similarly, for (IV) the bound (F.43) gives $|e^{i\omega z'}(\text{IV})| \sim e^{-(\text{Im}\omega)(z'-z)}$ for $\text{Im}\omega > 0$. Since $z' > z$, we again close the contour upstairs, and analyticity (cf. (F.42)) gives

$$\int_{-\infty}^{+\infty} \frac{d\omega}{2\pi} e^{i\omega z'}(\text{IV}) = 0. \quad (\text{G.9})$$

Thus only (I) and (II) remain. Define:

$$\tilde{S}(z) = \int_{-\infty}^{+\infty} \frac{d\omega}{2\pi} e^{i\omega z} [\mathcal{S}(\omega) - \mathcal{S}_\infty] \quad (\text{G.10})$$

Combining this definition with (G.6) gives the Marchenko equation for the kernels $C_{1,2}(z, z')$:

$$C_1(z, z') = \int_z^{+\infty} dz'' \tilde{S}(z' + z'') C_2(z, z''), \quad C_2(z, z') = \tilde{S}(z + z') + \int_z^{+\infty} dz'' \tilde{S}(z' + z'') C_1(z, z'') \quad (\text{G.11})$$

It is convenient to introduce

$$\tilde{h}(z_1, z_2) := \tilde{S}(z_1 + z_2), \quad \tilde{h}_z(z_1, z_2) := \tilde{S}(z_1 + z_2) \Theta(z_2 - z) \quad (\text{G.12})$$

and to regard $C_1, C_2, \tilde{h}, \tilde{h}_z$ as integral operators on $L^2(\mathbb{R})$. In operator notation, the Marchenko system becomes

$$C_1 = C_2 \tilde{h}_z^\top, \quad C_2 = \tilde{h} + C_1 \tilde{h}_z^\top \quad (\text{G.13})$$

Eliminating C_2 yields

$$C_1 = \tilde{h} \cdot \tilde{h}_z^\top (1 - \tilde{h}_z^\top)^{-1} \quad (\text{G.14})$$

By (G.5), the conformal factor is determined by the diagonal of C_1 , which we extract using a Fredholm determinant identity:

$$\begin{aligned} & \partial_z \log \det \left(\mathbf{1} - \tilde{h}_z^\top \right) \\ &= -\text{Tr} \left[(1 - \tilde{h}_z^\top)^{-1} (\partial_z \tilde{h}_z^\top \cdot \tilde{h}_z^\top + \tilde{h}_z^\top \cdot \partial_z \tilde{h}_z^\top) \right] \\ &= - \int dz_1 dz_2 dz_3 (1 - \tilde{h}_z^\top)^{-1}_{(z_1, z_2)} \left[(\partial_z \tilde{h}_z)_{(z_3, z_2)} (\tilde{h}_z^\top)_{(z_3, z_1)} + (\tilde{h}_z^\top)_{(z_2, z_3)} (\partial_z \tilde{h}_z)_{(z_1, z_3)} \right] \\ &= \int dz_1 dz_2 dz_3 (1 - \tilde{h}_z^\top)^{-1}_{(z_1, z_2)} \left[\tilde{S}(z_3 + z_2) \delta(z - z_2) (\tilde{h}_z^\top)_{(z_3, z_1)} + \tilde{S}(z_1 + z_3) \delta(z - z_3) (\tilde{h}_z^\top)_{(z_2, z_3)} \right] \\ &= \int dz_1 dz_3 \cdot \tilde{S}(z + z_3) (\tilde{h}_z^\top)_{(z_3, z_1)} (1 - \tilde{h}_z^\top)^{-1}_{(z_1, z)} + \int dz_1 dz_2 \cdot \tilde{S}(z + z_1) (1 - \tilde{h}_z^\top)^{-1}_{(z_1, z_2)} (\tilde{h}_z^\top)_{(z_2, z)} \\ &= (\tilde{h} \tilde{h}_z^\top (1 - \tilde{h}_z^\top)^{-1})_{(z, z)} + (\tilde{h} (1 - \tilde{h}_z^\top)^{-1} \tilde{h}_z^\top)_{(z, z)} \\ &= 2(\tilde{h} \tilde{h}_z^\top (1 - \tilde{h}_z^\top)^{-1})_{(z, z)} \\ &= 2C_1(z, z) \end{aligned} \quad (\text{G.15})$$

Combine with (G.5), we obtain:

$$m^2 \Omega(z)^2 = -\partial_z^2 \log \det \left(\mathbf{1} - \tilde{h}_z^\top \right) \quad (\text{G.16})$$

To streamline notation, introduce the projector $P_z = \mathbf{1}_{[z, +\infty)}$ so that $\tilde{h}_z = \tilde{h}P_z$. Using the expansion of $\log \det$ in traces and the identity $\text{Tr}[(P_z \tilde{h})^{2n}] = \text{Tr}[(P_z \tilde{h} P_z)^{2n}]$, we obtain

$$m^2 \Omega(z)^2 = -\partial_z^2 \log \det \left[\mathbf{1} - (P_z \tilde{h} P_z)^2 \right] \quad (\text{G.17})$$

Relative to (2.49) in the main text, the only difference is that here we used $\mathcal{S}(\omega) - \mathcal{S}_\infty$ in defining $\tilde{S}(z)$. Physically, subtracting $\mathcal{S}_\infty = -1$ removes the hard-wall contribution from the boundary scatterer at $z = 0$. Since we are interested in $\Omega(z)$ for $z > 0$, this subtraction is inessential: at leading order (cf. (E.8)) it only produces a $\delta(z)$ term, and in the pole expansion the constant piece does not affect the sum.

Accordingly, we may drop the $-\mathcal{S}_\infty$ subtraction and recover (2.49) exactly as stated in the main text.

To connect with (1.2) and (1.3), we now use the pole expansion of $S(z)$ on the upper half-plane (cf. (2.56) in the main text):

$$S(z) = \sum_i \beta_i e^{-\lambda_i z}, \quad z > 0 \quad (\text{G.18})$$

We only need the projected operator $\mathfrak{h}_z := P_z h P_z$, which acts on functions supported on $[z, \infty)$. To make the z -dependence explicit, shift variables $z_i = z + x_i$ with $x_i > 0$ and work on $\mathcal{H}_{\text{con}} := L^2(\mathbb{R}_{>0})$. Then \mathfrak{h}_z acts as

$$\begin{aligned} (\mathfrak{h}_z f)(x_1) &= \int_0^{+\infty} dx_2 S(2z + x_1 + x_2) f(x_2) \\ &= \sum_n \beta_n e^{-\lambda_n 2z} e^{-\lambda_n x_1} \int_0^{+\infty} dx_2 e^{-\lambda_n x_2} f(x_2) \end{aligned} \quad (\text{G.19})$$

This factorized form suggests introducing an auxiliary discrete space $\mathcal{H}_{\text{dis}} := \text{span}\{|n\rangle\}$ and operators

$$T_1 : \mathcal{H}_{\text{dis}} \rightarrow \mathcal{H}_{\text{con}}, \quad \langle x | T_1 | n \rangle := \beta_n e^{-\lambda_n 2z} e^{-\lambda_n x} \quad (\text{G.20})$$

$$T_2 : \mathcal{H}_{\text{con}} \rightarrow \mathcal{H}_{\text{dis}}, \quad \langle n | T_2 | x \rangle := e^{-\lambda_n x} \quad (\text{G.21})$$

so that $\mathfrak{h}_z = T_1 T_2$. Using Sylvester's determinant theorem, $\det(\mathbf{1} - T_1 T_2 T_1 T_2) = \det(\mathbf{1} - T_2 T_1 T_2 T_1)$, we obtain

$$m^2 \Omega(z)^2 = -\partial_z^2 \log \det(\mathbf{1} - \mathfrak{h}_z^2) = -\partial_z^2 \log \det(\mathbf{1}_{\mathcal{H}_{\text{con}}} - T_1 T_2 T_1 T_2) = -\partial_z^2 \log \det(\mathbf{1}_{\mathcal{H}_{\text{dis}}} - T_2 T_1 T_2 T_1) \quad (\text{G.22})$$

We now introduce the auxiliary matrix $B(z)$ acting on \mathcal{H}_{dis} ,

$$B(z) := T_2 T_1, \quad (\text{G.23})$$

with matrix elements

$$\begin{aligned} B(z)_{nm} &= \langle n | T_2 T_1 | m \rangle = \int_0^{+\infty} dx \langle n | T_2 | x \rangle \langle x | T_1 | m \rangle = \int_0^{+\infty} dx \cdot \beta_m e^{-\lambda_m 2z} e^{-(\lambda_m + \lambda_n)x} \\ &= \frac{\beta_m e^{-\lambda_m 2z}}{\lambda_n + \lambda_m} \end{aligned} \quad (\text{G.24})$$

Substituting into (G.22) yields the compact form of (1.2) and (1.3):

$$m^2\Omega(z)^2 = -\partial_z^2 \log \det[\mathbf{1} - B(z)^2] \quad (\text{G.25})$$

H Technical details of near horizon algebra

This appendix collects technical details related to the near-horizon algebra discussed in section 6. In section H.1 we benchmark that the definition of P^\pm and B in (6.7) matches the exact $\text{sl}(2, \mathbb{R})$ generators for a massive Majorana fermion in AdS_2 -Rindler with an asymptotic boundary and standard normalizable boundary conditions. In section H.2.2 we derive (6.13), showing that the commutator $[P^-, P^+]$ acting on bifurcate-horizon modes is proportional to the boost generator.

H.1 $\text{sl}(2, \mathbb{R})$ algebra in AdS_2 -Rindler

Consider a massive Majorana fermion on AdS_2 -Rindler, with metric:

$$ds^2 = \Omega(z)^2(-dt^2 + dz^2), \quad \Omega(z) = \frac{1}{\sinh z}, \quad z \geq 0 \quad (\text{H.1})$$

On any constant t slice, one can write down the three generators of $\text{sl}(2, \mathbb{R})$ represented in terms of fermion bilinear:

$$\begin{aligned} H(t) &:= \frac{i}{4\pi} \int_0^{+\infty} dz \cdot \Psi_L \partial_z \Psi_L - \Psi_R \partial_z \Psi_R - 2m\Omega(z) \Psi_L \Psi_R \\ L^+(t) &:= \frac{i}{4\pi} e^t \int_0^{+\infty} dz \cdot e^z \Psi_L \partial_z \Psi_L - e^{-z} \Psi_R \partial_z \Psi_R - 2m(\coth z) \Psi_L \Psi_R \\ L^-(t) &:= \frac{i}{4\pi} e^{-t} \int_0^{+\infty} dz \cdot e^{-z} \Psi_L \partial_z \Psi_L - e^z \Psi_R \partial_z \Psi_R - 2m(\coth z) \Psi_L \Psi_R \end{aligned} \quad (\text{H.2})$$

The boost generator $H(t)$ is the Hamiltonian, which follows from the action (2.9). The ladder operators L^\pm can be constructed by writing the corresponding Killing vector field $\xi^t \partial_t + \xi^z \partial_z$, then replacing ∂_t by the Hamiltonian density $\mathcal{H}(t, z) \propto \Psi_L \partial_z \Psi_L - \Psi_R \partial_z \Psi_R - 2m\Omega(z) \Psi_L \Psi_R$ and ∂_z by the momentum density $\mathcal{P}(t, z) \propto \Psi_L \partial_z \Psi_L + \Psi_R \partial_z \Psi_R$, and finally integrating along a constant-time slice.

A straightforward calculation shows that the $\text{sl}(2, \mathbb{R})$ algebra holds:

$$[H, L^\pm] = \pm iL^\pm, \quad [L^-, L^+] = -iRH, \quad \text{with } R = -2 \quad (\text{H.3})$$

where R is the Ricci scalar. Owing to the explicit factors $e^{\pm t}$ in L^\pm , one finds that the ladder operators are in fact time independent:

$$\frac{d}{dt} L^\pm(t) = \partial_t L^\pm + [iH, L^\pm] = 0. \quad (\text{H.4})$$

Thus they may be pushed to the future/past horizons at $t = \pm\infty$.

First, we consider pushing $L^+(t)$ to past horizon ($t = -\infty$). One first change to lightcone

coordinate:

$$L_+(t) = \frac{i}{4\pi} \int_t^{+\infty} dv e^v \Psi_L \partial_v \Psi_L - e^{2t-v} \Psi_R \partial_v \Psi_R - e^t 2m \coth \frac{v-t}{2} \Psi_L \Psi_R \quad (\text{H.5})$$

As $t \rightarrow -\infty$, the last two terms drop out due to the suppression by e^t and e^{2t} , and in the first term the fermion $\Psi_L(u, v)|_{u=2t-v}$ becomes the horizon mode $\Psi^p(v)$. Therefore,

$$L^+(-\infty) = \frac{i}{4\pi} \int_{-\infty}^{+\infty} dv \cdot \Psi^p(v) e^v \partial_v \Psi^p(v) = \frac{i}{4\pi} \int_{-\infty}^0 dV \cdot \Upsilon^p \partial_V \Upsilon^p \quad (\text{H.6})$$

where in the last equality we used (6.3), i.e. $\Psi^p(v) = e^{-v/2} \Upsilon^p(V)$, to pass to Kruskal coordinates. Comparing with (6.7), we find $L^+(-\infty) \equiv P^+$. A similar computation gives $L^-(+\infty) \equiv P^-$.

Then, we consider pushing $H(t)$ to past horizon ($t = -\infty$). Similarly, one first change to lightcone coordinate:

$$H(t) = \frac{i}{4\pi} \int_t^{+\infty} dv \cdot \Psi_L \partial_v \Psi_L - \Psi_R \partial_v \Psi_R - 2m (\sinh \frac{v-t}{2})^{-1} \Psi_L \Psi_R \quad (\text{H.7})$$

As $t \rightarrow -\infty$, the third term drops out due to $(\sinh \frac{t}{2})^{-1}$ suppression, and the second term also drops out since $\partial_v \Psi_R \rightarrow 0$. This is because, in light-cone quantization, the right-mover along the past horizon becomes non-dynamical. Therefore, we find:

$$H(-\infty) = \frac{i}{4\pi} \int_{-\infty}^{+\infty} dv \cdot \Psi_L \partial_v \Psi_L = -\frac{i}{4\pi} \int_{-\infty}^0 dV \cdot \Upsilon^p V \partial_V \Upsilon^p \quad (\text{H.8})$$

Comparing with (6.7), we indeed find $H(-\infty) \equiv B$. A similar calculation shows that $H(+\infty) \equiv B$.

To summarize, pushing the AdS_2 generators defined on a constant-time slice (H.2) to the future/past horizons yields the null-translation and boost generators on the horizon defined in (6.7).

H.2 Curvature from algebra at bifurcate horizon

In this appendix, we will explain how does the curvature at horizon shows up from the commutator $[P^-, P^+]$ acting on modes at bifurcate horizon. First, in section H.2.1 we will describe a useful contour prescription in frequency space. Based on this, in section H.2.2, we will derive (6.13). In the end, we will benchmark this result on AdS_2 -Rindler special case in section H.2.3.

H.2.1 Preparation: a contour prescription in frequency space

In this section we motivate and develop a contour prescription that will be important in section H.2.2.

Consider the anti-commutator between the bifurcate-horizon mode $\Upsilon^p(0)$ and a boundary operator $\chi(t)$. Since the bifurcate horizon is spacelike separated from any boundary point, one

expects $\{\Upsilon^p(0), \chi(t)\} = 0$ for all t . This can be checked directly:

$$\begin{aligned} \{\Psi^p(v), \chi(t)\} &= \int dt' \mathcal{K}^p(t' - v) A(t - t') \\ &= \int d\omega e^{-i\omega(v-t)} \mathcal{K}^p(-\omega) \mathcal{A}(\omega) \\ &= \int d\omega e^{-i\omega(v-t)} \mathcal{R}^p(\omega) \end{aligned} \quad (\text{H.9})$$

In the first line we used the definition of the horizon mode in (2.33). In the second and third lines we used $\mathcal{K}^p(\omega) \mathcal{A}(\omega) \mathcal{K}^p(-\omega) = 1$ from (2.37) and $\mathcal{R}^p(\omega) := \frac{1}{\mathcal{K}^p(\omega)}$. In section 2.3.1 we showed that, in the absence of bound states in the upper half-plane, $\mathcal{R}^p(\omega)$ has the same analyticity properties as $\mathcal{K}^p(\omega)$. It follows that $\{\Psi^p(v), \chi(t)\} = 0$ for $t < v$. Using $\Psi^p(v) = \sqrt{-2\lambda_0 V} \Upsilon^p(V)$ and $V = -e^{-2\lambda_0 v}$, we can send $v \rightarrow +\infty$ (equivalently $V \rightarrow 0$) to obtain $\Upsilon^p(0)$ at the bifurcate horizon, and hence $\{\Upsilon^p(0), \chi(t)\} = 0$ for all t , as expected.

Formally, the above computation corresponds to

$$\lim_{V \rightarrow 0} [\{\Upsilon^p(V), \chi(t)\}] = 0. \quad (\text{H.10})$$

It is illuminating to consider the opposite order of limits,

$$\{\lim_{V \rightarrow 0} [\Upsilon^p(V)], \chi(t)\}, \quad (\text{H.11})$$

i.e. to first take $V \rightarrow 0$ in $\Upsilon^p(V)$ and then compute the anti-commutator. Define $\beta_k^p := i \text{Res}[\mathcal{K}^p(\omega \rightarrow i\lambda_k)]$ in the upper half-plane, so that

$$\mathcal{K}^p(t) := \Theta(-t) \sum_k \beta_k^p e^{\lambda_k t}. \quad (\text{H.12})$$

Then

$$\Upsilon^p(V) = \frac{1}{\sqrt{2\lambda_0}} e^{\lambda_0 v} \int_{-\infty}^v dt' \mathcal{K}^p(t' - v) \chi(t') = \frac{1}{\sqrt{2\lambda_0}} \int_{-\infty}^v dt' \sum_k \beta_k^p e^{-(\lambda_k - \lambda_0)v} e^{\lambda_k t'} \chi(t'). \quad (\text{H.13})$$

As $V \rightarrow 0$ (i.e. $v \rightarrow +\infty$), only the $k = 0$ term survives, giving

$$\Upsilon^p(0) = \frac{\beta_0^p}{\sqrt{2\lambda_0}} \int_{-\infty}^{+\infty} dt' e^{\lambda_0 t'} \chi(t'). \quad (\text{H.14})$$

The corresponding anti-commutator is

$$\{\Upsilon^p(0), \chi(t)\} = \frac{\beta_0^p}{\sqrt{2\lambda_0}} \int_{-\infty}^{+\infty} dt' e^{\lambda_0 t'} A(t, t') = \frac{\beta_0^p}{\sqrt{2\lambda_0}} \int_{-\infty}^{+\infty} dt' e^{\lambda_0 t'} \sum_n c_n e^{-J_n |t - t'|}. \quad (\text{H.15})$$

The dt' integral diverges as $t' \rightarrow +\infty$ whenever there exists any $J_n \leq \lambda_0$. In particular, if $J_0 \leq \lambda_0$ then $\{\Upsilon^p(0), \chi(t)\} = \infty$ rather than 0. This contradiction shows that the two limits do not commute:

$$\lim_{V \rightarrow 0} [\{\Upsilon^p(V), \chi(t)\}] \neq \{\lim_{V \rightarrow 0} [\Upsilon^p(V)], \chi(t)\}. \quad (\text{H.16})$$

The second (naive) computation can nevertheless be repaired by a contour prescription. Rewriting (H.15) in frequency space gives

$$\{\Upsilon^p(0), \chi(t)\} = \frac{\beta_0^p}{\sqrt{2\lambda_0}} \int dt' d\omega e^{\lambda_0 t'} e^{i\omega(t-t')} A(\omega) = \frac{\beta_0^p}{\sqrt{2\lambda_0}} \int dt' d\omega e^{-i(\omega+i\lambda_0)t'} e^{i\omega t} A(\omega). \quad (\text{H.17})$$

Both t' and ω are initially integrated along \mathbb{R} . If we shift the ω contour from \mathbb{R} to $\mathbb{R} - i\lambda_0$, i.e. set $\omega = \omega' - i\lambda_0$ with $\omega' \in \mathbb{R}$, then the dt' integral produces $\delta(\omega')$, and we obtain

$$\{\Upsilon^p(0), \chi(t)\} \supset \frac{\beta_0^p}{\sqrt{2\lambda_0}} e^{\lambda_0 t} \mathcal{A}(-i\lambda_0) = 0, \quad (\text{H.18})$$

where we used that $-i\lambda_0$ is a zero of $A(\omega)$. This reproduces the expected result.

However, in shifting the ω contour from \mathbb{R} to $\mathbb{R} - i\lambda_0$, one crosses poles of $\mathcal{A}(\omega)$ at $\{-iJ_n \mid J_n < \lambda_0\}$. These poles generate precisely the divergent real-space contributions discussed below (H.15). The contour prescription is therefore: “When shifting the ω contour from \mathbb{R} to $\mathbb{R} - i\lambda_0$, ignore the poles at $\{-iJ_n \mid J_n < \lambda_0\}$.”

In the next section we will see that the same prescription is required to derive (6.13).

H.2.2 Derive (6.13)

The physics of the derivation is simple: $[P^-, P^+]$ is written as a bilocal operator on the past horizon, but when it acts on the bifurcate-horizon mode $\Upsilon^p(0)$ only the $V \rightarrow 0$ region matters, and the bilocal kernel collapses to a local boost action.

Starting from (6.12) and using (6.5) and (2.47), we can write

$$[P^-, P^+] = -\frac{(2\lambda_0)^{-2}}{8\pi^2} \int_{-\infty}^{+\infty} dv_1 dv_2 \Psi^p(v_1) \Psi^p(v_2) f(v_1 - v_2) \quad (\text{H.19})$$

with

$$\text{with: } f(v) := 2 \sinh(\lambda_0 v) \partial_v^2 \int_{-\infty}^{+\infty} du e^{-2\lambda_0 u} S\left(\frac{v}{2} - u\right) S\left(-\frac{v}{2} - u\right) \quad (\text{H.20})$$

To see how this becomes local, we go to Fourier space,

$$f(v) := \int d\omega e^{i\omega v} \tilde{f}(\omega). \quad (\text{H.21})$$

Expanding $\tilde{f}(\omega)$ around $\omega = 0$ packages the bilocal kernel into a local differential operator acting along the horizon coordinate v :

$$[P^-, P^+] = -\frac{(2\lambda_0)^{-2}}{4\pi} \int dv \Psi^p(v) \tilde{f}(-i\partial_v) \Psi^p(v). \quad (\text{H.22})$$

Now switch to Kruskal V using (6.3). The point is that ∂_v becomes a dilatation operator $2\lambda_0 V \partial_V$, and the extra $\sqrt{-V}$ factors shift the differential operator by $i\lambda_0$. Concretely,

$$[P^-, P^+] = -\frac{1}{4\pi} (2\lambda_0)^{-2} \int \frac{dV}{-2\lambda_0 V} \sqrt{-2\lambda_0 V} \Upsilon^p(V) \tilde{f}(i2\lambda_0 V \partial_V) \left[\sqrt{-2\lambda_0 V} \Upsilon^p(V) \right]. \quad (\text{H.23})$$

Using $(i2\lambda_0 V \partial_V)(\sqrt{-2\lambda_0 V}) = (\sqrt{-2\lambda_0 V})(i2\lambda_0 V \partial_V + i\lambda_0)$ and iterating, we obtain

$$[P^-, P^+] = -\frac{(2\lambda_0)^{-2}}{4\pi} \int dV \Upsilon^p(V) \tilde{f}(i2\lambda_0 V \partial_V + i\lambda_0) \Upsilon^p(V) \quad (\text{H.24})$$

so that

$$[[P^-, P^+], \Upsilon^p(V)] = (2\lambda_0)^{-2} \tilde{f}(2i\lambda_0 V \partial_V + i\lambda_0) \Upsilon^p(V). \quad (\text{H.25})$$

For generic V this is nonlocal, but at the bifurcate horizon $V = 0$ it collapses to

$$[[P^-, P^+], \Upsilon^p(0)] = (2\lambda_0)^{-2} \tilde{f}(i\lambda_0) \Upsilon^p(0). \quad (\text{H.26})$$

Finally, using (6.10),

$$[B, \Upsilon^p(0)] = i\frac{1}{2} \Upsilon^p(0), \quad (\text{H.27})$$

we conclude:

$$[[P^-, P^+], \Upsilon^p(0)] = -2i(2\lambda_0)^{-2} \tilde{f}(i\lambda_0) \times [B, \Upsilon^p(0)] \quad (\text{H.28})$$

Comparing with (6.13), we define the *algebraic curvature*

$$R_a := 2\beta_0^{-2} \tilde{f}(i\lambda_0). \quad (\text{H.29})$$

Our goal is to show that R_a equals the geometric curvature at the horizon, R_h . Using (H.20), we can express $\tilde{f}(i\lambda_0)$ via an inverse Fourier transform:

$$R_a/m^2 = (-2\beta_0^{-2}) \int_{-\infty}^{+\infty} dv (e^{2\lambda_0 v} - 1) \partial_v^2 \int_{-\infty}^{+\infty} du e^{-2\lambda_0 u} S(\frac{v}{2} - u) S(-\frac{v}{2} - u). \quad (\text{H.30})$$

We split the integrand according to $(e^{2\lambda_0 v} - 1)$:

$$R_a/m^2 := R_a^{(1)}/m^2 + R_a^{(2)}/m^2. \quad (\text{H.31})$$

$$\begin{aligned} \text{with: } R_a^{(1)}/m^2 &:= -\frac{\beta_0^{-2}}{2} \int dv_+ dv_- e^{-\lambda_0 v_+} e^{3\lambda_0 v_-} (\partial_{v_+} - \partial_{v_-})^2 S(v_+) S(v_-) \\ R_a^{(2)}/m^2 &:= 2\beta_0^{-2} \int dv du e^{-2\lambda_0 u} \partial_v^2 [S(\frac{v}{2} - u) S(-\frac{v}{2} - u)] \end{aligned} \quad (\text{H.32})$$

where for $R_a^{(1)}$ we changed variables to $v_{\pm} := \frac{v}{2} \pm u$ for later convenience; the integration contours for v_{\pm} lie along \mathbb{R} .

To analyze potential divergences, we recall the asymptotic behavior of $S(z)$. From (2.56), for $z > 0$ we have $S(z) = \sum_k \beta_k e^{-\lambda_k z}$. For $z < 0$, the decay is controlled by poles of $S(\omega)$ in the lower half-plane (at $\{-iJ_n\}$), so $S(z) = \sum_n \tilde{\beta}_n e^{J_n z}$ for $z < 0$, with $\tilde{\beta}_n \propto \text{Res}[S(\omega \rightarrow -iJ_n)]$.

Let's first focus on $R_a^{(1)}/m^2$.

For the v_- integral, a potential divergence arises as $v_- \rightarrow +\infty$, where the integrand behaves as $e^{(3\lambda_0 - \lambda_k)v_-}$. The leading divergence from the $k = 0$ term, $\sim e^{2\lambda_0 v_-}$, will be removed below by an appropriate choice of the order of integration. Additional divergences occur whenever there exists $k \geq 1$ with $\lambda_k < 3\lambda_0$. In particular, if $\lambda_1 < 3\lambda_0$ then the v_- integral diverges. This divergence is physical and reproduces Case III in section 3, where the horizon curvature diverges for $\lambda_1 < 3\lambda_0$.

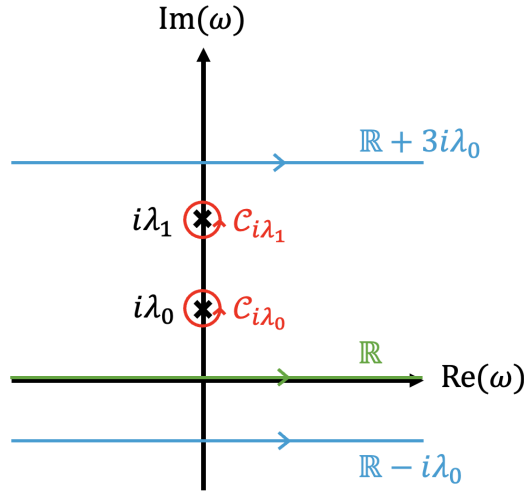


Figure 12: Various contours in the ω plane, used in [section H.2.2](#).

For the v_+ integral, a potential divergence arises as $v_+ \rightarrow -\infty$, where the integrand behaves as $e^{-(\lambda_0 - J_n)v_+}$. Thus, if there exists any $J_n \leq \lambda_0$ (in particular if $J_0 \leq \lambda_0$), the v_+ integral diverges. As discussed in [section H.2.1](#), this divergence is unphysical and reflects the wrong order of limits in defining $\Upsilon^p(0)$. We remove it by implementing the same contour prescription in Fourier space:

$$R_a^{(1)}/m^2 := \frac{\beta_0^{-2}}{2} \int dv_+ dv_- \frac{d\omega_+}{2\pi} \frac{d\omega_-}{2\pi} e^{i(\omega_+ + i\lambda_0)v_+} e^{i(\omega_- - 3i\lambda_0)v_-} (\omega_+ - \omega_-)^2 \mathcal{S}(\omega_+) \mathcal{S}(\omega_-) \quad (\text{H.33})$$

The defining contour of ω_{\pm} is along \mathbb{R} . To perform v_+, v_- integral, we will move the ω_+, ω_- contour to $\mathbb{R} - i\lambda_0$ and $\mathbb{R} + 3i\lambda_0$ respectively. As explained before, the contour prescription is that, when moving ω_+ contour, we ignore any possible poles of $\mathcal{S}(\omega_+)$ at $\{-iJ_n | J_n \leq \lambda_0\}$. When moving ω_- , we will pick up poles of $\mathcal{S}(\omega_-)$ at $i\lambda_0$ and possibly at $i\lambda_k$ if $k \geq 1, \lambda_k < 3\lambda_0$ (we will use λ_1 as representative). See [fig. 12](#).

Therefore, $R_a^{(1)}$ is further separated into three terms denoted as $R_a^{(1)} := R_a^{(1,1)} + R_a^{(1,2)} + R_a^{(1,3)}$:

$$\underbrace{\int_{\mathbb{R}} d\omega_+ \int_{\mathbb{R}} d\omega_-}_{R_a^{(1)}} \equiv \underbrace{\int_{\mathbb{R} - i\lambda_0} d\omega_+ \int_{\mathbb{R} + 3i\lambda_0} d\omega_-}_{R_a^{(1,1)}} + \underbrace{\int_{\mathbb{R}} d\omega_+ \int_{C_{i\lambda_1}} d\omega_-}_{R_a^{(1,2)}} + \underbrace{\int_{\mathbb{R}} d\omega_+ \int_{C_{i\lambda_0}} d\omega_-}_{R_a^{(1,3)}} \quad (\text{H.34})$$

We first evaluate $R_a^{(1,1)}$. One first change $\omega_+ := \tilde{\omega}_+ - i\lambda_0, \omega_- = \tilde{\omega}_- + 3i\lambda_0$, with $\tilde{\omega}_{\pm}$ along \mathbb{R} . Then, integration of v_+, v_- along \mathbb{R} is convergent and impose $\delta(\tilde{\omega}_+) \delta(\tilde{\omega}_-)$. We eventually obtain:

$$R_a^{(1,1)}/m^2 = -2\beta_0^{-2} (2\lambda_0)^2 \mathcal{S}(3i\lambda_0) \mathcal{S}(-i\lambda_0) \quad (\text{H.35})$$

Notice that, $\mathcal{S}(-i\lambda_0) = \frac{1}{\mathcal{S}(i\lambda_0)} = 0$, since $i\lambda_0$ is a simple pole of $\mathcal{S}(\omega)$. So, $R_a^{(1,1)}$ is zero in general, unless $\mathcal{S}(3i\lambda_0)$ hit another pole. This is precisely the critical case when $\lambda_1 = 3\lambda_0$, where $R_a^{(1,1)}$

will become finite. To summarize:

$$R_a^{(1,1)}/m^2 = \begin{cases} 0, & \lambda_1 > 3\lambda_0 \\ (-2)\frac{4\lambda_0^2\beta_1}{\beta_0}, & \lambda_1 = 3\lambda_0 \\ \text{finite value,} & \lambda_1 < 3\lambda_0 \end{cases} \quad (\text{H.36})$$

Now, we evaluate $R_a^{(1,2)}$. One first integrates over ω_- along $\mathcal{C}_{i\lambda_1}$, the integrand becomes $e^{i(\omega_++i\lambda_0)v_+} e^{(3\lambda_0-\lambda_1)v_-} (\omega_+ - i\lambda_1)^2 \mathcal{S}(\omega_+) \beta_1$. Then, we further change v_{\pm} back to u, v coordinate, and the two exponential becomes $e^{i(\omega_+-2i\lambda_0+i\lambda_1)\frac{v}{2}} e^{i(\omega_++4i\lambda_0-i\lambda_1)u}$. When $\lambda_0 < \lambda_1 < 3\lambda_0$, we have $-\lambda_0 < \lambda_1 < \lambda_0$. Therefore, we can move the contour of ω_+ from \mathbb{R} to $\mathbb{R} + i(2\lambda_0 - \lambda_1)$, to make v integral convergent. By our contour prescription, we ignore the possible poles at $\{-iJ_n | J_n \leq \lambda_0\}$. So, we change variable $\omega_+ := \tilde{\omega}_+ + i(2\lambda_0 - \lambda_1)$, $\tilde{\omega}_+ \in \mathbb{R}$. Integrate over v along \mathbb{R} impose $\delta(\tilde{\omega})$. The remaining du integral along \mathbb{R} is divergent due to integrand $e^{-(3\lambda_0-\lambda_1)(2u)} (\lambda_0 - \lambda_1)^2 \mathcal{S}(2i\lambda_0 - i\lambda_1) \beta_1$. Therefore, we conclude:

$$R_a^{(1,2)}/m^2 = \begin{cases} \infty, & \lambda_1 < 3\lambda_0 \\ 0, & \text{otherwise} \end{cases} \quad (\text{H.37})$$

Then, we evaluate $R_a^{(1,3)}$. The procedure is similar as $R_a^{(1,2)}$. One first integrates over ω_- along $\mathcal{C}_{i\lambda_0}$, the integrand becomes $e^{i(\omega_++i\lambda_0)v_+} e^{2\lambda_0 v_-} (\omega_+ - i\lambda_0)^2 \mathcal{S}(\omega_+) \beta_0$. Then, we further change v_{\pm} back to u, v coordinate, and the two exponential becomes $e^{i(\omega_+-i\lambda_0)\frac{v}{2}} e^{i(\omega_++3i\lambda_0)u}$. Now, to make v integral convergent, we shift contour of ω_+ from \mathbb{R} to $\mathbb{R} + i\lambda_0$. In this process, no pole is crossed. One might worry that $\mathcal{S}(\omega_+)$ has a simple pole at $\omega_+ = i\lambda_0$, which exactly sit on deformed contour $\mathbb{R} + i\lambda_0$, but the pole is canceled by double zero $(\omega_+ - i\lambda_0)^2$ term in the front. So, we change variable $\omega_+ := \tilde{\omega}_+ + i\lambda_0$, $\tilde{\omega}_+ \in \mathbb{R}$. Integrate over v along \mathbb{R} impose $\delta(\tilde{\omega}_+)$. The integrand of the remaining du integral, $\lim_{\tilde{\omega}_+ \rightarrow 0} [e^{i(4i\lambda_0+\tilde{\omega}_+)u} \tilde{\omega}_+^2 \mathcal{S}(\tilde{\omega}_+ + i\lambda_0) \beta_0]$, is zero, again due to the fact that double zero factor cancels a simple pole and leaving a simple zero. Therefore, if we delay the du integral to the last, we conclude that:

$$R_a^{(1,3)}/m^2 = 0 \quad (\text{H.38})$$

Finally, we calculate $R_a^{(2)}$. In Fourier space, (H.32) becomes:

$$R_a^{(2)}/m^2 = -\frac{\beta_0^{-2}}{2} \int dudv \frac{d\omega_1}{2\pi} \frac{d\omega_2}{2\pi} e^{i(\omega_1-\omega_2)\frac{v}{2}} e^{i(-\omega_1-\omega_2+2i\lambda_0)u} (\omega_1 - \omega_2)^2 \mathcal{S}(\omega_1) \mathcal{S}(\omega_2) \quad (\text{H.39})$$

First imagine moving the first pole slightly above: $\lambda_0 \rightarrow \lambda_0 + \epsilon$, where one replace $\mathcal{S}(\omega)$ by $\mathcal{S}_{\epsilon}(\omega)$. Then one can safely move the contour of $\omega_{1,2}$ from \mathbb{R} to $\mathbb{R} + i\lambda_0$. So, define $\omega_{1,2} := \tilde{\omega}_{1,2} + i\lambda_0$. In this process no pole is crossed. Then one can integrate u, v along \mathbb{R} and get:

$$\begin{aligned} R_a^{(2)}/m^2 &= -\frac{\beta_0^{-2}}{2} \int d\tilde{\omega}_1 d\tilde{\omega}_2 \delta\left(\frac{\tilde{\omega}_1 - \tilde{\omega}_2}{2}\right) \delta(\tilde{\omega}_1 + \tilde{\omega}_2) (\tilde{\omega}_1 - \tilde{\omega}_2)^2 \mathcal{S}_{\epsilon}(i\lambda_0 + \tilde{\omega}_1) \mathcal{S}_{\epsilon}(i\lambda_0 + \tilde{\omega}_2) \\ &= -2\beta_0^{-2} \int d\tilde{\omega}_1 \delta(\omega_1) \tilde{\omega}_1^2 \mathcal{S}_{\epsilon}(i\lambda_0 + \tilde{\omega}_1) \mathcal{S}_{\epsilon}(i\lambda_0 - \tilde{\omega}_1) \\ &= (-2\beta_0^{-2}) \lim_{\tilde{\omega}_1 \rightarrow 0} \lim_{\epsilon \rightarrow 0} [\tilde{\omega}_1^2 \mathcal{S}_{\epsilon}(i\lambda_0 + \tilde{\omega}_1) \mathcal{S}_{\epsilon}(i\lambda_0 - \tilde{\omega}_1)] \\ &= -2 \end{aligned} \quad (\text{H.40})$$

where in the second line, we integrate over $d\tilde{\omega}_2\delta(\tilde{\omega}_1 + \tilde{\omega}_2)$, and in the last line we notice that $-i\beta_0$ is the residual of $\mathcal{S}(\omega)$ at $i\lambda_0$.

To summarize, combining $R_a^{(1,1)}$, $R_a^{(1,2)}$, $R_a^{(1,3)}$, and $R_a^{(2)}$ from (H.36), (H.37), (H.38), and (H.40), we obtain

$$R_a/m^2 = \begin{cases} -2, & \lambda_1 > 3\lambda_0 \\ -2(1 + \frac{4\lambda_0^2\beta_1}{\beta_0^2}), & \lambda_1 = 3\lambda_0 \\ \infty, & \lambda_1 < 3\lambda_0 \end{cases} \quad (\text{H.41})$$

This matches the three cases of horizon curvature discussed in section 3. Therefore,

$$R_a = R_h. \quad (\text{H.42})$$

This completes the derivation of (6.13).

H.2.3 Benchmark on AdS₂-Rindler case

In the special case of AdS₂-Rindler, we expect the nonlocal kernel (H.19) to become local and $[P^-, P^+]$ to be exactly proportional to B . To check this, we first take the inverse Fourier transform of $f(v)$ in (H.20) to obtain $\tilde{f}(\omega)$:

$$\tilde{f}(\omega) = (i\lambda_0 + \omega)^2 \mathcal{S}(2i\lambda_0 + \omega) \mathcal{S}(-\omega) - (i\lambda_0 - \omega)^2 \mathcal{S}(2i\lambda_0 - \omega) \mathcal{S}(\omega) \quad (\text{H.43})$$

For a massive Majorana fermion with non-integer mass and standard normalizable boundary conditions at the asymptotic boundary, the S-matrix is given in (F.58). Together with $\lambda_0 = \frac{1}{2}$, this yields

$$\tilde{f}(\omega) = 2i\omega. \quad (\text{H.44})$$

Substituting into (H.24) gives a local operator:

$$[P^-, P^+] = \frac{1}{2\pi} \int dV \Upsilon^p(V) V \partial_V \Upsilon^p(V). \quad (\text{H.45})$$

Comparing with (6.7), we find

$$[P^-, P^+] = 2iB, \quad (\text{H.46})$$

in agreement with the $\mathfrak{sl}(2, \mathbb{R})$ algebra (H.3).

I Examples of two-point function that doesn't have a continuous limit

Not every boundary two-point function $A(t, t')$ admits a sensible bulk-QFT description in the continuum limit (2.8). The basic diagnostic is the gate angle: from (2.12), obtaining an $O(1)$ conformal factor requires $\theta_N = \frac{\pi}{2} - O(\Delta t)$. If instead θ_N stays $O(1)$ away from $\pi/2$ (or approaches 0), the would-be bulk interpretation breaks down. Here we record two explicit examples where this happens.

Example I. Consider

$$A(t, t') = \frac{1}{\cosh(t - t')} \quad (\text{I.1})$$

which can be obtained by analytically continuing the large- q SYK two-point function (5.2) to $q = 2$ and infinite temperature. Using the determinant formula (2.20), we compute the gate angles. The relevant Toeplitz matrix is

$$A_{N+1} = \begin{bmatrix} 1 & \text{sech}(\Delta t) & \text{sech}(2\Delta t) & \cdots & \text{sech}(N\Delta t) \\ \text{sech}(\Delta t) & 1 & \text{sech}(\Delta t) & \cdots & \text{sech}((N-1)\Delta t) \\ \text{sech}(2\Delta t) & \text{sech}(\Delta t) & 1 & \cdots & \text{sech}((N-2)\Delta t) \\ \vdots & \vdots & \vdots & \ddots & \vdots \\ \text{sech}(N\Delta t) & \text{sech}((N-1)\Delta t) & \text{sech}((N-2)\Delta t) & \cdots & 1 \end{bmatrix} \quad (\text{I.2})$$

Using the block-determinant identity²⁵

$$\det A_{N+1} = \det \begin{bmatrix} 1 & x_N^\top \\ x_N & A_N \end{bmatrix} = \det(A_N - x_N x_N^\top) \quad (\text{I.3})$$

with $(x_N)_i := \text{sech}(i\Delta t)$, we find

$$(A_N - x_N x_N^\top)_{ij} = \text{sech}((i-j)\Delta t) - \text{sech}(i\Delta t) \text{sech}(j\Delta t) = (A_N)_{ij} \tanh(i\Delta t) \tanh(j\Delta t) \quad (\text{I.4})$$

and hence, defining $(\Lambda_N)_{ij} = \delta_{ij} \tanh(i\Delta t)$,

$$\det(A_{N+1}) = \det(\Lambda_N A_N \Lambda_N) = \det(A_N) \prod_{i=1}^N \tanh^2(i\Delta t) \quad (\text{I.5})$$

The determinant formula (2.20) then gives

$$\sin \theta_N = \tanh(N\Delta t) \quad (\text{I.6})$$

so in the continuum limit (2.8),

$$\sin \theta(z) = \tanh(z) \quad (\text{I.7})$$

In particular, θ remains $O(1)$ rather than approaching $\pi/2$, so this $A(t, t')$ does not admit the desired bulk-QFT limit.

Example II. Consider

$$A(t, t') = e^{-(t-t')^2} \quad (\text{I.8})$$

A direct computation of the first few gate angles (e.g. in Mathematica; we checked up to $N = 12$) gives

$$\sin^2 \theta_N = 1 - e^{-2N(\Delta t)^2} \quad (\text{I.9})$$

In the continuum limit (2.8) this implies $\sin \theta(z) = 0$, i.e. the gates approach near-perfect reflection rather than SWAP (cf. fig. 9(c),(d)). In this case the appropriate scaling limit is instead the Krylov limit (7.1), which yields an $O(1)$ Krylov coefficient $b_n \equiv \sqrt{2n}$ via (7.2).

²⁵We thank Xinyu Sun for explaining the following computation.

References

- [1] L. Susskind, “The World as a hologram,” *J. Math. Phys.* **36** (1995) 6377–6396, [arXiv:hep-th/9409089](#).
- [2] J. M. Maldacena, “The Large N limit of superconformal field theories and supergravity,” *Adv. Theor. Math. Phys.* **2** (1998) 231–252, [arXiv:hep-th/9711200](#).
- [3] E. Witten, “Anti de Sitter space and holography,” *Adv. Theor. Math. Phys.* **2** (1998) 253–291, [arXiv:hep-th/9802150](#).
- [4] S. S. Gubser, I. R. Klebanov, and A. M. Polyakov, “Gauge theory correlators from noncritical string theory,” *Phys. Lett. B* **428** (1998) 105–114, [arXiv:hep-th/9802109](#).
- [5] O. Aharony, S. S. Gubser, J. M. Maldacena, H. Ooguri, and Y. Oz, “Large N field theories, string theory and gravity,” *Phys. Rept.* **323** (2000) 183–386, [arXiv:hep-th/9905111](#).
- [6] A. Strominger, “The dS / CFT correspondence,” *JHEP* **10** (2001) 034, [arXiv:hep-th/0106113](#).
- [7] V. Chandrasekaran, R. Longo, G. Penington, and E. Witten, “An algebra of observables for de Sitter space,” *JHEP* **02** (2023) 082, [arXiv:2206.10780 \[hep-th\]](#).
- [8] L. Susskind, “Entanglement and Chaos in De Sitter Space Holography: An SYK Example,” *JHAP* **1** no. 1, (2021) 1–22, [arXiv:2109.14104 \[hep-th\]](#).
- [9] V. Narovlansky and H. Verlinde, “Double-scaled SYK and de Sitter holography,” *JHEP* **05** (2025) 032, [arXiv:2310.16994 \[hep-th\]](#).
- [10] E. Coleman, E. A. Mazenc, V. Shyam, E. Silverstein, R. M. Soni, G. Torroba, and S. Yang, “De Sitter microstates from $T\bar{T} + \Lambda_2$ and the Hawking-Page transition,” *JHEP* **07** (2022) 140, [arXiv:2110.14670 \[hep-th\]](#).
- [11] J. Maldacena, “Real observers solving imaginary problems,” [arXiv:2412.14014 \[hep-th\]](#).
- [12] V. Ivo, J. Maldacena, and Z. Sun, “Physical instabilities and the phase of the Euclidean path integral,” [arXiv:2504.00920 \[hep-th\]](#).
- [13] Y. Chen, D. Stanford, H. Tang, and Z. Yang, “On the phase of the de Sitter density of states,” [arXiv:2511.01400 \[hep-th\]](#).
- [14] Z. Yang, Y. Zhang, and W. Zheng, “Comments on the de Sitter Double Cone,” [arXiv:2505.08647 \[hep-th\]](#).
- [15] S. Collier, L. Eberhardt, and B. Mühlmann, “A microscopic realization of dS₃,” *SciPost Phys.* **18** no. 4, (2025) 131, [arXiv:2501.01486 \[hep-th\]](#).
- [16] T. Banks, W. Fischler, S. H. Shenker, and L. Susskind, “M theory as a matrix model: A conjecture,” *Phys. Rev. D* **55** (1997) 5112–5128, [arXiv:hep-th/9610043](#).
- [17] T. Nebabu and X.-L. Qi, “Bulk reconstruction from generalized free fields,” *JHEP* **08** (2024) 107, [arXiv:2306.16687 \[hep-th\]](#).

- [18] A. Hamilton, D. N. Kabat, G. Lifschytz, and D. A. Lowe, “Local bulk operators in AdS/CFT: A Boundary view of horizons and locality,” *Phys. Rev. D* **73** (2006) 086003, [arXiv:hep-th/0506118](#).
- [19] A. Hamilton, D. N. Kabat, G. Lifschytz, and D. A. Lowe, “Holographic representation of local bulk operators,” *Phys. Rev. D* **74** (2006) 066009, [arXiv:hep-th/0606141](#).
- [20] A. Hamilton, D. N. Kabat, G. Lifschytz, and D. A. Lowe, “Local bulk operators in AdS/CFT: A Holographic description of the black hole interior,” *Phys. Rev. D* **75** (2007) 106001, [arXiv:hep-th/0612053](#). [Erratum: *Phys.Rev.D* 75, 129902 (2007)].
- [21] A. Borodin and A. Okounkov, “A fredholm determinant formula for toeplitz determinants,” *Integral Equations and Operator Theory* **37** no. 4, (Dec, 2000) 386–396. <https://doi.org/10.1007/BF01192827>.
- [22] J. S. Geronimo and K. M. Case, “Scattering theory and polynomials orthogonal on the unit circle,” *J. Math. Phys.* **20** (1979) 299–310.
- [23] O. Aharony, J. Marsano, S. Minwalla, K. Papadodimas, and M. Van Raamsdonk, “The Hagedorn - deconfinement phase transition in weakly coupled large N gauge theories,” *Adv. Theor. Math. Phys.* **8** (2004) 603–696, [arXiv:hep-th/0310285](#).
- [24] R. Arai, S. Fujiwara, Y. Imamura, and T. Mori, “Finite N corrections to the superconformal index of toric quiver gauge theories,” *PTEP* **2020** no. 4, (2020) 043B09, [arXiv:1911.10794 \[hep-th\]](#).
- [25] R. Arai, S. Fujiwara, Y. Imamura, and T. Mori, “Finite N corrections to the superconformal index of orbifold quiver gauge theories,” *JHEP* **10** (2019) 243, [arXiv:1907.05660 \[hep-th\]](#).
- [26] R. Arai and Y. Imamura, “Finite N Corrections to the Superconformal Index of S-fold Theories,” *PTEP* **2019** no. 8, (2019) 083B04, [arXiv:1904.09776 \[hep-th\]](#).
- [27] R. Arai, S. Fujiwara, Y. Imamura, T. Mori, and D. Yokoyama, “Finite- N corrections to the M-brane indices,” *JHEP* **11** (2020) 093, [arXiv:2007.05213 \[hep-th\]](#).
- [28] D. Gaiotto and J. H. Lee, “The giant graviton expansion,” *JHEP* **08** (2024) 025, [arXiv:2109.02545 \[hep-th\]](#).
- [29] Y. Imamura, “Finite- N superconformal index via the AdS/CFT correspondence,” *PTEP* **2021** no. 12, (2021) 123B05, [arXiv:2108.12090 \[hep-th\]](#).
- [30] S. Murthy, “Unitary matrix models, free fermions, and the giant graviton expansion,” *Pure Appl. Math. Quart.* **19** no. 1, (2023) 299–340, [arXiv:2202.06897 \[hep-th\]](#).
- [31] D. S. Eniceicu, “Comments on the Giant-Graviton Expansion of the Superconformal Index,” [arXiv:2302.04887 \[hep-th\]](#).
- [32] Y. Chen, R. Mahajan, and H. Tang, “Giant graviton expansion from eigenvalue instantons,” [arXiv:2407.08155 \[hep-th\]](#).

- [33] R. G. Newton, *Scattering Theory of Waves and Particles*. Theoretical and Mathematical Physics. Springer Berlin, Heidelberg, 2 ed., 1982.
- [34] G. T. Horowitz and V. E. Hubeny, “Quasinormal modes of AdS black holes and the approach to thermal equilibrium,” *Phys. Rev. D* **62** (2000) 024027, [arXiv:hep-th/9909056](#).
- [35] E. Berti, V. Cardoso, and A. O. Starinets, “Quasinormal modes of black holes and black branes,” *Class. Quant. Grav.* **26** (2009) 163001, [arXiv:0905.2975 \[gr-qc\]](#).
- [36] G. Batra, G. B. De Luca, E. Silverstein, G. Torroba, and S. Yang, “Bulk-local dS₃ holography: the matter with $T\bar{T} + \Lambda_2$,” *JHEP* **10** (2024) 072, [arXiv:2403.01040 \[hep-th\]](#).
- [37] D. Anninos, R. Arias, D. A. Galante, and C. Maneerat, “Gravitational observatories in AdS₄,” *JHEP* **07** (2025) 234, [arXiv:2412.16305 \[hep-th\]](#).
- [38] S. Sachdev and J. Ye, “Gapless spin-fluid ground state in a random quantum heisenberg magnet,” *Phys. Rev. Lett.* **70** (1993) 3339–3342.
- [39] A. Kitaev, “A simple model of quantum holography.” Talks at kitp, april and may 2015, 2015. Available online (KITP seminar recordings/notes).
- [40] J. Maldacena and D. Stanford, “Remarks on the sachdev-ye-kitaev model,” *Phys. Rev. D* **94** no. 10, (2016) 106002, [arXiv:1604.07818 \[hep-th\]](#).
- [41] J. Polchinski and V. Rosenhaus, “The spectrum in the sachdev-ye-kitaev model,” *JHEP* **04** (2016) 001, [arXiv:1601.06768 \[hep-th\]](#).
- [42] H. W. Lin and D. Stanford, “A symmetry algebra in double-scaled SYK,” *SciPost Phys.* **15** no. 6, (2023) 234, [arXiv:2307.15725 \[hep-th\]](#).
- [43] Wikipedia contributors, “Cholesky decomposition,” 2026. https://en.wikipedia.org/wiki/Cholesky_decomposition.
- [44] Wikipedia contributors, “Szegő limit theorem,” 2026. https://en.wikipedia.org/wiki/Szeg%C5%91_limit_theorem.
- [45] D. S. Eniceicu, C. Murdia, and A. Torchylo, “The complete non-perturbative partition function of minimal superstring theory and JT supergravity,” *JHEP* **06** (2025) 178, [arXiv:2412.08698 \[hep-th\]](#).
- [46] D. S. Eniceicu, R. Mahajan, and C. Murdia, “Complex eigenvalue instantons and the Fredholm determinant expansion in the Gross-Witten-Wadia model,” *JHEP* **01** (2024) 129, [arXiv:2308.06320 \[hep-th\]](#).
- [47] Wikipedia contributors, “Kramers–kronig relations,” 2026. https://en.wikipedia.org/wiki/Kramers%E2%80%93Kronig_relations.
- [48] G. Festuccia and H. Liu, “Excursions beyond the horizon: Black hole singularities in Yang-Mills theories. I.,” *JHEP* **04** (2006) 044, [arXiv:hep-th/0506202](#).

- [49] G. Festuccia and H. Liu, “A Bohr-Sommerfeld quantization formula for quasinormal frequencies of AdS black holes,” *Adv. Sci. Lett.* **2** (2009) 221–235, [arXiv:0811.1033 \[gr-qc\]](#).
- [50] M. Dodelson, C. Iossa, R. Karlsson, and A. Zhiboedov, “A thermal product formula,” *JHEP* **01** (2024) 036, [arXiv:2304.12339 \[hep-th\]](#).
- [51] B. Swingle, “Entanglement Renormalization and Holography,” *Phys. Rev. D* **86** (2012) 065007, [arXiv:0905.1317 \[cond-mat.str-el\]](#).
- [52] V. de Alfaro, S. Fubini, and G. Furlan, “Conformal Invariance in Quantum Mechanics,” *Nuovo Cim. A* **34** (1976) 569.
- [53] D. Anninos, S. A. Hartnoll, and D. M. Hofman, “Static Patch Solipsism: Conformal Symmetry of the de Sitter Worldline,” *Class. Quant. Grav.* **29** (2012) 075002, [arXiv:1109.4942 \[hep-th\]](#).
- [54] C. Liu, H. Tang, and H. Zhai, “Krylov complexity in open quantum systems,” *Phys. Rev. Res.* **5** no. 3, (2023) 033085, [arXiv:2207.13603 \[cond-mat.str-el\]](#).
- [55] J. Maldacena, D. Stanford, and Z. Yang, “Conformal symmetry and its breaking in two dimensional Nearly Anti-de-Sitter space,” *PTEP* **2016** no. 12, (2016) 12C104, [arXiv:1606.01857 \[hep-th\]](#).
- [56] A. Almheiri and J. Polchinski, “Models of AdS₂ backreaction and holography,” *JHEP* **11** (2015) 014, [arXiv:1402.6334 \[hep-th\]](#).
- [57] K. Jensen, “Chaos in AdS₂ Holography,” *Phys. Rev. Lett.* **117** no. 11, (2016) 111601, [arXiv:1605.06098 \[hep-th\]](#).
- [58] T. G. Mertens and G. J. Turiaci, “Solvable models of quantum black holes: a review on Jackiw–Teitelboim gravity,” *Living Rev. Rel.* **26** no. 1, (2023) 4, [arXiv:2210.10846 \[hep-th\]](#).
- [59] M. Berkooz, M. Isachenkov, V. Narovlansky, and G. Torrents, “Towards a full solution of the large N double-scaled SYK model,” *JHEP* **03** (2019) 079, [arXiv:1811.02584 \[hep-th\]](#).
- [60] M. Berkooz, P. Narayan, and J. Simon, “Chord diagrams, exact correlators in spin glasses and black hole bulk reconstruction,” *JHEP* **08** (2018) 192, [arXiv:1806.04380 \[hep-th\]](#).
- [61] L. Susskind, “De Sitter Space, Double-Scaled SYK, and the Separation of Scales in the Semiclassical Limit,” *JHAP* **5** no. 1, (2025) 1–30, [arXiv:2209.09999 \[hep-th\]](#).
- [62] L. Susskind, “Scrambling in Double-Scaled SYK and De Sitter Space,” [arXiv:2205.00315 \[hep-th\]](#).
- [63] A. Rahman and L. Susskind, “Infinite Temperature is Not So Infinite: The Many Temperatures of de Sitter Space,” [arXiv:2401.08555 \[hep-th\]](#).
- [64] H. Verlinde, “Double-scaled SYK, chords and de Sitter gravity,” *JHEP* **03** (2025) 076, [arXiv:2402.00635 \[hep-th\]](#).

- [65] H. Lin and L. Susskind, “Infinite Temperature’s Not So Hot,” [arXiv:2206.01083 \[hep-th\]](#).
- [66] Y. Chen, N. Lashkari, and K. L. Leung, “Local approximations of global Hamiltonian from inclusion of algebras,” [arXiv:2512.25062 \[hep-th\]](#).
- [67] K. Furuya, N. Lashkari, M. Moosa, and S. Ouseph, “Information loss, mixing and emergent type III₁ factors,” *JHEP* **08** (2023) 111, [arXiv:2305.16028 \[hep-th\]](#).
- [68] S. Ouseph, K. Furuya, N. Lashkari, K. L. Leung, and M. Moosa, “Local Poincaré algebra from quantum chaos,” *JHEP* **01** (2024) 112, [arXiv:2310.13736 \[hep-th\]](#).
- [69] N. Lashkari, K. L. Leung, M. Moosa, and S. Ouseph, “Modular intersections, time interval algebras and emergent AdS₂,” *JHEP* **10** (2025) 153, [arXiv:2412.19882 \[hep-th\]](#).
- [70] S. A. W. Leutheusser and H. Liu, “Emergent Times in Holographic Duality,” *Phys. Rev. D* **108** no. 8, (2023) 086020, [arXiv:2112.12156 \[hep-th\]](#).
- [71] S. Leutheusser and H. Liu, “Causal connectability between quantum systems and the black hole interior in holographic duality,” *Phys. Rev. D* **108** no. 8, (2023) 086019, [arXiv:2110.05497 \[hep-th\]](#).
- [72] S. Leutheusser and H. Liu, “Subregion-subalgebra duality: Emergence of space and time in holography,” *Phys. Rev. D* **111** no. 6, (2025) 066021, [arXiv:2212.13266 \[hep-th\]](#).
- [73] E. Witten, “Gravity and the crossed product,” *JHEP* **10** (2022) 008, [arXiv:2112.12828 \[hep-th\]](#).
- [74] E. Witten, “Algebras, regions, and observers,” *Proc. Symp. Pure Math.* **107** (2024) 247–276, [arXiv:2303.02837 \[hep-th\]](#).
- [75] E. Witten, “A background-independent algebra in quantum gravity,” *JHEP* **03** (2024) 077, [arXiv:2308.03663 \[hep-th\]](#).
- [76] V. Chandrasekaran, G. Penington, and E. Witten, “Large N algebras and generalized entropy,” *JHEP* **04** (2023) 009, [arXiv:2209.10454 \[hep-th\]](#).
- [77] G. Penington and E. Witten, “Algebras and States in JT Gravity,” [arXiv:2301.07257 \[hep-th\]](#).
- [78] J. Kudler-Flam, S. Leutheusser, and G. Satishchandran, “Generalized black hole entropy is von Neumann entropy,” *Phys. Rev. D* **111** no. 2, (2025) 025013, [arXiv:2309.15897 \[hep-th\]](#).
- [79] C.-H. Chen and G. Penington, “A clock is just a way to tell the time: gravitational algebras in cosmological spacetimes,” [arXiv:2406.02116 \[hep-th\]](#).
- [80] A. Goel, V. Narovlansky, and H. Verlinde, “Semiclassical geometry in double-scaled SYK,” *JHEP* **11** (2023) 093, [arXiv:2301.05732 \[hep-th\]](#).
- [81] A. Almheiri, A. Goel, and X.-Y. Hu, “Quantum gravity of the Heisenberg algebra,” *JHEP* **08** (2024) 098, [arXiv:2403.18333 \[hep-th\]](#).

- [82] B. Czech, L. Lamprou, S. McCandlish, and J. Sully, “Integral Geometry and Holography,” *JHEP* **10** (2015) 175, [arXiv:1505.05515 \[hep-th\]](#).
- [83] V. Balasubramanian, B. D. Chowdhury, B. Czech, J. de Boer, and M. P. Heller, “Bulk curves from boundary data in holography,” *Phys. Rev. D* **89** no. 8, (2014) 086004, [arXiv:1310.4204 \[hep-th\]](#).
- [84] B. Czech, L. Lamprou, S. McCandlish, and J. Sully, “Tensor Networks from Kinematic Space,” *JHEP* **07** (2016) 100, [arXiv:1512.01548 \[hep-th\]](#).
- [85] D. E. Parker, X. Cao, A. Avdoshkin, T. Scaffidi, and E. Altman, “A Universal Operator Growth Hypothesis,” *Phys. Rev. X* **9** no. 4, (2019) 041017, [arXiv:1812.08657 \[cond-mat.stat-mech\]](#).
- [86] P. Nandy, A. S. Matsoukas-Roubeas, P. Martinez-Azcona, A. Dymarsky, and A. del Campo, “Quantum dynamics in Krylov space: Methods and applications,” *Phys. Rept.* **1125-1128** (2025) 1–82, [arXiv:2405.09628 \[quant-ph\]](#).
- [87] M. Dodelson, “Ringdown in the SYK model,” *SciPost Phys.* **19** no. 3, (2025) 081, [arXiv:2408.05790 \[hep-th\]](#).
- [88] M. Dodelson, “Black holes from chaos,” [arXiv:2501.06170 \[hep-th\]](#).
- [89] V. Chandrasekaran and É. É. Flanagan, “Subregion algebras in classical and quantum gravity,” [arXiv:2601.07915 \[hep-th\]](#).
- [90] S. H. Shenker and D. Stanford, “Stringy effects in scrambling,” *JHEP* **05** (2015) 132, [arXiv:1412.6087 \[hep-th\]](#).
- [91] M. Gärttner, J. G. Bohnet, A. Safavi-Naini, M. L. Wall, J. J. Bollinger, and A. M. Rey, “Measuring out-of-time-order correlations and multiple quantum spectra in a trapped-ion quantum magnet,” *Nature Physics* **13** no. 8, (Aug, 2017) 781–786. <https://doi.org/10.1038/nphys4119>.
- [92] J. Li, R. Fan, H. Wang, B. Ye, B. Zeng, H. Zhai, X. Peng, and J. Du, “Measuring out-of-time-order correlators on a nuclear magnetic resonance quantum simulator,” *Phys. Rev. X* **7** (Jul, 2017) 031011. <https://link.aps.org/doi/10.1103/PhysRevX.7.031011>.
- [93] S. Xu and B. Swingle, “Scrambling Dynamics and Out-of-Time-Ordered Correlators in Quantum Many-Body Systems,” *PRX Quantum* **5** no. 1, (2024) 010201, [arXiv:2202.07060 \[quant-ph\]](#).
- [94] “NIST Digital Library of Mathematical Functions.” <https://dlmf.nist.gov/>, release 1.2.5 of 2025-12-15. <https://dlmf.nist.gov/>.